E.O. Paton Electric Welding Institute of the National Academy of Science of Ukraine
International Association «Welding»
LLC «Scientific Journals»

The Paton Welding Journal

10
2021

International Scientific-Technical and Production Journal
Founded in January 2000 (12 Issues Per Year)

EDITORIAL BOARD

Editor-in-Chief
I.V. Krivtsun — E.O. Paton Electric Welding Institute, Kyiv, Ukraine

Deputy Editor-in-Chief
S.V. Akhonin — E.O. Paton Electric Welding Institute, Kyiv, Ukraine

Deputy Editor-in-Chief
L.M. Lobanov — E.O. Paton Electric Welding Institute, Kyiv, Ukraine

Editorial Board Members

O.M. Berdnikova	E.O. Paton Electric Welding Institute, Kyiv, Ukraine
Chang Yunlong	School of Materials Science and Engineering, Shenyang University of Technology, Shenyang, China
V.V. Dmitrik	NTUU «Kharkiv Polytechnic Institute», Kharkiv, Ukraine
Dong Chunlin	China-Ukraine Institute of Welding of Guangdong Academy of Sciences, Guangzhou, China
A. Gumenyuk	Bundesanstalt für Materialforschung und –prüfung (BAM), Berlin, Germany
V.V. Knysh	E.O. Paton Electric Welding Institute, Kyiv, Ukraine
V.M. Korzhyk	E.O. Paton Electric Welding Institute, Kyiv, Ukraine
V.V. Kvasnytskyi	NTUU «Igor Sikorsky Kyiv Polytechnic Institute», Kyiv, Ukraine
Yu.M. Lankin	E.O. Paton Electric Welding Institute, Kyiv, Ukraine
S.Yu. Maksymov	E.O. Paton Electric Welding Institute, Kyiv, Ukraine
M.O. Pashchin	E.O. Paton Electric Welding Institute, Kyiv, Ukraine
Ya. Pilarczyk	Welding Institute, Gliwice, Poland
V.D. Poznyakov	E.O. Paton Electric Welding Institute, Kyiv, Ukraine
U. Reisgen	Welding and Joining Institute, Aachen, Germany
I.O. Ryabtsev	E.O. Paton Electric Welding Institute, Kyiv, Ukraine
V.M. Uchanin	Karpenko Physico-Mechanical Institute, Lviv, Ukraine
Yang Yongqiang	South China University of Technology, Guangzhou, China

Managing Editor
O.T. Zelnichenko — International Association «Welding», Kyiv, Ukraine

Address of Editorial Board
E.O. Paton Electric Welding Institute, 11 Kazymyr Malevych Str. (former Bozhenko), 03150, Kyiv, Ukraine
Tel./Fax: (38044) 200 82 77, E-mail: journal@paton.kiev.ua
https://patonpublishinghouse.com/eng/journals/tpwj

State Registration Certificate 24933-14873 ПР from 13.08.2021
ISSN 0957-798X, DOI: http://dx.doi.org/10.37434/tpwj

Subscriptions, 12 issues per year:
$384 — annual subscription for the printed (hard copy) version, air postage and packaging included;
$312 — annual subscription for the electronic version
(sending issues in pdf format or providing access to IP addresses).

The content of the journal includes articles received from authors from around the world in the field of welding and related technologies and selectively includes translations into English of articles from the following journals, published by PWI in Ukrainian:

- Automatic Welding (https://patonpublishinghouse.com/eng/journals/as);
- Technical Diagnostics & Nondestructive Testing (https://patonpublishinghouse.com/eng/journals/tdnk);
- Electrometallurgy Today (https://patonpublishinghouse.com/eng/journals/sem).

© E.O. Paton Electric Welding Institute of NASU, 2021
© International Association «Welding» (Publisher), 2021
© LLC «Scientific Journals», 2021

CONTENTS

ORIGINAL ARTICLES

*Translation Article(s) from «Automatic Welding», No. 10, 2021.

**Translation Article(s) from «Electrometallurgy Today», No. 3, 2021.

https://doi.org/10.37434/tpwj2021.10.01

INFLUENCE OF MODIFICATION AND MICROALLOYING ON DEPOSITED METAL STRUCTURE AND PROPERTIES (Review)

A.A. Babinets and **I.O. Ryabtsev**

E.O. Paton Electric Welding Institute of the NASU
11 Kazymyr Malevych Str., 03150, Kyiv, Ukraine

ABSTRACT

Proceeding from published data, the influence of modification and microalloying by boron, titanium, tungsten, zirconium, yttrium, etc., on the deposited metal structure, mechanical and service properties is shown. It is demonstrated that addition of these elements or their compounds with carbon and nitrogen in the quantity of up to 0.2 %, allows producing a fine-grained, homogeneous structure of metal, a more uniform distribution of alloying elements, that makes a positive effect on the values of strength, ductility, wear and heat resistance. It was determined that introducing small additives of boron or its compounds (in the quantity of up to 0.2 %), cerium or yttrium (in the quantity of up to 0.015 % of each), or application of complex master alloys, which can have the above-mentioned elements in their composition, as well as such modifiers, as zirconium, titanium carbides and borides or tungsten carbides, looks promising in terms of increase of wear and heat resistance of the deposited metal. Proceeding from the performed analysis, it was also shown that addition of titanium and zirconium diborides to the composition of flux-cored wire charge, promotes activation of the processes of formation of molten metal drops at the electrode wire tip, resulting in improvement of the quality of metal transfer in the welding arc that leads to greater values of the coefficients of alloying element transition into the deposited metal and improves deposited bead formation.

KEY WORDS: arc surfacing, deposited metal, tool steel, modification, microalloying, metal structure, wear resistance, heat resistance

It is widely known that mechanical and service properties of steels and alloys are determined by their chemical composition and structure. Thus, influencing the metal structure allows changing its properties within a certain range. In work [1] the main methods of deposited metal modification and microalloying were analyzed, and it was shown that the simplest and most rational of the considered methods is introducing small additives (up to 0.2 %) of chemical elements or their compounds directly through the charge of flux-cored electrode wires.

The objective of this work is analysis of published data on the influence of small additives (up to 0.2 %) of chemical elements or their compounds on the deposited metal structure, and its service properties, as well as on indices of stability of electric arc surfacing process.

It should be noted that in the majority of works, analyzed in this paper, studied was the influence of individual chemical elements or their compounds of exactly the modifying particles, that is those, the action of which consists in regulation of primary crystallization and/or change of the degree of dispersity of the crystallizing phases. As to microalloying, this term is mostly applied to such an element as boron and its compounds with other elements, the role of which is manifested predominantly as a result of an impact on the solid state of the metal (formation of interstitial or substitutional solid solution, etc.) [1].

Influence of elements-modifiers and their compounds on the deposited metal structure, its mechanical and service properties. In the general case it can be noted that application of modifiers leads to refinement of the deposited metal grain, and producing a more uniform structure that has a positive effect on its ductile characteristics, and influences the technological and other properties of the metal [2–6, etc.].

As the grain size depends on the ratio of the rates of crystal nucleation and growth, its modification is essentially aimed at the change of these parameters in the required direction. Usually, a large number of crystallization centers form in the liquid metal at modification. Their further growth depends on the nature of the influence of modifying additives or physical impacts on the situation in the crystal–melt near-boundary zone [1]. In the majority of the cases, the soluble or insoluble additives demonstrate an inhibitory effect on crystal growth. Here, the specific braking mechanism depends on the modifying additive nature and mechanism of its action. Two types of the influence of modifier content on the metal structure were found [2]: monotonic refinement of the grain at gradual increase of modifier content and nonmonotonic grain refinement with the area of optimum concentration of modifiers in the range of 0.01–0.10 %, going above which again leads to coarsening of the grain.

Copyright © The Author(s)

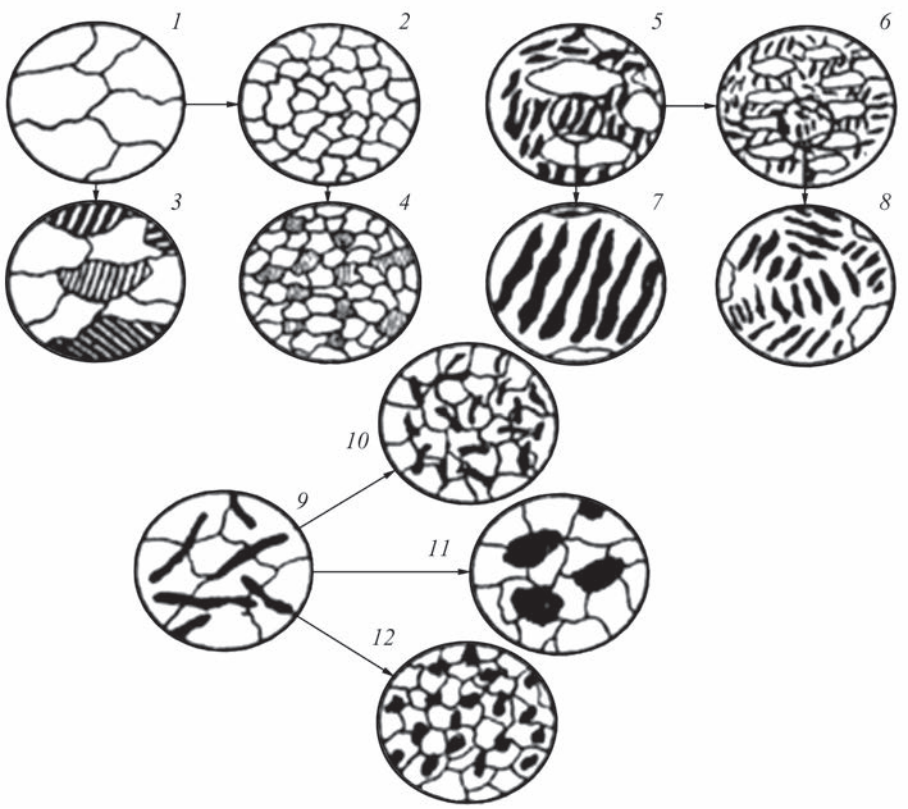

Figure 1. Influence of modifiers on the alloy structural components [2]

The variant of monotonic refinement of the grain with increase of modifier concentration is characteristic for insoluble catalyst additives (for instance, titanium in aluminium), while the variant of nonmonotonic grain refinement is characteristic for surface-active soluble additives (for instance, magnesium in zinc) [2]. Influence of modifiers on individual structural components of steel (alloy) is schematically shown in Figure 1 and in the Table 1.

Let us consider the influence of modification and microalloying on the structure and properties of steels and alloys in greater detail, grouping the data available in technical literature by the name of the respective chemical elements.

Boron. It is widely known that boron microadditives are used to improve a set of mechanical properties of steels, subjected to quenching and tempering. Here, the influence of boron is associated with increase of hardening and refinement of austenite grain [3–6].

In addition to refinement of the grain size, boron microalloying influences the deposited metal hardness and microhardness of solid solution grains, while the carbide phase microhardness remains practically unchanged. Increase of the deposited metal hardness at a slight lowering of hardness of austenite decomposition products, in the opinion of the authors of [7], is related to greater density and branching of intergranular boundaries, strengthened by boron.

In work [5] it was established that application of flux-cored wire with microadditives of boron nitride is promising for restoration by surfacing of the rollers of machines for continuous casting of billets (MCCB). It results in formation on the surface of MCCB rollers of a wear-resistant layer of the deposited metal of 30Kh5M2V2GF type with the hardness of up to

Table 1. Results of the influence of modifiers on the structure of steels and alloys [2]

Alloy type	Result	Structure (see Figure 1)
Alloys — solid solutions (carbon steels with ferrite-pearlite structure)	Initial grain refinement	1, 2
	Phase recrystallization	1, 3
	Secondary grain refinement after phase recrystallization	1, 2, 4
Alloys with primary precipitates and eutectics (grey and high-strength cast iron)	Refinement of both the structural components	5, 6
	Coarse-crystalline eutectics	7
	Thin-plate eutectics with very short plates	8
	Refinement of individual coarse structural components	9, 10
	Coagulation and spheroidization of structural components	11, 12

HRC 57, high heat-resistance and low coefficient of friction, compared to a layer deposited by unmodified material.

On the other hand, the data on the influence of boron microadditives on the ductility properties of steels are quite ambiguous. In work [8] it is shown that at boron content in the metal on the level of 0.0015–0.0025 % it is possible to effectively control the ductility properties of low-alloyed steels of K40 strength class. Microalloying of low-alloyed steels of 08G2S, 10G2S type, etc., by boron (0.002–0.004 %) promotes an improvement of their metallurgical purity, resulting in increase of the level of steel impact toughness [9], but a decrease of its ductility [10]. Lowering of ductility and impact toughness of structural steel 35 is reported in work [11] at microalloying with boron in the same amounts (up to 0.005 %).

Such an unambiguous influence of boron on the steel properties is associated with the fact that it is a more active deoxidizer, compared to silicon and manganese, and has high surface activity. Due to that boron is predominantly located along the grain boundaries, which leads to impurity redistribution also on the grain boundaries, and the concentration of sulphur, manganese, nitrogen and titanium decreases markedly. More over, boron can form an interstitial solid solution in combination with the ability to drive the impurities from the boundaries into the grain volume [10].

Titanium. Titanium in the form of its compounds with carbon, nitrogen and boron is rather widely used at steel modification, primarily due to the high melting temperature of these compounds (> 3000 K). Titanium carbonitrides are most often used as modifiers. By the data of works [12, 13], microalloying of high-alloyed steels of 10Kh15N4AM3 type by titanium carbonitride leads to marked refinement of the macrograin, elimination of grain columnarity and different grain size. Carbides take a compact equiaxed shape and are uniformly distributed in the grain volume: in an unmodified alloy, carbides have an elongated shape, and reach the size of 50 μm, while in the modified alloy carbides take a compact shape of 4–8 μm size. Such a change of the microstructure is favourable for the long-term strength, wear and heat resistance of the samples, raising it up to 2–3 times.

We can assume that the particles of titanium carbonitride, which have a high thermodynamic stability, only slightly dissolving in the metal melt, migrate from the flux-cored wire charge into the weld pool, influencing the kinetics of molten metal crystallization [12]. By the data of [13], carbonitride particles have the role of effective inoculants, promoting refinement of primary grain of the alloy matrix. Increase of the quantity of modifier in the wire above 0.4 wt.% does not lead to further refinement of the grains.

The influence of steel modification by titanium nitride is less unambiguous. In keeping with the data of [14], the average width of primary crystallites in low-alloyed structural steel becomes smaller, but the scatter of width values becomes greater. There is also information that addition of titanium nitride particles leads to formation of pores in the weld metal. Opposite results are reported in [4], where it is shown that addition of up to 0.4 wt.% of titanium nitride particles in the composition of filler flux-cored wire to high-carbon chromium steel of 320Kh12M2NR type does not lead to formation of pores and promotes increase of the deposited metal hardness from *HRC* 55 to *HRC* 57, while increasing the abrasive wear resistance of high-alloyed chromium-molybdenum deposited metal by 20 %. Such an ambiguous influence of titanium nitride is attributable to different class of materials used in the above studies.

In work [6] it was shown that modification of structural steel 45 by titanium diborides lowers the dendritic heterogeneity, fragmentation of columnar den-

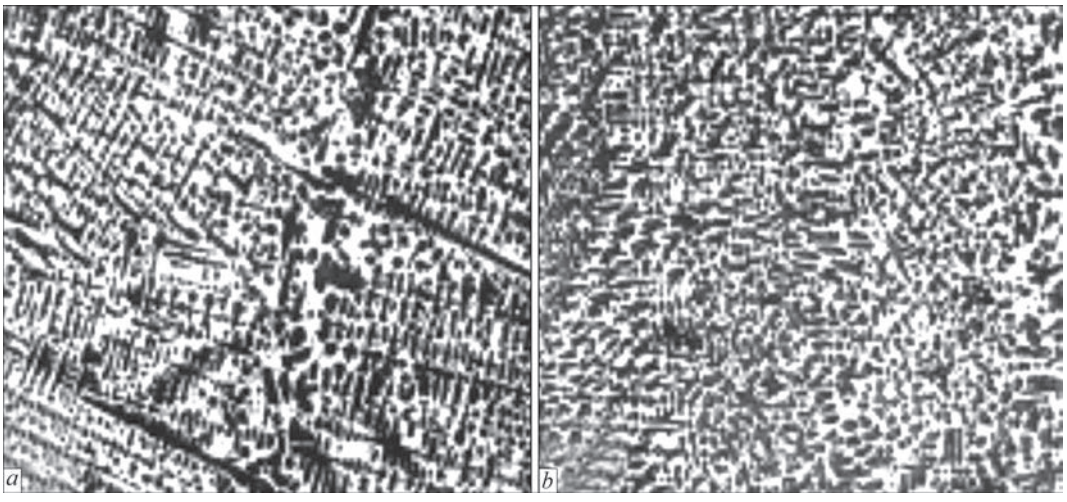

Figure 2. Influence of TiB_2 modifier on the deposited layer structure (×100) [6]: *a* — without modifier; *b* — with modifier

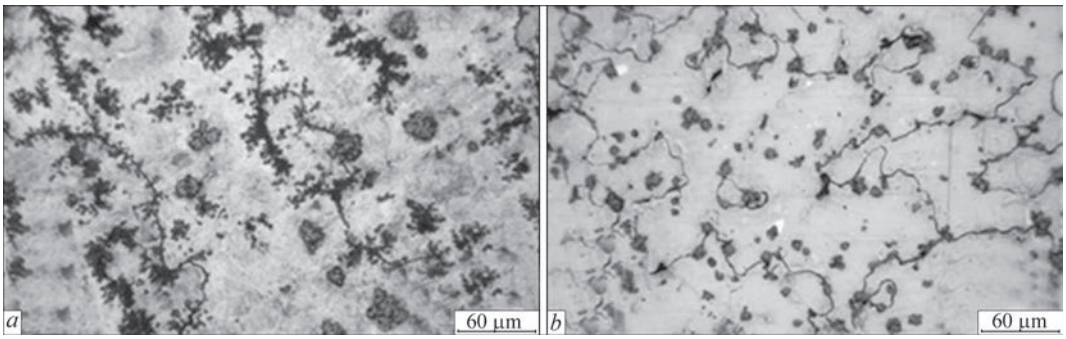

Figure 3. Initial structure of metal deposited by ESS with flux-cored wire (*a*), and with the same wire, but with the charge containing tungsten nanocrabides (*b*) (×200) [16]

drites, structure refinement, and elimination of coarse primary precipitates of the carbide phase (Figure 2). Here, the structural changes, that have taken place, did not influence the metal hardness, while increasing its wear resistance [6]. By the data of works [12, 15] addition of titanium dioxide to the filler material in welding raises the yield limit and ultimate strength of welds in medium- and high-alloyed steels.

Tungsten. Refinement of the structure of low-carbon low-alloyed [14, 16], as well as medium- and high-alloyed metal of chromium steel type [16] was found at their modification by powders of tungsten carbide at their content in the metal of up to 0.04 %. It was noted that in the modified metal of the type of low-alloyed steel the structure becomes more homogeneous, demonstrating the positive influence on the ductility characteristics [14].

A similar influence of tungsten carbide additives was noted in work [16], where it was shown that the structure of the deposited metal of the type of high-carbon chromium steel in the initial state is a ferrite-pearlite mixture (Figure 3, *a*). Addition of tungsten nanocarbides leads to transformation of the metal structure into a modified subdispersed solid solution based on α-Fe with residual austenite, located on the grain boundaries (Figure 3, *b*). The quantity of nonmetallic inclusions, which at some time had rather arbitrary contours and were nonuniformly distributed in the metal, decreased by 15–20 %. The remaining inclusions are more uniformly distributed and are of a globular shape. Such a structure of the metal, in the opinion of the authors of the work, should promote an increase of its ductility properties under cyclic loading.

Zirconium. Use of zirconium is due to its ability to inhibit grain growth, and actively interact with carbon and nitrogen (more actively than titanium does), leading to formation of dispersed carbides and nitrides [3, 17]. Their influence on the joint properties is manifested in the form of grain refinement, improvement of mechanical properties, lowering of cold brittleness threshold and sensitivity to stress raisers of both steels and alloys, including those from light metals [11, 18]. For instance, aluminium alloy modification by adding potassium fluorozirconate (K_2ZrF_6) to the composition of the flux-cored wire charge [18] leads to refinement of weld pool metal and increase of the total number of crystallization centers, resulting in the deposited metal having a fine-grained structure with uniform distribution of alloying elements that causes 1.2 times increase in wear resistance. By the data of work [11], zirconium nitrides and carbides exceed similar compounds of titanium, vanadium and molybdenum by their strength and resistance. This leads to an essential increase of strength and ductility values of structural steels (Figure 4).

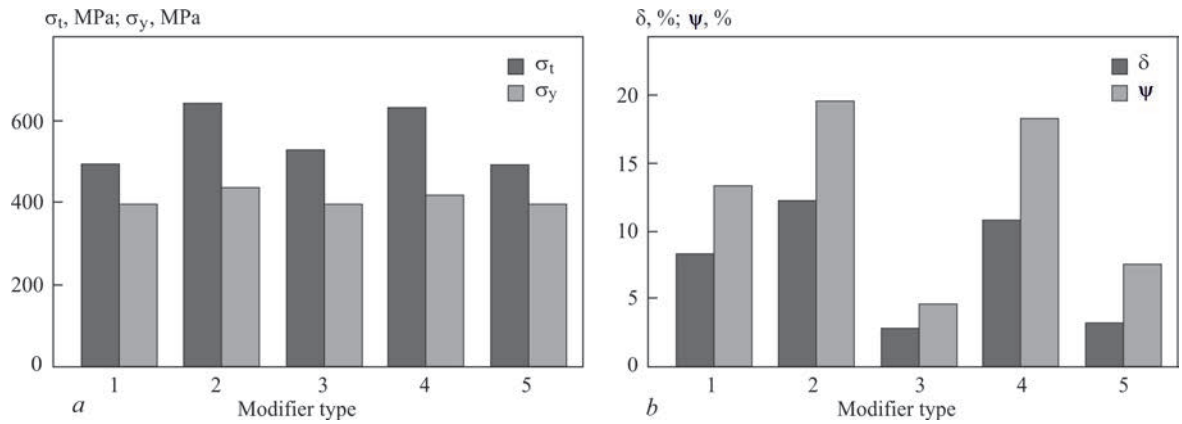

Figure 4. Influence of different elements on the values of strength (*a*) and ductility (*b*) of structural steel, unmodified (1) and modified by vanadium (2), molybdenum (3), zirconium (4) and boron (5) [11]

Cerium. Cerium is known due to its ability to neutralize the influence of surface-active sulphur during deposited metal solidification and at long-term high-temperature heating [19]. Modification of steels of 30KhGSA, Kh5MF, Kh12MF type by cerium in the quantities of up to 0.009 %, leads to increase of the technological strength, impact toughness and resistance to thermal fatigue failure of the deposited metal [19, 20]. This effect is achieved through sulphur binding into refractory finely-dispersed compounds, lowering of microchemical heterogeneity and refinement of austenite grain. Here, weld metal contamination by nonmetallic inclusions is also reduced [21].

Yttrium. Yttrium has an exceptionally high affinity to oxygen, nitrogen, sulphur and other elements, forming thermodynamically stable compounds with them. Among the rare-earth elements (REM) the affinity of yttrium to oxygen at weld pool temperatures is the highest. According to the data of [17], investigations of yttrium-modified deposited metal of 15Kh8N2M2F type showed that it has certain technological advantages, compared to cerium: at its addition to liquid metal the pyroeffect is absent, it is assimilated by liquid steel in a more stable manner and, in addition, 3–4 times smaller amount of it is required, in order to obtain optimum steel properties, than that of cerium. Optimum yttrium content in the deposited metal is in the range of 0.013–0.015 % [17].

So, deposited metal microalloying by yttrium leads to an increase of mechanical and service properties, namely wear resistance and heat resistance by 20–30 % (Figure 5), which is, apparently, attributable to metal structure refinement, change of the shape, size and nature of distribution of nonmetallic inclusions, cleaning of grain boundaries from sulphur and other harmful impurities [17, 22].

Calcium. In the general case, addition of calcium to steel increases its fluidity, modifies the oxide and sulphide inclusions, improves the ductility properties, etc. Calcium features low solubility in the metal and low melting and boiling temperatures, so that it is practically completely removed from the metal. Therefore, in order to preserve the modification effect, it is necessary to add a lot of other elements to the master alloy composition, which promote prolongation of calcium effect [3].

Strontium. By its physico-chemical properties strontium takes up an intermediate position between calcium and barium, and it also has a limited use to improve the effectiveness of metal modification [3].

Barium. Barium is often used in combination with calcium to improve its absorption and enhance the positive impact of the latter, although the effectiveness of using just barium (without calcium) is noted in a number of cases [3].

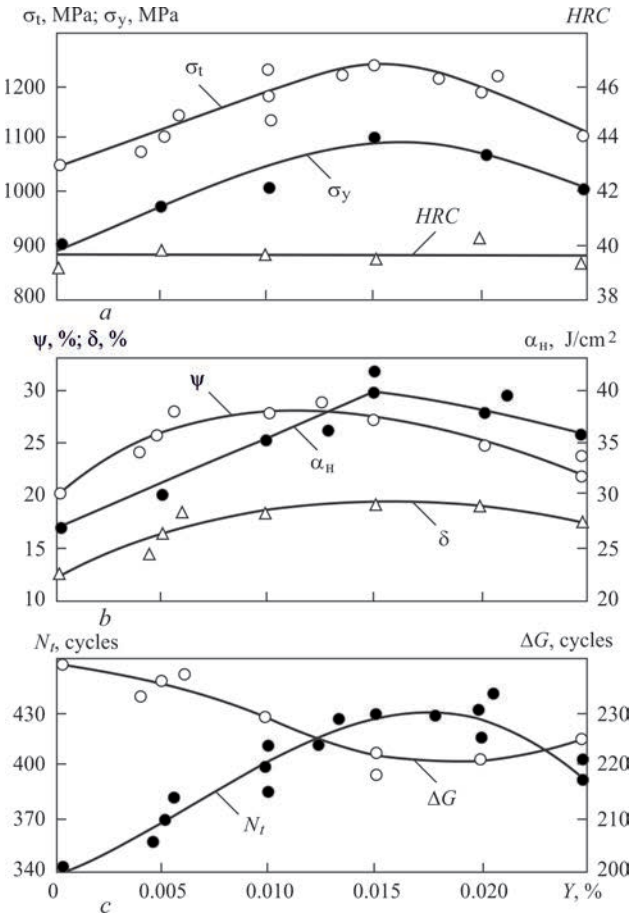

Figure 5. Influence of yttrium on mechanical properties (*a*, *b*), wear resistance Δ*G* and heat resistance *Nt* (*c*) of deposited metal of 15Kh8N2M2F type [17]

Influence of complex modifiers on the deposited metal structure, its mechanical and service properties. Proceeding from the fact that some additives-modifiers refine the structure and block the impurity elements on the intergranular and interphase boundaries, while others inhibit the recrystallization processes and intragranular decomposition, the idea of steel modifying by complex additives looks promising. In combination they can promote formation of a homogeneous structural-phase state, enhancement of the effects from each other, etc.

So, for instance, microalloying of low-alloyed steels of 08G2S, 10G2S type by titanium and zirconium, led to a significant improvement of metal strength and ductility [23]. In works [19, 24] the joint effect of fine powder of titanium and zirconium diborides, and well as cerium dioxide was studied. It was shown [24], that weld microalloying by titanium and boron at multiarc welding using neutral or slightly acidic fluxes improves the structure of metal of the type of low-alloyed steel 10G2FB, resulting in 1.5–2.5 times increase of the steel impact toughness. The optimum content of titani-

um and boron in the weld metal is equal to 0.022–0.038 and 0.0025–0.0065 wt.%, respectively.

In work [11], introducing microadditives (up to 0.2 %) of highly active elements (V, Mo, Zr, B) to the composition of structural steel St. 35 allowed improving the material structure and service properties.

Similarly, by applying an optimum combination of surface-active modifying additives of Ti, Al, B, Ce, Ca and V, at simultaneous alloying of the welds (wire material was 10KhGNM steel, base metal was 33KhSN2MA steel), in work [25] it was possible to achieve a stable crack resistance of welded joints, while ensuring rather high strength of the weld metal. Due to reaching a certain balance between Ti, B, Ni and Mo, in work [26] an increase of the homogeneity of chemical composition of welds and, consequently, improvement of impact toughness of welded joints on low-alloyed steel 08G2S, was achieved.

In work [27] the influence of addition to the charge of flux-cored wire, used as filler wire at plasma surfacing, of a complex master alloy, containing fluorine, alumocalcium, ferrocerium and copper-beryllium alloy, was studied. Beryllium was added to strengthen the steel, and improve its high-temperature mechanical properties. Alumocalcium and ferrocerium were added to remove oxygen, sulphur and phosphorus. Presence of fluorine in the arc, which has a high ionization potential, leads to improvement of the arc self-regulation and increase of the surfacing process stability. As a result, deposited metal of 2Kh13N12GD2Yu type with higher mechanical and service properties was produced, in particular with high resistance to thermocyclic loading.

Influence of modification and microalloying on welding-technological properties of surfacing materials. It is known that one of the ways to improve the stability of melting and transfer of electrode metal in the arc, is application of a process with superposition of additional current pulses of a certain frequency [19]. However, in the case of application of flux-cored wires, controlling the frequency of detachment of electrode metal drop requires ensuring the synchronism of melting of the sheath and the core (filler) that at practical application of pulsed-arc processes is quite successfully applied only when small diameter wires are used.

Another method of influencing the process of electrode wire melting is addition to its charge of modifying microadditives of various elements, the action of which is based on the change of electrophysical characteristics of the welding arc, and of the conditions of heat transfer in the arc gap, respectively. At the same time, technical literature contains practically no data on the influence of modifying additives on such welding-technological properties of surfacing materials as arcing stability, coefficient of alloying element transfer, quality of deposited bead formation and their geometrical dimensions. There are just a few works, devoted to these subjects.

By the data of [18], use of potassium fluorozirconate in the composition of the flux-cored wire charge not only refines the deposited metal structure, but also improves the arc process stability and deposited metal formation. This effect is achieved at the action of surface-active elements, which lower the surface tension force, holding the drop at the electrode tip. In addition, the alkaline element potassium with a low ionization potential enhances the arc burning stability due to lowering the effective ionization potential of the arc gap.

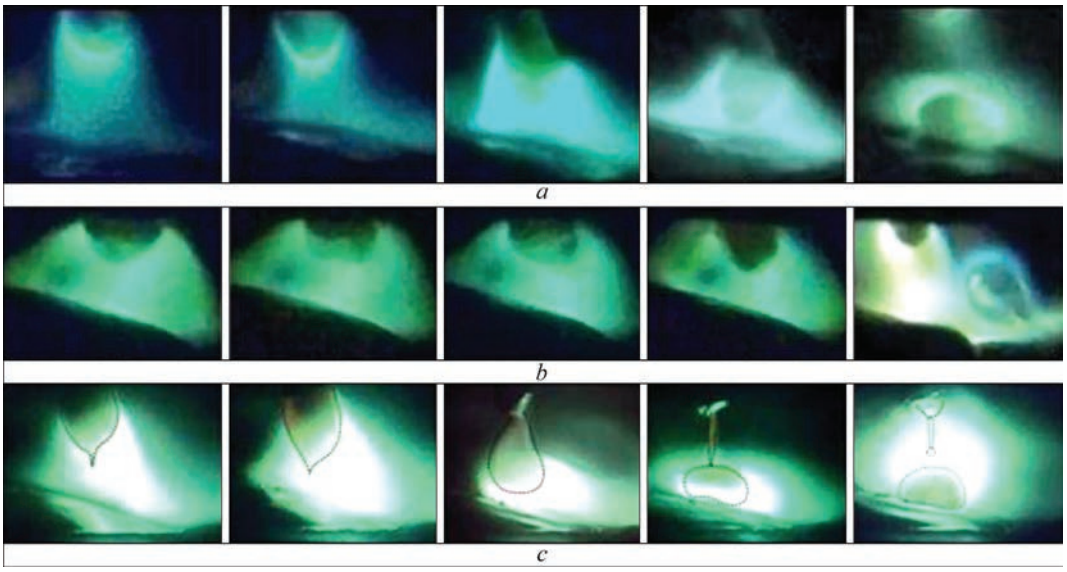

Figure 6. Nature of formation of electrode metal drop at deposition by flux-cored wire, using particles of TiB_2 (*a*), CeO_2 (*b*) and without them (*c*) [19]

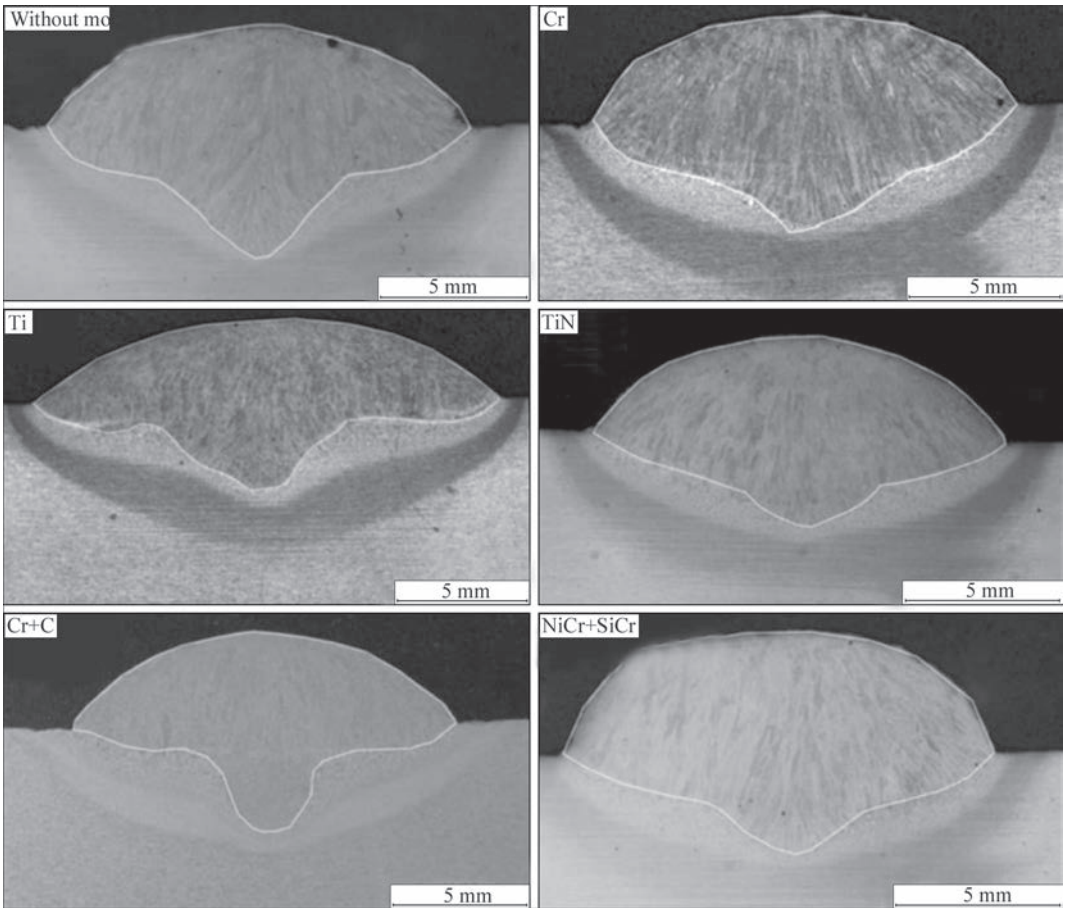

Figure 7. Influence of modifier type on penetration shape and depth at gas-shielded welding with solid wire with a modified coating [28]

In work [19] it was established that introducing into electrode material composition microadditives of titanium and zirconium diborides promotes creation of the conditions, at which the sheath and components of flux-cored wire core, dissimilar by their thermophysical properties, more actively melt and form into a metal drop (Figure 6). It results in reduction of the drop size and increase of their detachment frequency that is accompanied by increase of the periodicity with which the arc anode spot moves between the refractory core end face and metal drop surface. The result of such an influence is improvement of the quality of metal transfer in the welding arc, leading to greater values of the coefficients of alloying element transfer into the deposited metal. It is also noted that at > 0.05 % boron content in the deposited metal, liquation areas with chemical heterogeneity and metal embrittlement were detected.

By the data of [28], the impact on the arc and drop transfer can be applied through thin coatings, deposited on electrode wire surface, which also affects the geometrical dimensions of the deposited beads. The influence of some coatings is shown in Figure 7, from which one can see that the smallest penetration depth was reported for the case of deposition of a pure titanium coating. In this case, a considerable increase of weld metal resistance at cyclic loading was also noted.

CONCLUSIONS

1. As one can see from the results of analyzed studies, modification or microalloying of steels, leading to their grain refinement, redistribution of nonmetallic inclusions, cleaning of grains boundaries, etc., on the whole has a positive effect on the deposited metal mechanical and service properties, in particular, increase of wear- and heat resistance take place.

2. Various compounds of titanium, tungsten, zirconium and boron are the most often used for modification and microalloying of steels and alloys. Here, complex modification by such elements can demonstrate a more significant influence on the steel properties, than use of such elements as monoadditives.

3. From the view point of ensuring a high stability of arc burning, lowering of spattering and improvement of the quality of deposited metal formation, application of zirconium and titanium as modifiers in combination with such elements as potassium, calcium, fluorine, etc., looks promising.

REFERENCES

1. Babinets, A.A., Ryabtsev, I.O. (2021) Classification of methods of modification and microalloying of deposited metal

(Review). *The Paton Welding J.*, **9**, 3–11. DOI: https://doi.org/10.37434/tpwj2021.09.01
2. Zadiranov, A.N., Kats, A.M. (2008) *Theory of crystallization of metals and alloys*. Moscow, MGIU [in Russian].
3. Zubenko, L.N. (2015) Application of modifiers in composition of functional coatings. *Tekhnologii i Materialy*, **2**, 20–23 [in Russian].
4. Antonov, A.A., Artemiev, A.A., Sokolov, G.N. et al. (2016) Argon-arc flux-cored wire surfacing with feed of modifiers to welding pool. *Izv. Volgograd. GTU*, **15**, 102–105 [in Russian].
5. Makarov, A.V., Kudryashov, A.E., Vladimirov, A.A., Titova, A.P. (2019) Application of surfacing materials modified by refractory components for restoration of rollers of billet continuous casting machines. *Vestnik Bryanskogo GTU*, **8**, 41–48 [in Russian].
6. Poletika, I.M., Borisov, M.D., Kozlov, A.V. et al. (2005) Formation of metal structure by electroslag surfacing at alloying of boron and chrome carbides. *Perspektivnye Materialy*, **4**, 78–82 [in Russian].
7. Krivchikov, S.Yu. (2012) Modification by boron of deposited metal of white cast iron type. *The Paton Welding J.*, **6**, 19–21.
8. Maksimov, S.Yu., Machulyak, V.V., Sheremeta, A.V., Goncharenko, E.I. (2014) Investigation of influence of microalloying with titanium and boron of weld metal on its mechanical properties in underwater welding. *Ibid*., **6–7**, 76–79. DOI: https://doi.org/10.15407/tpwj2014.06.15
9. Vashchenko, I.P. (2007) Structure and properties of low-carbon low-alloyed steels. *Vestnik MGTU, 94*, 558–560 [in Russian].
10. Orlov, L.N., Sharapov, M.G., Volynets, V.L. (2010) Influence of microalloying by boron on properties of weld metal in rutile flux-cored wire welding of shipbuilding steels. *Sudostroenie*, **5**, 54–58 [in Russian].
11. Korovin, V.A., Palavin, R.N., Leushin, I.O., Kostromin, S.V. (2011) Microalloying of cast structural steel. *Trudy NGTU*, **2**, 199–207 [in Russian].
12. Litvinenko-Arkov, V.B., Sokolov, G.N., Kyazymov, F.A. (2012) Structure and properties of heat-resistant metal, deposited by flux-cored wires with TiCN nanoparticles. I*zv. Volgograd. GTU*, **9**, 194–197 [in Russian].
13. Sokolov, G.N., Artemiev, A.A., Dubtsov, Yu.N. et al. (2018) Influence of nitrogen and titanium carbonitride particles on structure and properties of metal of Fe–C–Cr–Ni–Mo system. *Omsky Nauchny Vestnik*, **2**, 15–19 [in Russian].
14. Aleshin, N.P., Grigor'ev, M.V., Kobernik, N.V. et al. (2018) Modification of weld metal with tungsten carbide and titanium nitride nanoparticles in twin submerged arc welding. *High Energy Chemistry*, 52(**5**), 440–445.
15. Kuznetsov, V.D., Stepanov, D.V. (2015) Structure and properties of weld metal modified by nanooxides. *The Paton Welding J.*, **11**, 10–16. DOI: https://doi.org/10.15407/tpwj2015.11.01
16. Sokolov, G.N., Lysak, V.I., Troshkov, A.S. et al. (2009) Modification of structure of metal deposited by nanodisperse tungsten carbides. *Fizika i Khimiya Obrabotki Materialov*, **6**, 41–47 [in Russian].
17. Gladky, P.V., Mikaelyan, G.S. (2015) Microalloying and modification of wear-resistant deposited metal. In: *Surfacing. Technologies. Materials. Equipment*. Kiev, PWI, 71–73 [in Russian].
18. Zusin, V.Ya. (2011) Study of modification of metal deposited by flux-cored wire with aluminium sheath. *Vestnik Priazov. GTU. Seriya: Tekhnicheskie Nauki*, **23**, 180–183 [in Russian].
19. Zorin, I.V., Dubtsov, Yu.N., Sokolov, G.N. et al. (2020) Influence of particles of refractory chemical compounds on metal transfer in welding arc during surfacing by composite wire. *Izv. Volgograd. GTU*, **4**, 43–48 [in Russian].
20. Bondareva, O.P., Gonik, I.L. (2009) Influence of microalloying on structure and properties of sparcely-alloyed ferritic-austenitic steel 02Kh22N5. *Ibid*., **11**, 137–140 [in Russian].
21. Stepnov, K.K., Matvienko, V.N., Oldakovsky, A.I. (2011) Modification of medium-chromium deposited metal. *The Paton Welding J.*, **8**, 10–12.
22. Efimenko, N.G. (2002) Modifying, refining and alloying with yttrium in welding of steels. *Ibid*., **6**, 8–12.
23. Pu, J., Yu, Sh., Li, Yu. (2017) Effects of Zr–Ti on the microstructure and properties of flux aided backing submerged arc weld metals. *J. of Alloys and Compounds*, **692**, 351–358.
24. Fejnberg, L.I., Rybakov, A.A., Alimov, A.N., Rosert, R. (2007) Weld microalloying with titanium and boron in multiarc welding of large diameter gas and oil pipes. *The Paton Welding J.*, **5**, 12–16.
25. Kabatsky, V.I., Kabatsky, A.V. (2004) Effect of modifying of weld metal on delayed fracture resistance of high-strength steel welded joints. *Ibid*., **3**, 21–25.
26. Yakovlev, D.S., Shakhmatov, M.V. (2015) Microalloying of welded joints by flux-cored wire. *Tekhnologii i Materialy*, **2**, 23–28 [in Russian].
27. Chigarev, V.V., Kondrashov, K.A., Makarenko, N.A., Granovsky, A.V. (2002) Surfacing material for plasma strengthening and restoration of press moulds. V*estnik Priazov. GTU, Seriya: Tekhnicheskie Nauki*, **12**, 153–156 [in Russian].
28. Wesling, V., Schram, A., Muller, T. (2016) Influencing the arc and the mechanical properties of the weld metal in GMA-welding processes by additive elements on the wire electrode surface. In: *Proc. of 18th Chemnitz Seminar on Materials Engineering, MAR 10–11. IOP Conf. Series-Materials Science and Engineering.*

ORCID
A.A. Babinets: 0000-0003-4432-8879,
I.O. Ryabtsev: 0000-0001-7180-7782

CONFLICT OF INTEREST
The Authors declare no conflict of interest

CORRESPONDING AUTHOR
I.O. Ryabtsev
E.O. Paton Electric Welding Institute of the NASU
11 Kazymyr Malevych Str., 03150, Kyiv, Ukraine
E-mail: ryabtsev39@gmail.com

SUGGESTED CITATION
A.A. Babinets and I.O. Ryabtsev (2021) Influence of modification and microalloying on deposited metal structure and properties (Review). *The Paton Welding J.*, **10**, 3–10.

JOURNAL HOME PAGE
https://pwj.com.ua/en

Received: 15.07.2021
Accepted: 11.11.2021

https://doi.org/10.37434/tpwj2021.10.02

STRUCTURAL INHOMOGENEITY IN WELDED JOINTS OF HEAT-RESISTANT STEELS OF CHROMIUM-MOLYBDENUM-VANADIUM SYSTEM WITH DIFFERENT CHROMIUM CONTENT

M.O. Nimko, V.Yu. Skulskyi, A.R. Gavryk, S.I. Moravetskyi and **I.G. Osypenko**

E.O. Paton Electric Welding Institute of the NASU
11 Kazymyr Malevych Str., 03150, Kyiv, Ukraine

ABSTRACT

Welded joints of dissimilar steels are widely used in different assemblies of the steam-water mixture loop in electric power plants. Difference in alloying by chromium and other carbide-forming elements results in carbon migration from the lower alloyed to the higher alloyed steel in such joints after tempering and in high-temperature service. Decarbonization in the HAZ near-weld zone of the lower alloyed steel can lead to formation of defects and subsequent failures. In this work we studied the influence of the type of 15Kh2M2FBS steel joint (single-pass, multipass), made using electrodes with 9 % Cr, on the nature of formation and development of structural inhomogeneity in the HAZ at high-temperature annealing. It is shown that depending on joint type, development of ferrite interlayer takes place in different zones of the HAZ: in the normalized zone and in the zone of intercritical temperatures A_{C1}–A_{C3} at a distance from the fusion line at single-pass welding; and in the near-weld zone through the HAZ coarse-grained region at multipass welding. Proceeding from the features of decarbonizastion on the surfaces of butt joints and near the fusion line, a scheme was proposed, that allows explaining the nature of development of structural inhomogeneity in the multipass joint of dissimilar steels.

KEY WORDS: carbon diffusion, dissimilar steel joints, heat-affected zone, decarbonized interlayer

The main thermodynamic cycle of thermal power plants used in modern heat power engineering, is the Rankine cycle with steam overheating. To implement this thermal cycle different sections of steam-water loop at the power plant should have different parameters of working medium temperature and pressure. In order to lower the cost of power plant construction, the sections with lower steam parameters are made from low-alloy bainitic steels with 0.5–2.25 % Cr (wall-mounted screen boiler pipes; up to 600 °C temperatures) and martensitic steels with 9–12 % Cr (upper pipe sections of wall-mounted screens of the boiler, headers, main steam lines; up to 625–630 °C temperatures), while sections with higher steam parameters are made from more expensive austenitic steels (superheater coils; up to 660–680 °C) [1]. To realize a closed steam-water loop all these sections are connected to each other by welding, forming a dissimilar steel joints.

In such joints a decarbonized interlayer forms on the side of the lower alloyed steel in high-temperature service, as a result of carbon migration. It is known that chromium and some other carbide-forming elements lower the chemical potential of carbon in steel, thus promoting carbon diffusion from the lower alloyed to the higher alloyed steel [2].

Influence of a decarbonized interlayer on the long-term strength of the joint has been the subject of discussions for many years. Most of the authors believe that the interlayer has a noticeable influence on the mechanical properties [3–6]. In some works, however, no influence of the interlayer on creep fracture was reported [7]. The authors of all the published papers, however, agree in that the decarbonized interlayer has a lower hardness. The main difference in the opinions is related to fracture mode.

It is known from publications that there are two main types of creep damage accumulation processes that pertain to welded joints of low-alloy and high-alloy ferritic steels. One mode prevails at longer fracture time and lower loads, the other is prevalent at shorter time-to-fracture and higher loads. The first process is called cracking of type IV, and it is characterized by damage accumulation and crack initiation in the zone of normalizing temperatures and intercritical temperatures A_{C1}–A_{C3} in the HAZ. The other process is called cracking of IIIa type, and it is characterized by high local stresses and damage accumulation in the decarbonized interlayer in the HAZ near the fusion line [4].

The decarbonized interlayer is harmful for long-term strength of the welded joint not only because of formation of a microstructure, susceptible to microcracking, but also through localization of shear stresses and three-axial loads, in connection with the softness and higher ductility of the interlayer and high strength and lower ductility of the weld metal adjacent to the interlayer on the boundary with the base metal [8]. Dissolution of M_2C, M_7C_3 and $M_{23}C_6$ carbides within this area during the thermal cycle is also noted as an

Copyright © The Author(s)

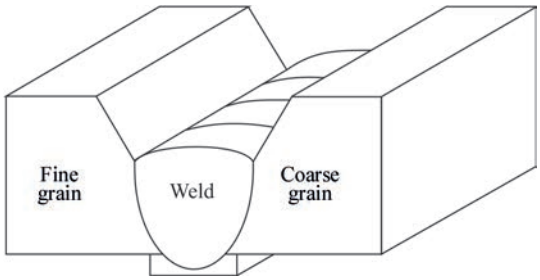

Figure 1. Scheme of welded joint with different grain size

additional factor for early destruction [9, 10]. In work [11] a statistical study on formation of cracks of type IV and IIIa was performed during inspection of power plants in Great Britain. The author came to the conclusion that a significant number of the defects were of IIIa type, and that carbon diffusion from low-alloy steels to high-alloy steels was the main cause for it.

As regards cracks of type IV, their formation is related to softening in the HAZ fine-grained zone and in the incomplete recrystallization zone (of intercritical temperatures A_{C1}–A_{C3}) [12]. One of the phenomena, accompanying the softening in these zones of low-alloy steels, is appearance of white etching interlayer (so-called white interlayer) [13, 14] at tempering and high-temperature service, which is formed by ferrite grains.

The objective of the work was revealing the features of inhomogeneity formation in the joints of dissimilar ferritic steels at tempering and an attempt to connect the phenomenon of formation of a decarbonized interlayer in the HAZ near-weld zone of low-alloy steel in a combined multipass welded joint and of the white etching interlayer in the zone of normalizing and intercritical temperatures A_{C1}–A_{C3}.

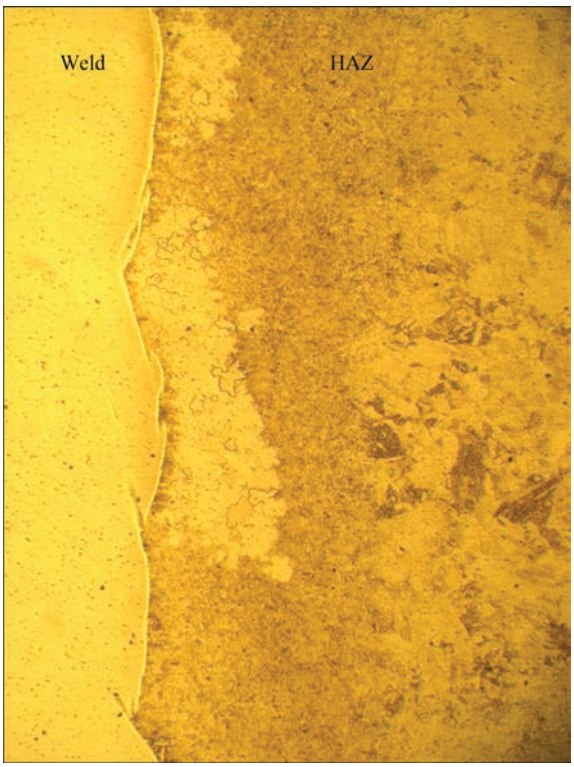

Figure 2. HAZ of multipass welds of P3 steel, welded by 9 % Cr electrodes, after tempering at 750 °C, for 8 h (×25 magnification)

Investigation procedure. Within the framework of microstructural studies of welded joints of 15Kh1M1F steel (reference designation P3; wt.%; 0.115 C; 0.648 Si; 0.67 Mn; 1.95 Cr; 0.16 Ni; 1.12 Mo; 0.32 V; 0.072 Nb; 0.15 Cu) with steels with 9 % Cr, experiments were conducted with the purpose of obtaining the structural inhomogeneity in the HAZ of the lower alloyed steel after high-temperature tempering, using different approaches to welding:

1) multipass welding of P3 steel with R91 steel using Thermanit Chromo 9V electrodes (wt.%): 0.09 C; 0.2 Si; 0.6 Mn; 9.0 Cr; 0.8 Ni; 1.1 Mo; 0.2 V; 0.05 Nb; 0.04 Ni) of 4 mm diameter, I_w = 130–135 A, U_a = = 24 V; preheating and concurrent heating ~200 °C; higher welding speeds were used to produce beads of a small cross-section.

Welding was followed by tempering at 750 °C, for 8 h and 760 °C, for 4 h. Tempering at the temperatures of 750–760 °C was recommended both for R91 steel, Chromo 9V electrodes, and for P3 steel [14];

2) single-pass submerged-arc welding of P3 steel, using wire with 9 % Cr. The sides of the butt joints differed by the size of grains in the microstructure: one side of the butt joint, welded in as-delivered condition, had a fine-grained structure (grain size number G = 9 to DSTU EN ISO 643): the other side of the butt joint was subjected to prior heat treatment at 1200 °C, for 30 min (cooling in air) + 730 °C, for 3 h to obtain a coarse-grained structure (grain size number G = 4 to DSTU EN ISO 643). After that the joint was welded using Thermanit MTS 3 wire (wt.%: 0.1 C; 0.3 Si; 0.5 Mn; 9.0 Cr; 0.7 Ni; 1.0 Mo; 0.2 V) of 2.4 mm diameter with Bohler Marathon 543 flux in the following mode: I_w = = 360–380 A, U_a = 34.4 V; v_w = 20.7 m/h (Figure 1).

For development of structural inhomogeneity welding was followed by tempering at the temperature of 750 °C, for 3 and 18 h.

3) deposition of two beads on PZ steel using Thermanit Chromo 9V electrodes of 3.2 mm diameter, I_w = 115–120 A, U_a = 24 V.

After deposition, tempering was performed at the temperature of 750 °C, for 3 and 18 h.

After welding and surfacing the templates were used to prepare microsections, which where photographed in the optical microscope, and hardness was measured.

In the first experiment, hardness was measured at 5 kg load in the weld and HAZ at the distance of ~0.3, ~0.9 and ~1.4 mm from the fusion line. In the second experiment microhardness with 100 g load was measured for comparison on the joint sides with the fine and coarse grain. In the third experiment microhardness was

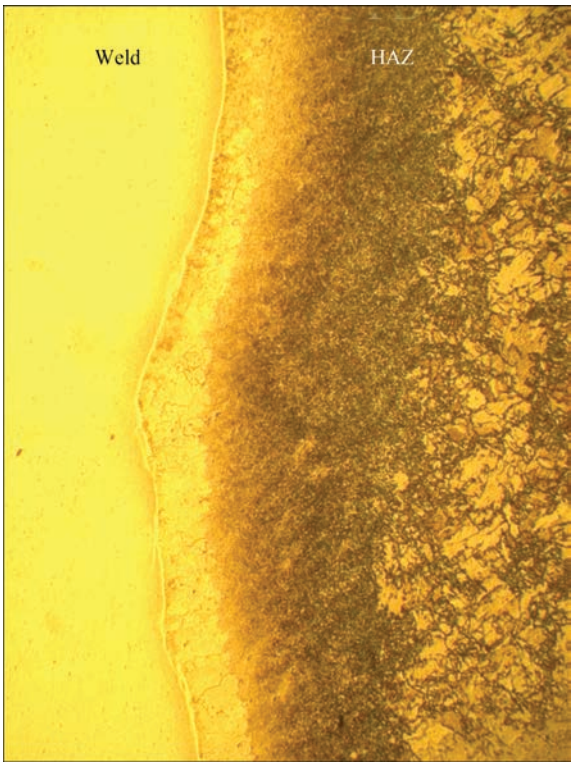

Figure 3. HAZ of multipass joints of P3 steel, welded by 9 % Cr electrodes, after tempering at 760 °C, for 4 h (×25 magnification)

measured with 100 g load, both in the section between the two beads, and under the middle of the second bead.

Experimental results and their analysis. In the first experiment after tempering at 750 °C, for 8 h and 760 °C, for 4 h formation of ferrite zones and ferrite interlayer is observed in the HAZ of P3 steel (Figures 2, 3). These interlayers form nonuniformly, and at a certain distance from the fusion line in some places (Figure 4), so that they cannot be directly related to carbon diffusion through the fusion surface. A characteristic feature of the microstructure in Figure 3 is presence of two interlayers in it: one in immediate vicinity of the fusion line, and the other, less pronounced, at a distance from the fusion line, approximately in the zone of intercritical temperatures A_{C1}–A_{C3}.

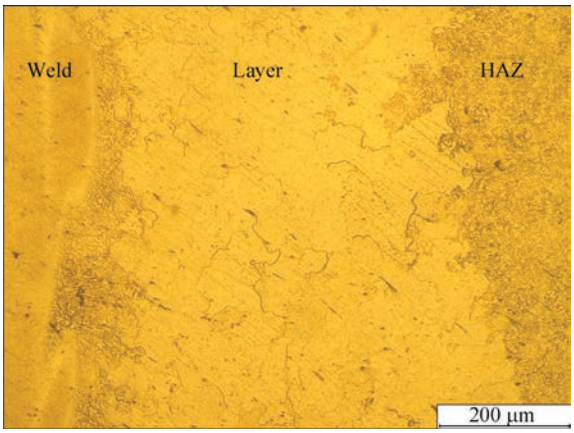

Figure 4. HAZ of multipass joints of P3 steel, welded by 9 % Cr electrodes, after tempering at 750 °C, for 8 h (×160 magnification)

Both the micrographs, and hardness distribution (Figure 5) point to the fact that with temperature rise, the processes of structural inhomogeneity formation and softening in the near-weld zone begin to develop more rapidly in the HAZ of P3 steel.

In the second experiment in the joints of P3 steel with different grain size, a wide ferrite interlayer of a lower hardness (Figure 6) was observed in an area at a distance from the fusion line on the fine grain side after tempering at 750 °C for 18 h, while no such interlayer was found on the coarse grain side. Note that after tempering at 750 °C for 3 h, the interlayer was not observed on the fine grain side, either. The ferrite interlayer forms approximately in the HAZ fine grain zone, and in the zone that is heated during welding in A_{C1}–A_{C3} temperature range. Variation of the interlayer width (it becomes wider on the top and at the bottom of the joint, near the butt surfaces) is attributable to considerable decarbonization of the surface, where the coefficient of carbon diffusion is the highest. Kinetics of ferrite interlayer formation is very well seen on thin single-pass samples after heat treatment (Fig-

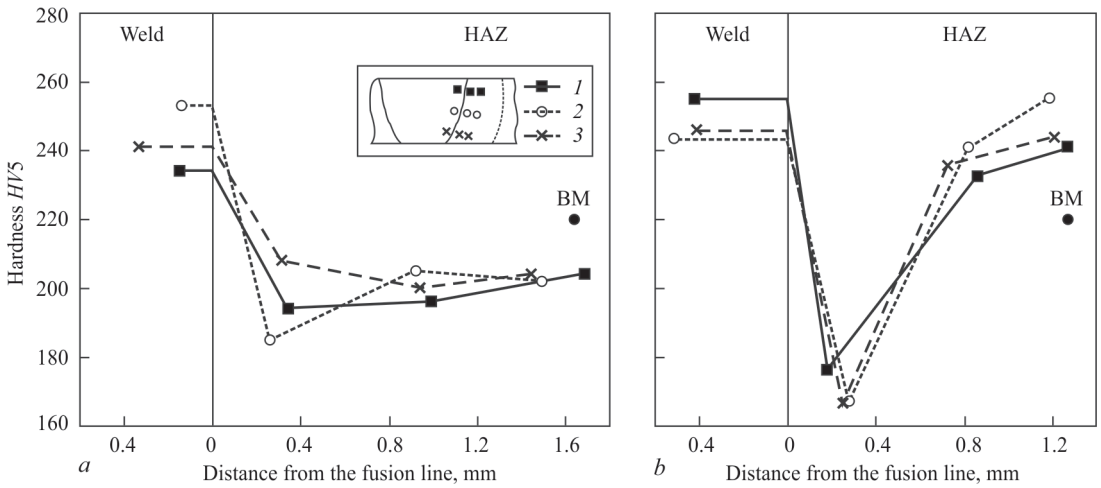

Figure 5. Hardness profile for the HAZ of multipass joints of P3 steel, welded with 9 % Cr electrodes, after tempering at 750 °C, for 8 h (*a*) and 760 °C, for 4 h (*b*)

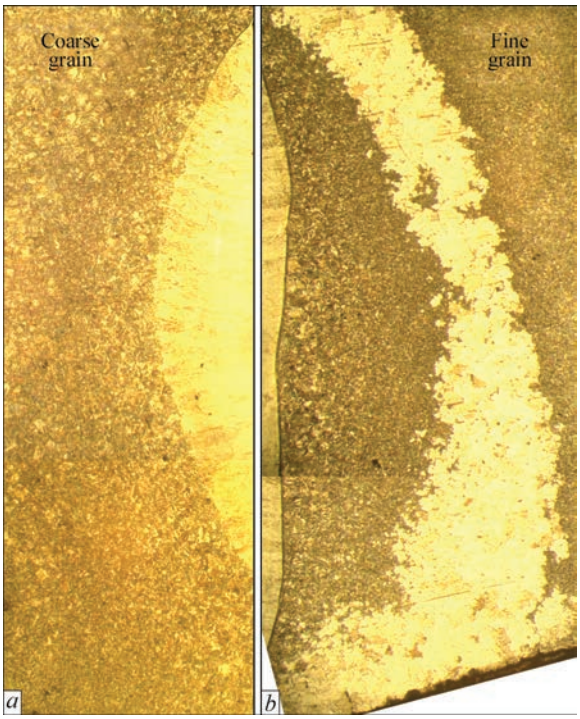

Figure 6. Microstructure of the HAZ of single-pass joint on P3steel with large $G = 4$ (*a*) and small $G = 9$ (*b*) initial grain size after tempering at 750 °C, for 18 h (×25 magnification)

ure 7). It is important to note that even in the case of thin samples decabonization develops exactly along the fine grain zone of normalizing and intercritical temperatures.

Microhardness measurement on both sides of the butt joint also indicates softening in the ferrite interlayer (Figure 8). However, neither the panoramic photo of the microsection, nor the hardness profile demonstrate any noticeable decarbonization or softening in the near-weld zone near the fusion line, as in the case of multipass welding.

The main idea of the third experiment was simulation of the simplest variant of multipass welding, which would enable in each specific case determination of the factors, affecting formation of the ferrite interlayer in the near-weld zone of low-alloy steel HAZ.

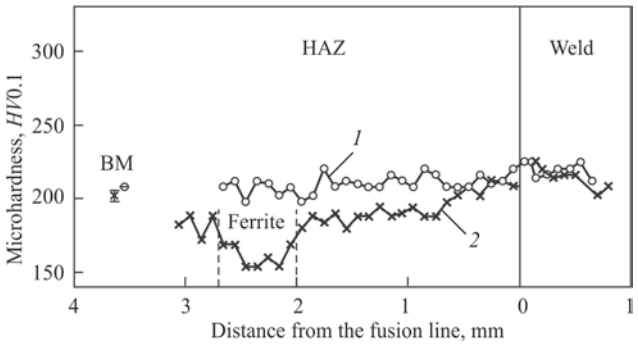

Figure 8. Microhardness measurement in a single-pass joint of P3 steel with different grain size after tempering at 750 °C for 18 h (*1* — coarse grain; *2* — fine grain)

A characteristic feature of the HAZ structure in as-deposited condition is formation of fine-grain structure in the near-weld zone of the first bead that is located approximately in the normalizing zone and the intercritical zone from the second bead.

After soaking for 750 °C for 18 h, a ferrite area develops in this fine-grain zone of the first bead HAZ, formed at the second bead deposition. This area spreads perpendicular to the fusion line of the first bead, to the zone of normalizing and intercritical temperatures of the second bead (Figure 9). Similar results were obtained in work [15], where in a similar experiment decarbonization at tempering also began developing under the first bead through the zone of normalizing and intercritical temperatures from the second bead.

In the HAZ of P3 steel a drop in microhardness is observed in the intercritical temperature zone from the second bead after such a tempering, compared to microhardness under the second bead (Figure 10). Microhardness drop and formation of ferrite areas in the intercritical zone point to development of structural instability of this zone at high-temperature soaking. In other sections of deposition no ferrite areas or other structural inhomogeneities were reported.

These data point to the fact that the mechanism of the process of formation and development of the ferrite interlayer in the near-weld zone of the multi-

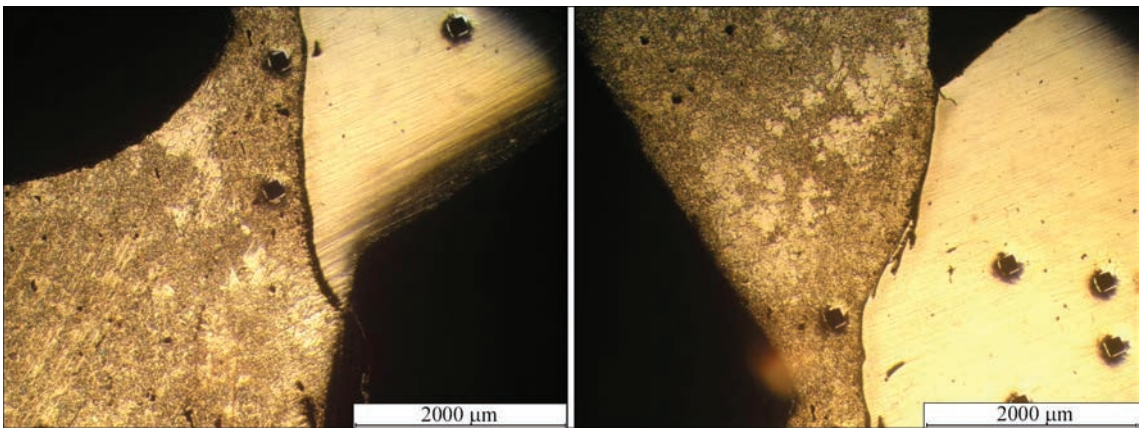

Figure 7. Single-pass joints of 15KH2M2FBS steel, welded with 9 % Cr electrodes, after tempering at 740 °C, for 4 h

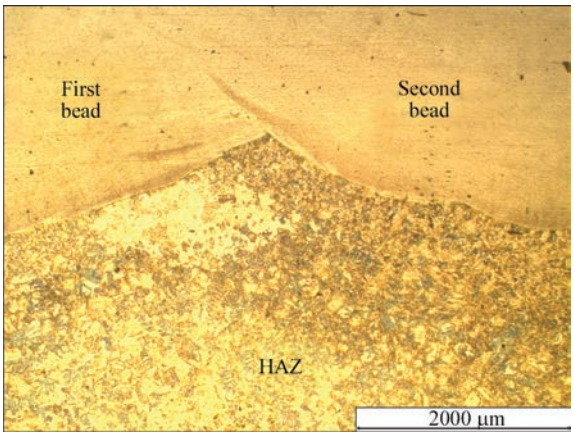

Figure 9. Microstructure of an area between the two beads at surfacing of 15Kh2M2FBS steel by 9 % Cr electrodes, after tempering at 750 °C, for 18 h (×25 magnification)

pass joint is similar to the process of formation and development of the white etching interlayer in the single-pass welded joint:

- in single-pass welded joint the role of diffusion intensifier was taken by the butt joint surfaces, which have a greater coefficient of diffusion, and where intensive decarbonization occurs (as a result of oxidation in the furnace atmosphere), whereas decarbonization developed in the fine-grain zone of normalizing and intercritical temperatures A_{C1}–A_{C3} at a distance from the weld (Figures 6, 7);
- in a multipass welded joint the surface of fusion with the higher alloyed weld with a smaller chemical potential for carbon penetration, has the role of diffusion intensifier, while decarbonization developed in the fine-grain zone of normalizing and intercritical temperatures A_{C1}–A_{C3} from the next beads, gradually covering the entire near-weld zone of the HAZ (Figure 11). Decarbonization can additionally develop in the vicinity of the intercritical zone at a distance from the weld (Figure 3).

This mechanism accounts for formation and development of ferrite areas near the fusion line in a multipass welded joint of R91+PZ steels. As was shown earlier, these ferrite areas in many places move away from the fusion line and develop in a less fine-grain zone at a slightly greater distance from the fusion line, making it impossible to explain this phenomenon by just the mechanism of direct diffusion from the near-weld zone into the weld. At multipass welding a complex superposition of the fields of temperature distribution from each of the beads develops in the near-weld zone of the low-alloy steel HAZ, both of those, which are directly superimposed on the base metal, and those, located in the second-third layer in-depth of the weld (Figure 11). This may result in development of a distribution of finer and coarser grains in the near-weld zone. The structure with the coarser grains has a smaller area of the grain boundaries per a unit of volume. However, diffusion along the high-angle grain boundaries with their less densely-packed structure has the most important role at the temperatures of high-temperature tempering (up to the temperature of $0.6T_m$), compared to diffusion over dislocations and through the crystalline lattice [16]; in most cases the following ratio of the values of the coefficients of diffusion is realized in the metal volume:

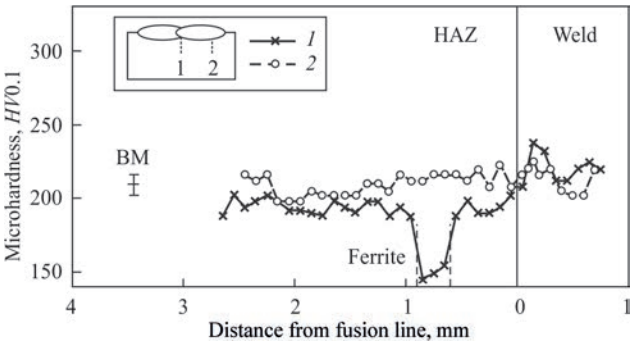

Figure 10. Microhardness measurement in a bead on 15Kh2M-2FBS steel, deposited by 9 % Cr electrodes, after tempering at 750 °C, for 18 h

$$D_{\text{lattice}} << D_{\text{dislocation}} \leq D_{\text{grain boundaries}} \leq D_{\text{surface}},$$

Therefore, reduction of the boundary area leads to lowering of the rate of carbon diffusion, and to lowering of the rate of decarbonized interlayer development, respectively, and vice versa.

This is exactly why the coarse-grain area in the near-weld zone directly at the fusion line in a multipass welded joint (Figure 4) has higher resistance to formation of structural inhomogeneity, unlike the normalizing zone, removed from the fusion line, through which the structural inhomogeneity develops (Figure 11). The same resistance to development of a «white interlayer» is demonstrated also by the side of the butt joint with initially coarse grain in the second experiment (Figure 6,

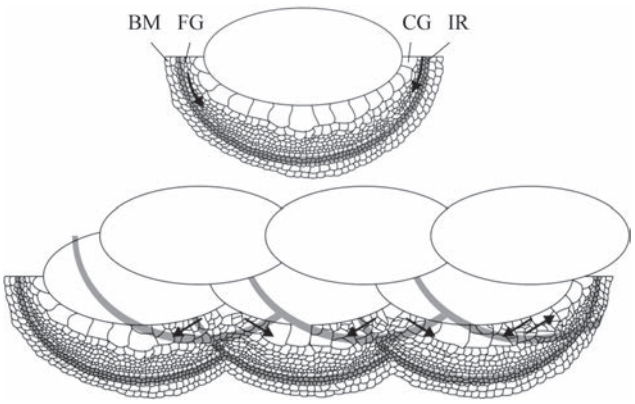

Figure 11. Superposition of intercritical zones in a multipass deposits and its comparison with a single-pass deposit: CG — coarse-grain HAZ; FG — fine-grain HAZ; IR — incomplete recrystallization zone (grey bands); BM — base metal; arrows show the direction of spreading of the decarbonized interlayer

a), in which the white etching interlayer does not develop even after tempering at 750 °C for 18 h.

These results allow noting the important role of the size of the grains in the processes of ferrite interlayer formation. It is envisaged that in the zones of normalizing and intercritical temperatures carbon fluctuation develops at high-temperature soaking, as a result of nonuniform distribution of carbon concentration in steel, fine grain sizes and high diffusion rates, respectively, and presence of surfaces with a higher coefficient of diffusion and lower chemical potential, leading to critical decarbonization and ferrite grain formation in some areas.

Additional factors, which may affect strength lowering in the incomplete recrystallization zone are [17]: 1) lath martensite transformation into subgrains with a low density of dislocations; 2) coagulation and coalescence of carbides (in particular, $M_{23}C_6$). Plastic deformation of the zone during tempering is mentioned as another reason for recrystallization and further growth of α-grains [13].

Figure 11 shows one of the examples of superposition of the temperature fields from the next beads. However, depending on the bead location and their orientation, a different distribution of the coarse and fine grains can form in the near-weld zone that may lead to another profile of decarbonization development in this zone.

Experimental results show that the white etching interlayer at a distance from the weld and the decarbonized interlayer in the HAZ near-weld zone of low-alloy steels, which develop in combined welded joints of dissimilar steels at tempering and in high-temperature service, can have the same mechanism of formation and propagation, and accordingly, the damages of IIIa and IV types in low-alloy steels operating in dissimilar steel joints at high temperatures can have the same initial cause: this is the influence of the thermal cycle of welding in the range of normalizing and incomplete recrystallization temperatures.

The main task, arising as a result of the study, is determination of the optimum geometrical configuration of surfacing or welding, at which the zones of normalizing and intercritical temperatures from the next beads at multipass welding will have the smallest specific length along the fusion line. For instance, in the case of deposition on surfaces of the same width, a compromise arises between making a smaller number of wider beads in the modes with a higher heat input that also have wider zones of normalizing and intercritical temperatures, and making a greater number of narrower beads, having narrower zones of normalizing and intercritical temperatures. It is assumed that in the first case wider individual ferrite accumulations will form (Figure 3), and in the second case a more uniform narrower interlayer will appear (Figure 4).

CONCLUSIONS

1. It is shown that zones with different decarbonization kinetics are observed in multipass welded joints of dissimilar ferritic steels after tempering, which was determined by the degree of microstructure etchability.

2. It was found that formation of white etching interlayer in the zone of normalizing and intercritical temperatures in the HAZ of pearlitic steels can depend on base metal grain size: the susceptibility to formation of a «white interlayer» in the incomplete recrystallization zone decreases with increase of the grain size.

3. It is shown that intensification of white etching interlayer formation can take place on the open surfaces of the butt joints.

4. It is also shown that at multipass welding of dissimilar steels intensification of formation of a decarbonized interlayer in the near-weld zone of the HAZ of lower alloyed steel occurs in the zones of normalizing and intercritical temperatures in the HAZ from the next beads.

5. It is noted that the phenomenon of development of a decarbonized interlayer near the fusion line can have a similar formation and propagation mechanism to that of the phenomenon of white etching interlayer formation in the zone of normalizing and intercritical temperatures.

REFERENCES

1. Di Gianfrancesco, A. (2017) *Materials for ultra-supercritical and advanced ultra-supercritical power plants*. Woodhead Publ.
2. DuPont, J.N. (2012) Microstructural evolution and high temperature failure of ferritic to austenitic dissimilar welds. *Int. Materials Reviews*, 57(**4**), 208–234.
3. Gotalsky, Yu.N. (1981) *Welding of dissimilar steels*. Kiev, Tekhnika [in Russian].
4. Helander, T., Andersson, H. C. M., Oskarsson, M. (2000) Structural changes in 12–2.25 % Cr weldments — an experimental and theoretical approach. *Materials at High Temperatures*, 17(**3**), 389–396.
5. Zhao, Y., Gong, J., Wang, X. et al. (2015) Carbon diffusion in dissimilar joints between P91 and 12Cr1MoV steels welded by different consumables at high temperature. *Ibid.*, 32(**6**), 557–565.
6. Khromchenko, F.A. (2010) *Peculiarities and causes of damages of pipeline welded joints (Background materials)*. Moscow, STC Energoprogress [in Russian].
7. Jandová, D., Kasl, J., Kanta, V. (2006) Creep resistance of similar and dissimilar weld joints of P91 steel. *Materials at High Temperatures*, 23(**3–4**), 165–170.
8. Mayr, P., Schlacher, C., Siefert, J. A., Parker, J. D. (2018) Microstructural features, mechanical properties and high temperature failures of ferritic to ferritic dissimilar welds. *Int. Materials Reviews*, 64(**1**), 1–26.
9. Dawson, K. E., Tatlock, G. J., Chi, K., Barnard, P. (2013) Changes in precipitate distributions and the microstructural evolution of P24/P91 dissimilar metal welds during PWHT. *Metallurgical and Materials Transact. A*, **44**, 5065–5080.
10. Laha, K., Chandravathi, K.S., Bhanu Sankara Rao, K. et al. (2001) An assessment of creep deformation and fracture

behavior of 2.25Cr–1Mo similar and dissimilar weld joints. *Ibid.*, **32**, 115–124.
11. Brett, S.J. (2004) Type IIIa cracking in 1/2CrMoV steam pipework systems. *Sci. and Technol. of Welding and Joining*, 9(**1**), 41–45.
12. Cerjak, H., Mayr, P. (2008) *Creep strength of welded joints of ferritic steels.* In: *Creep-resistant steels.* Ed. by F. Abe, T.-U. Kern, R. Viswanathan. Woodhead Publ.
13. Hrivnak, I., Malinovska, E., Mosny, Ya. (1983) To problem of formation of «white layer» in narrow-gap submerged arc welding. *VUZ*, XIX, **1**.
14. German, S.I. (1972) *Electric arc welding of heat-resistant steels of pearlite class.* Moscow, Mashinostroenie [in Russian].
15. Lundin, C.D., Khan, K.K., Yang, D. (1995) Effect of carbon migration in Cr–Mo weldments on metallurgical structure and mechanical properties. *Welding Research Council Bulletin,* **407**, 1–49.
16. Mehrer, H. (2007) *Diffusion in Solids. Fundamentals, Methods, Materials, Diffusion-Controlled Processes*. Springer-Verlag.
17. Laha, K., Chandravathi, K.S., Parameswaran, P. et al. (2007) Characterization of microstructures across the heat-affected zone of the modified 9Cr–1Mo weld joint to understand its role in promoting type IV cracking. *Metallurgical and Materials Transact. A*, **38**, 58–67.

ORCID
M.O. Nimko: 0000-0002-9672-4921,
V.Yu. Skulskyi: 0000-0002-4766-5355

CONFLICT OF INTEREST
The Authors declare no conflict of interest

CORRESPONDING AUTHOR
V.Yu. Skulskyi
E.O. Paton Electric Welding Institute of the NASU
11 Kazymyr Malevych Str., 03150, Kyiv, Ukraine
E-mail: vsku@paton.kiev.ua

SUGGESTED CITATION
M.O. Nimko, V.Yu. Skulskyi, A.R. Gavryk, S.I. Moravetskyi and I.G. Osypenko (2021) Structural inhomogeneity in welded joints of heat-resistant steels of chromium-molybdenum-vanadium system with different chromium content. *The Paton Welding J.*, **10**, 11–17.

JOURNAL HOME PAGE
https://pwj.com.ua/en

Received 22.07.2021
Accepted: 11.11.2021

https://doi.org/10.37434/tpwj2021.10.03

CORROSION-MECHANICAL RESISTANCE OF 2219 ALLOY WELDED JOINTS UNDER SIMULATED SERVICE CONDITIONS*

L.I. Nyrkova[1], **T.M. Labur**[1], **E.I. Shevtsov**[2], **O.P. Nazarenko**[2] and **A.V. Dorofeev**[2]

[1]E.O. Paton Electric Welding Institute of the NASU
11 Kazymyr Malevych Str., 03150, Kyiv, Ukraine
[2]SC «DB Pivdenne»
3 Kryvorizzka Str., 49008, Dnipro, Ukraine

ABSTRACT

We studied the corrosion resistance, including local corrosion resistance, of welded joints of aluminium 2219 alloy, made by nonconsumable electrode single-pass welding along (L) and across (T) the rolled metal heat-treated to the T81 condition. It is shown that resistance of welded joints of 2219 alloy to general and local corrosion in amyl and its vapors does not depend on the direction of workpieces during welding. An increase in ductility and strength values of welded joint specimens was found after soaking them in amyl and amyl vapors. The coefficient of welded joints strength after soaking in amyl rises from 0.65 up to 0.67 in the longitudinal direction, and from 0.64 to 0.66 in the transverse direction. After soaking in amyl vapors, the strength properties of the welded joint almost do not change: strength coefficient was the same in both orientation directions and it was equal to 0.64. Fracture ran along the fusion line of the weld with the base metal, where melting of grain boundaries and their thickening take place during the thermal cycle of welding at crystallization, as well as decomposition of copper over saturated solid solution in aluminium, which is accompanied by precipitation and coagulation of the strengthening phases.

KEY WORDS: 2219 aluminium alloy, welded joints, heat treatment, corrosion resistance, mechanical properties, microstructure, mechanical fracture at tension

Aluminium structural 2219-T31 alloy (USA) belongs to the grade of thermally strengthened alloys of Al–Cu–Mn alloying system, which have a high specific heat capacity. Ultimate strength of wrought heat-treated aluminium alloys can reach 500 MPa and higher at a density lower than 2850 kg/m^3 [1–3]. It belongs to the most used structural materials, in particular, for the manufacture of fuel tanks in various systems of carrier rockets (Saturn V, Apollo, Space Shuttle, etc.).

The specific strength of alloys has high values and is close to the specific strength of high-strength steels. When the temperature decreases, the mechanical properties are not deteriorated and so they are used in a wide temperature range from –250 to +200 °C (at the condition of short-term heating to 250–300 °C). Therefore, the alloy is often used in the structures of cylinders and tanks in which liquid gases are stored. In addition, the alloy is also characterized by technological ductility in the cold and hot state at a high level of corrosion resistance of the metal, which distinguishes this alloy among other structural aluminium alloys [4]. It has a unique combination of physicomechanical and technological properties [1–17]. Its weldability and high strength under cryogenic temperatures are especially valued. Such structures require high ductility in cold and hot states at a high level of corrosion resistance.

2219-T31 alloy belongs to the group of structural materials and to the dispersion-hardened alloys. This alloy contains almost 6 % of copper, and its hardening characteristics are similar to the two-component Al-Cu alloy. The structure of the alloy consists of a solid solution and several phase inclusions: $\Theta'(A1_2Cu)$, $T(Al_{12}Mn_2Cu)$, $A1_3Zr$, $Al_{11}V$, etc., whose presence in the alloy provides a good combination of strength and ductility [18]. Numerous scientific studies indicate the influence of technological conditions of heating, under the action of which structural transformations occur, reduces the indices of mechanical and corrosion properties [1–16]. The degree of their reduction is influenced by the sizes and shape of crystallites and grains of the metal in the heat-affected-zone, the morphology of the distribution of structural components and their number in the volume of the metal. Moreover, the previous deformation has a significant effect, which enhances the action of the mechanism of precipitation of a metastable phase $\Theta'(Al_2Cu)$ and causes the appearance of a stable phase Θ, which initiates the formation of a crack during fracture [14].

*In the work participated: S.O. Osadchuk, M.R. Yavorska, A.G. Poklyatskyi, V.E. Fedorchuk.

Copyright © The Author(s)

Typically, structures of aluminium 2219 alloy, which operate under pressure, are subjected to heat treatment after welding or used in the state of delivery [1]. During heat treatment, various modes are used, including T81 (ageing of workpieces at 177 °C for 18 h in the T4 condition), as well as T87 (ageing of workpieces, heat treated with subsequent deformation of 8 % until the T37 condition, at 163 °C for 24 h).

At the same time, the alloy is very sensitive to temperature effect during welding.Therefore, during melting and crystallization of welds a significant softening of the base material in the HAZ occurs [5, 6]. The morphology of weld microstructure is determined by the temperature gradient on the surface of the distribution of the solid solution of liquid metal and phases, the value of the crystallization rate, as well as the nature of the distribution of alloying elements over the volume of the weld metal. Overheating of the metal causes a decrease in its strength in the HAZ and formation of an inhomogeneous structure as a result of segregation of alloying elements and impurities along the boundaries of crystallites and grains [7–12]. In addition, between the grains brittle interlayers of supersaturated phases appear, especially at the fusion boundary with the base metal, where the interlayers form a dense framework around the grains [14, 15].

Methods of experiments. In the work the aluminium 2219-T31 alloy of the alloying system Al–Cu with a thickness of 3 mm was investigated. The analysis of the chemical composition was performed spectrally in a spectrometer «Spectrovak-1000» of Baird Company. The obtained results were compared with the chemical composition of the alloy given in AMS-QQ-A-250/30A [17] (Table 1). It was found that as to the content of the basic alloying elements and impurities (except for vanadium, the content of which was not determined), the specimen of the investigated semi-finished workpieces of the aluminium alloy meets the requirements of the standard AMS-QQ-A-250/30A.

The plates of 2219-T31 alloy with a size of 300×150×3 mm, cut out along and across to the rolled metal direction were welded. Before welding, the workpieces of the alloy were treated in 10 % NaOH solution and clarified in 30 % HNO_3 solution. Welding of workpieces was performed in a flat position with a nonconsumable tungsten electrode with a lanthanum coating using filler wire of grade 2319 of a diameter 1.6 mm on the conditions: I_w = 280 A, v_w = 20 m/h, filler wire feed rate is 117 m/h. The power source — MW-450 of Fronius Company, an alternating current with a rectangular waveform of 200 Hz frequency was used. The fusion zone was protected with argon. A full penetration of welded edges in a one pass and the formation of the penetration (root) was achieved in the presence of a removable stainless steel backing with a rectangular groove of 4 mm width and 1 mm depth, which allowed obtaining a high-quality formation of butt joints with appropriate technological reinforcement.

The quality of weld formation of butt joints of 2219-T31 alloy was evaluated visually and using radiography method (GOST 7512 [18]) in the RAP-150/300 installation. The density of the weld metal was tested in the DP-30 densitometer.

To measure geometric parameters of the welds, an electronic caliper of grade ART-34460-150 with a graduation mark of 0.01 mm was used.

The specimens for mechanical and corrosion tests were made from welded billets in accordance with the relevant standard documents. The specimens of welded joints were heat treated to the T81 condition (artificial ageing) on the mode: $T = 180 \pm 5$ °C during 18 h.

Corrosion tests were performed in amyl and amyl vapors at a temperature of 50 °C continuously during 45 days on the base of the testing laboratory of the DB «Pivdenne». Then, the corrosion resistance (general corrosion rate, resistance to MCC, exfoliating corrosion and corrosion cracking) as well as mechanical properties were evaluated. Evaluation of the resistance of the base metal specimens to continuous corrosion was performed by the massometry method in accordance with GOST 9.908 [19]. The rate of weight loss of the specimens was determined by the change in their mass and duration of corrosion studies by the formula:

$$K = \frac{\Delta m}{ST}, \quad (1)$$

where $\Delta m = m_1 - m_2$ are corrosion losses of the specimen, g; m_1 is the mass of the specimen before the tests, g; m_2 is the mass of the specimen after the corro-

Table 1. Results of analysis of chemical composition of specimen of 2219-T31 alloy with a thickness of 3 mm

Reference specimen, or standard requirements	Mass fraction of elements, %									
	Cu	Mn	Zr	V	Ti	Fe	Si	Zn	Mg	Other elements: each one/in general
Specimen	6.7	0.34	0.18	–	0.05	0.16	0.09	0.03	0.02	0.01 (Ni)
AMS-QQ-A-250/30A	5.8–6.8	0.20–0.40	0.10–0.25	0.05–0.15	0.02–0.10	≤0.30	≤0.20	≤0.10	≤0.02	≤0.05/≤0.15

sion tests; S is the surface area of the specimen, m^2; T is the duration of investigations, h.

The corrosion rate was calculated by the formula:

$$\Pi = \frac{8760K}{d}, \quad (2)$$

where K is the corrosion rate, g/(m²·h); d is the metal density, g/cm³; 8760 is the number of hours per year.

The density of aluminium alloys is 2.7 g/cm³, which was taken into account during calculation.

The evaluation of resistance to exfoliating corrosion was carried out on the specimens of the base metal and welded joints according to GOST 9.904 [20]. While evaluating the condition of the experimental specimens, the change of colour, presence of ulcers and exfoliations on the working surfaces of the specimens and cracks on the ends were noted. The following symbols were taken. The letter «A» indicates the surface, on which marking is applied, and for the welded joints it indicates the surface with a facial weld, B indicates the back surface and for the welded joints it means the surface with penetration; *1*, *2* — ends of the sides with the length of 60 mm (80 mm for welded joints), *3*, *4* — ends of sides with the length of 40 mm (25 mm — for welded joints).

The evaluation of resistance of the alloy to MCC was carried out by a metallographic method at a magnification ×(100–200) according to GOST 9.021 [21] on the specimens of welded joints, all structural zones of the welded joint were evaluated, namely: base metal, heat-affected-zone and weld.

The tests of resistance to corrosion cracking were carried out on rectangular specimens with the size of 150.0×25.0×3.0 mm. The specimens were loaded according to a four-point bending scheme according to GOST 9.901.2 (method 4), the level of continuous deformation was agreed with the SE DB «Pivdenne» and amounted to 957 kgf/cm². The presence (absence) of cracks was revealed visually by means of a magnification glass.

The determination and evaluation of mechanical properties was performed on the plane specimens with technological reinforcement on the facial and back surfaces of the weld. Mechanical tests were carried out in accordance with GOST 1497 [22] in the Instron-1126 machine at a speed of traverses movement of 6 mm/min until fracture. To monitor the indice of relative elongation of the specimens, an extensometer No.G-51-12-M-A was used. During the tests with the help of a personal computer, the values of load and deformation were continuously recorded, according to the results of which, yield strength, ultimate tensie stength and relative elongation were calculated.

Metallographic analysis of the base metal and welded joints before and after corrosion tests was performed by means of a microscope MMT-1600V. The studies were conducted on the sections cut out from the butt joints, welded along (L) and across (T) the rolled sheet semifinished product. The microstructure was detected by etching in the solution of such composition: chloric acid — 1000 cm³ + ice acetic acid — 75 cm³.

Results and their discussion. *Geometric parameters of welds.* After welding butts, geometric parameters of produced welds were determined (B is the width of a weld from a facial surface of joints, H is the width of a weld from a back surface of joints (weld root); δ is the penetration depth of the base metal (in this case it is equal to its thickness); b is the height of convexes of technological reinforcement, h is the height of weld root). According to the results of measurements, the width of welds in the joints of 2219-T31 alloy cut out along the rolled metal, amounts from 9.56 to 9.72 mm, and across the rolled metal it is from 9.47 to 9.65 mm. The weld factor according to the formula $K = B/(b + \delta)$ for the joints welded along and across the rolled metal by nonconsumable electrode, is equal to 2.13 and 2.03, respectively.

Investigation of resistance to general and local corrosion. After the tests, a nonuniform darkening of surface of the specimens (Figure 1) and formation of corrosion spots of various sizes from 20 to 40 % was observed. After the contact with amyl vapors, darkening of the surface was also nonuniform, the area of corrosion spots amounted from 10 to 20 %. The spots are characterized by a change in colour of the surface layer (darkening) and a small depth of damage.

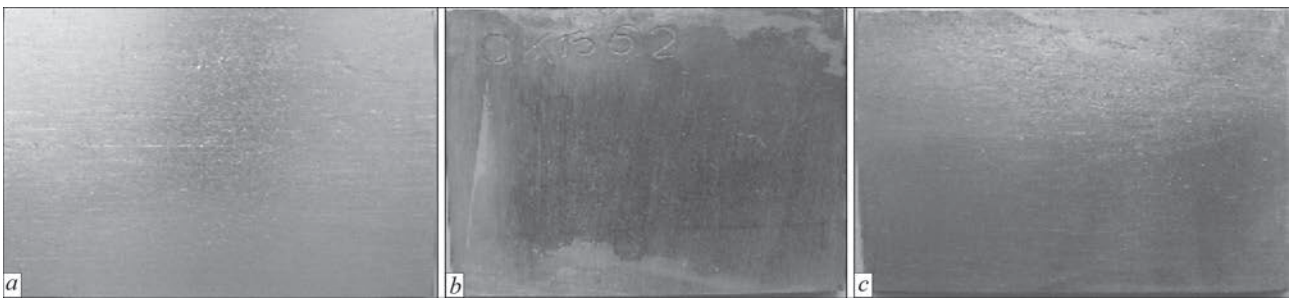

Figure 1. Appearance of base metal surface of aluminium 2219 alloy, heat-treated to the T81 condition, before (*a*) and after tests in amyl (*b*) and amyl vapors (*c*)

Table 2. Results of evaluation of resistance to exfoliating corrosion of base metal specimens of 2219-T31 alloy and welded joints produced along (L) and across (T) the rolled metal, as well as heat-treated to the T81 condition, after staying in amyl and its vapors

Marking	Rolled metal direction	Corrosion test conditions	Indice description										
			Nature of change in the appearance of specimens		Largest diameter of exfoliating, mm		Exfoliating area on each surface, %		Total length of ends with cracks, mm				Resistance to exfoliating corrosion according to GOST 9.904, point
			A	B	A	B	A	B	1	2	3	4	
Base metal	L	Amyl	Slight darkening		0	0	0	0	0	0	0	0	2
		Amyl vapors	Change of color by spots. Slight darkening. Spots with temper colors		0	0	0	0	0	0	0	0	2
		Ref.	Without changes		0	0	0	0	0	0	0	0	1
Welded joint	L	Amyl	Slight darkening. Spots with temper colors		0	0	0	0	0	0	0	0	2
		Amyl vapors	Slight darkening		0	0	0	0	0	0	0	0	2
		Ref.	Without changes		0	0	0	0	0	0	0	0	1
Base metal	T	Amyl	Slight darkening. Spots with temper colors		0	0	0	0	0	0	0	0	2
		Amyl vapors	Same		0	0	0	0	0	0	0	0	2
		Ref.	Without changes		0	0	0	0	0	0	0	0	1
PCK.11.81	T	Amyl	Slight darkening		0	0	0	0	0	0	0	0	2
PCK.13.81		Amyl vapors	Same		0	0	0	0	0	0	0	0	2
PCK.15.81		Ref.	Without changes		0	0	0	0	0	0	0	0	1

After removing the corrosion products, the surfaces are brilliant, local corrosion damages of the surface were not detected. According to the results of visual examination, after the tests in amyl environment (liquid and vapors), corrosion of aluminium 2219 alloy was identified according to GOST 9.908 as a continuous nonuniform, type of damages — corrosion spots. High-speed indices of continuous corrosion of the specimens of the base metal of aluminium 2219 alloy in the T81 condition, determined in accordance with GOST 9.908, are the following: weight loss rate in amyl is 0.00111 g/(m^2·h), in amyl vapors they are 0.00346 g/(m^2·h); linear rate of corrosion in amyl is 0.00362 mm/year, in amyl vapors it is 0.01120 mm/year.

Thus, to some extent amyl vapors are more corrosion-aggressive relative to the aluminium 2219 alloy as compared to liquid amyl: the rate of corrosion in the amyl vapors grows by 3.1 times as compared to amyl. According to a ten-point scale of corrosion resistance according to GOST 9.502 [23], the resistance of aluminium 2219 alloy, heat-treated to the T81 condition, in amyl is evaluated by a point 2, in amyl vapors it has a point 4, which corresponds to the group of metal resistance «highly resistant» and «resistant», respectively.

According to the evaluation results, it was found (Table 2) that resistance of the base metal of 2219 alloy to the exfoliating corrosion after the tests in amyl and its vapors and welded joints along (L) and across (T) the rolled metal, heat-treated to the T81 condition, corresponds to the point 2 according to GOST 9.904.

Thus, ressitance of welded joints of the base metal to exfoliating corrosion in amyl and its vapors does not affect the direction of a rolled semifinished product and the thermal cycle of welding.

After the corrosion tests in amyl and its vapors, the fracture of welded joints of 2219 alloy along the grain boundaries was not detected, and these joints are resistant to intercrystalline corrosion in accordance with GOST 9.021. Their resistance is not affected by the direction of rolled metal and thermal cycle of welding. The specimens of welded joints of 2219 alloy along (L) and across (T) the rolled metal in the T81 condition are resistant also to corrosion cracking in amyl and its vapors.

The welded joints of 2219 alloy along (L) and across (T) the rolled metal in the T81 condition are resistant to intercrystalline corrosion and corrosion cracking in amyl and its vapors. Resistance to exfoliating corrosion is evaluated by the point 2, the rate of corrosion of the base metal in amyl is 00362 mm/year, in vapors it is 0.01120 mm/year. Their resistance is not affected by the direction of rolled metal and thermal cycle of welding.

Examination of microstructure. Metallographic analysis of the microstructure of the base metal of 2219-T31 alloy showed that its morphology consists of α-phase enriched with aluminium (solid solution) and a stable θ($CuAl_2$)-phase. To the intermediate phases θ′($CuAl_2$) and S′(Al_2CuMg) belong. The main alloying elements are copper and manganese. The presence of

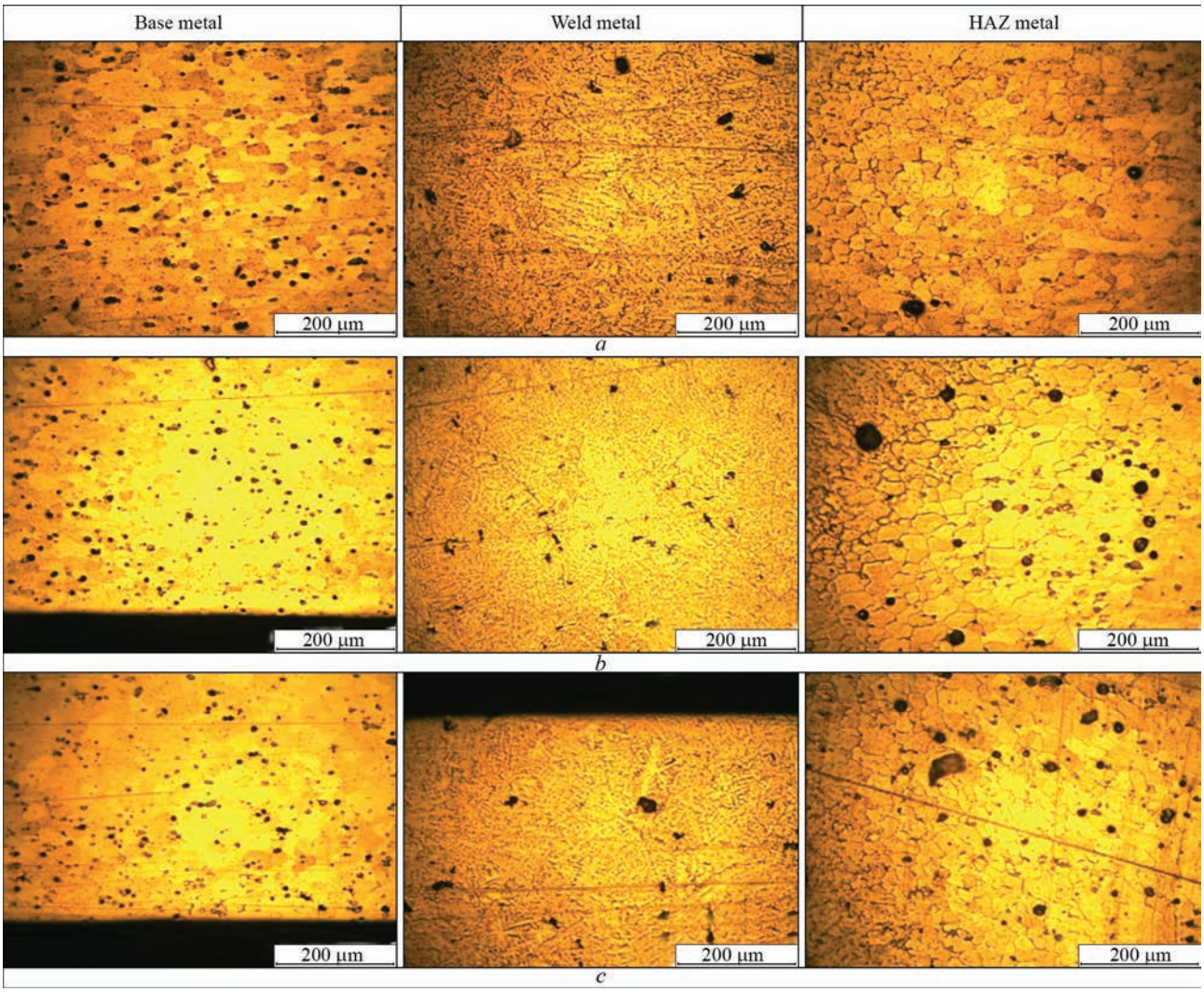

Figure 2. Microstructure of welded joints of aluminium 2219 alloy, heat-treated to the T81 condition, along (L) the rolled metal before corrosion tests (*a*), after tests in amyl environment (*b*) and its vapors (*c*)

the phases θ(Al_2Cu), T($Al_{12}Mn_2Cu$) and $A1_3Zr$, $A1_{11}V$ in the structure of the alloy provides a proper level of physical and mechanical properties of both the alloy itself and its welded joints. This is predetermined by a characteristic special mechanism of decomposition of a solid solution and the morphology of the location of phase precipitates during heating, as well as the ratio of their volumetric density in the structure. The number of phase components is determined by the total amount of alloying elements for a specific alloy.

The structure of the base metal of 2219 alloy in the T81 condition before the corrosion tests is characterized by the presence of grains of a solid solution of the main alloying elements in aluminium. Grains have an elongated shape along the direction of the rolled metal. In the volume of the alloy, precipitates of saturated phases are observed that contain the main alloying element of the alloy — copper. Nonmetallic inclusions are uniformly located over the whole metal cross-section (Figure 2). Signs of macro- and microchemical heterogeneity in structural components are not observed, indicating a high quality of the examined alloy.

In the specimens cut out in the longitudinal direction (Figure 2), along the rolled semifinished product, the length of grains is in average 60 μm, and the width is 35 μm (perpendicular to the thickness of the sheets). In a transverse direction, the size of grains is 60×35 μm, indicating the absence of anisotropy of the metal not only relative to a semifinished product, but also over the thickness (Figure 3).

A more thorough study of the structural features by the method of optical microscopy in a dark field showed that dark inclusions of irregular shape, which are uniformly located in the volume of the alloy, are intermetallic phases. A part of the inclusions has a spherical shape with a maximum size of about 12 μm. Taken into account their size, these intermetallics precipitated from a solid solution during heat treatment of the specimens. Other phase inclusions have a more elongated oval shape with a maximum size of 35×12 μm. They are not dissolved during arc welding and were formed

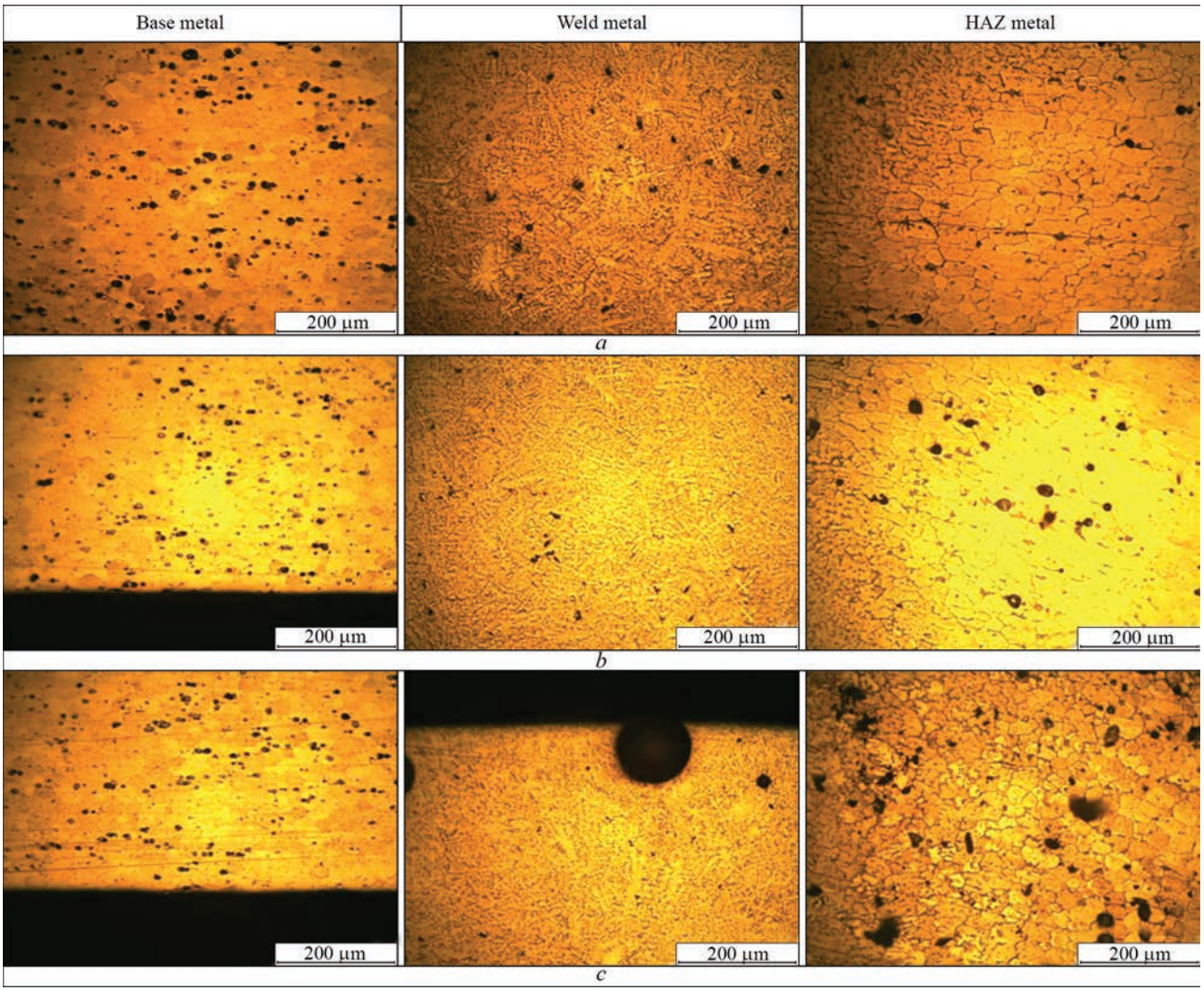

Figure 3. Microstructure of zone of welded joints of aluminium 2219 alloy, heat-treated to the T81 condition across (T) the rolled metal before corrosion tests (*a*), after tests in amyl environment (*b*) and its vapors (*c*)

at the metallurgical stage of manufacturing semifinished products and acquired an elongated shape in the process of plastic deformation in the sheets.

In the structure of welded joints, the zones can be distinguished, that differ from each other. Cast metal is observed in the welds. It has a dendritic structure. In the center of the weld, dendrites are located along the direction of welding. Directly near the fusion boundary of the weld with the base metal, dendrites have a columnar structure and directed from the fusion line to the center of the weld crystallization. Along the dendrites boundaries, the precipitates of eutectic origin (Figures 2, 3) are present, which have a size of not more than 15 μm. A uniform porosity is observed, typical to alloys of this alloying system. The size of pores does not exceed 50 μm. Their density is 7–12 pcs per 1 mm^2. On separate areas of the weld, single pores of up to 0.4 mm were detected, which is admissible according to DSTU EN ISO 10042 [14].

The fusion line separates the weld metal, which was completely melted during welding, from the base metal, which completely or partially remains in a solid state. It can not always be clearly determined, but it separates dendritic structure of the cast weld metal and the grain structure of the deformed HAZ metal (Figures 2, 3).

In HAZ intensive recrystallization processes were not detected. The size of the grains in this zone is not significantly different from the grains of the base metal. At the same time, precipitation of low-melting eutectics along the boundaries of grains is observed, which is associated with the redistribution of alloying elements between the structural components of the alloy under the influence of heating the HAZ metal to the temperatures higher than the solidus temperature (Figures 2, *c* and 3, *c*). This leads to the fact that in the HAZ near the fusion line the structure is formed characteristic to the state of heat treatment of alloys called «overburning» and is accompanied by a decrease in hardness (Figure 4).

This structural area is an integral part of any welded joint of aluminium alloys produced by fusion welding. At the distance from the fusion line to the base metal, the areas of annealing and over-

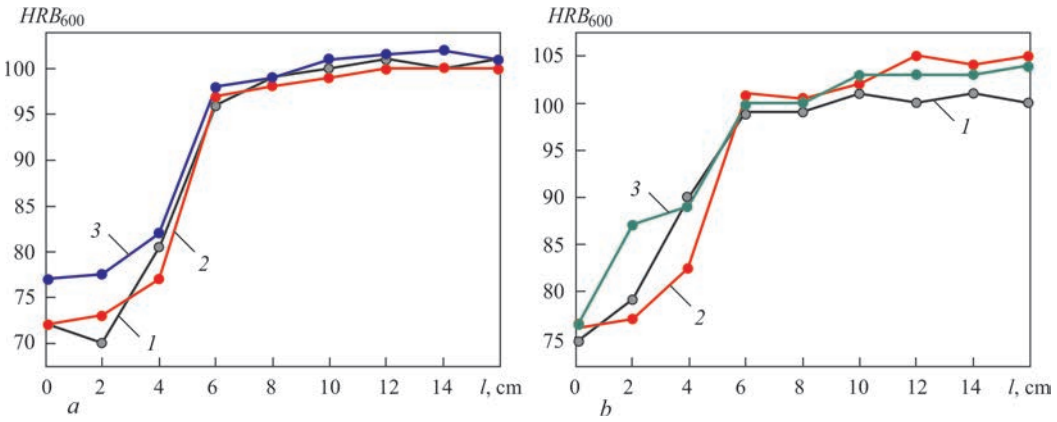

Figure 4. Nature of distribution of hardness over different zones of welded joint of 2219 alloy in the T81 condition along (*a*) and across (*b*) the rolled metal before corrosion tests (*1*), after corrosion tests in amyl environment (*2*) and its vapors (*3*)

ageing are also present, formed under the influence of heat of the welding arc. In these areas, as a result of coagulation processes, intermetallic phase precipitates are observed, which are increased up to 25 μm. The total width of the HAZ of the specimens of welded joints in the T81 condition is 6 mm. In the specimens, welded along and across the rolled metal, significant differences in the width of the HAZ area were not detected.

After the corrosion tests in amyl (Figures 2, 3, *b*) and amyl vapors (Figures 2, 3, *c*), any changes in the microstructure and grain size in the base metal, weld metal and HAZ are not observed.

Investigation of the mechanical properties. Figure 5 shows the averaged values of indices of mechanical properties: tensile strength, yield strength and relative elongation (Figure 5). The value of yield strength ($\sigma_{0.2}$) of the reference specimens of the base metal, cut out along the direction of the rolled metal (Figure 5, *a*), amounts from 365 to 367 MPa, and the tensile strength σ_t is from 462 to 463 MPa (Figure 5, *b*). In the specimens cut out in a transverse direction $\sigma_{0.2}$ is 362–365 MPa (Figure 5, *c*), σ_t is 468–469 MPa (Figure 5, *d*), which is slightly higher than for the specimens cut in the longitudinal direction.

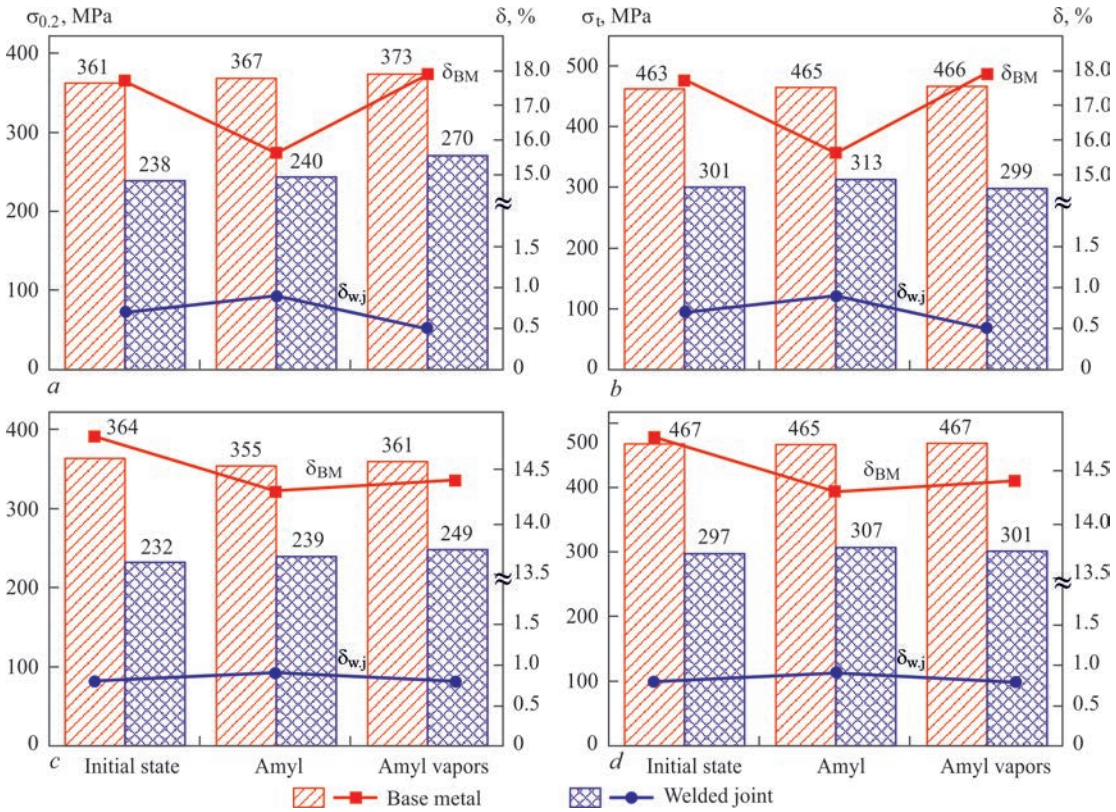

Figure 5. Mechanical properties of base metal and welded joint of 2219 alloy in the T81 condition along (*a*, *b*) and across (*c*, *d*) the rolled metal before corrosion tests and after corrosion tests in amyl and its vapors. Columns are tensile and yield strength, line is relative elongation

An analysis of the results of tests of the reference specimens of the welded joints, welded along the rolled metal, showed that the yield strength decreased by about 34–36 % as compared to the base metal — to 234–241 MPa (Figure 5, *a*). The tensile strength of the welded joints is 293–308 MPa (Figure 5, *b*), which is by 33–37 % lower than the strength of the base metal. The strength coefficient of the reference specimens of the welded joints is equal to 0.65.

A similar pattern was observed for the specimens of welded joints made across the direction of the rolled metal. The values of the yield strength of the reference specimens of welded joints was 229–234 MPa (Figure 5, *c*), which is approximately by 36–37 % lower than of the base metal. The tensile strength of the welded joints was from 271 to 323 MPa, which is lower than the strength of the base metal by approximately 31–45 %. The strength coefficient of the reference specimens of the welded joints, made across the rolled metal, was equal to 0.64.

After the tests of the specimens in amyl, the values of the yield strength of the base metal of 2219-T81 alloy in the longitudinal direction increased by almost 3 % and amounted from 355 to 373 MPa. At the same time, the level of strength increased by 1 % — 464–466 MPa. Soaking of the specimens in amyl vapors also caused an increase in yield stregnth by 4–5 % — up to 371–374 MPa and tensile strength by 1 % — up to 465–467 MPa.

After the corrosion tests of the specimens of joints, welded along the direction of the rolled metal, in amyl an increase in the value of the yield strength by ~1 % to 230–257 MPa (Figure 5, *a*) was observed. The tensile strength of the joints increased by ~4 %, to 309–315 MPa (Figure 5, *b*), indicating strengthening of the phase components of the metal structure after the contact with amyl. The tests of the longitudinal specimens of the welded joints in the amyl vapors contributed to an increase in the yield strength by ~13 % (up to 261–271 MPa), but a slight decrease in strength by ~1 % (to 290–308 MPa) (Figure 5, *a*, *b*).

The specimens of the base metal, cut out in the transverse direction relative to the rolled metal after soaking in amyl have the following properties: yield strength is 352–357 MPa, tensile strength is 465–467 MPa, i.e., both indices slightly decreased as compared to the indices for the specimens in the initial state. After the tests in amyl vapors, the yield strength decreased slightly (to 353–370 MPa), tensile strength did not change and amounted to 466–468 MPa.

In the specimens, welded across the direction of the rolled metal, after the action of amyl, the value

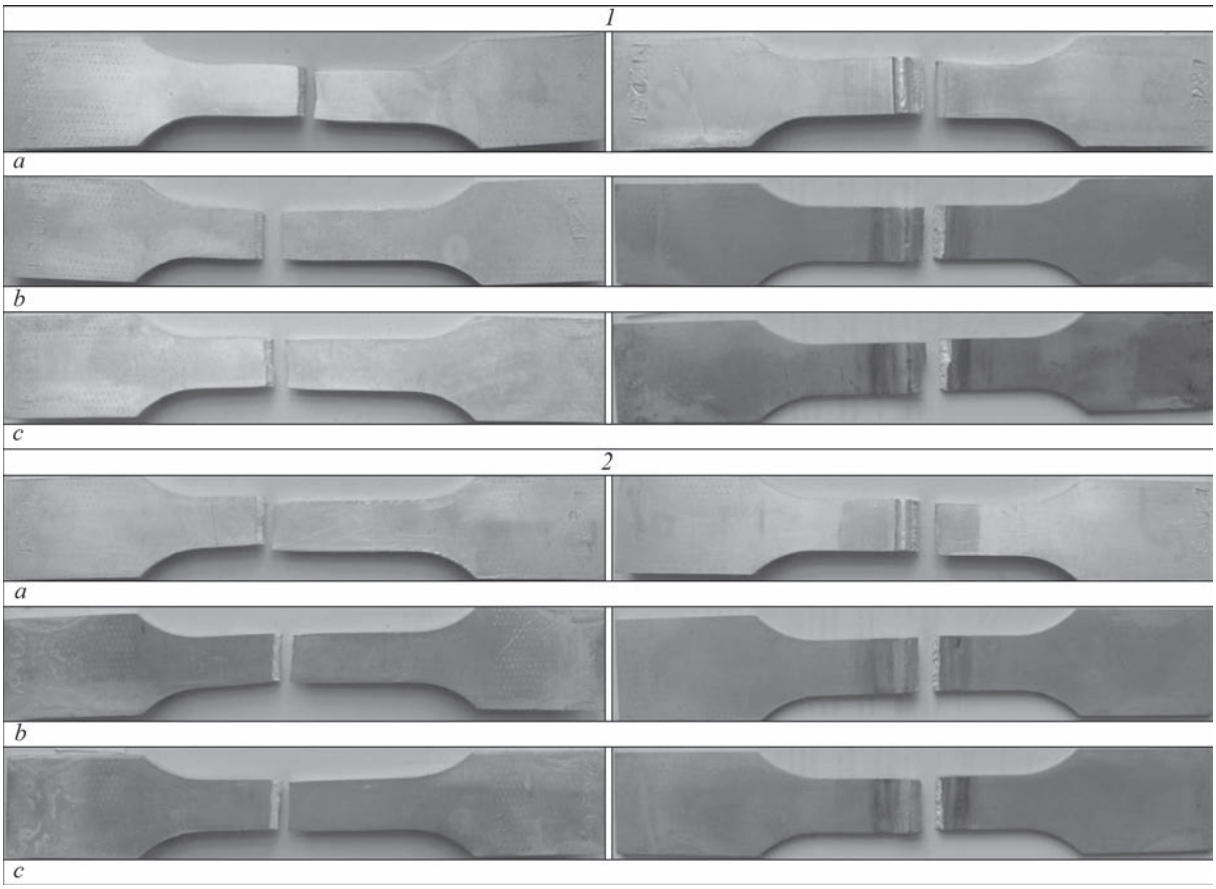

Figure 6. Appearance of base metal and welded joint of 2219 alloy specimens in the T81 condition along (*1*) and across (*2*) the rolled metal before corrosion tests (*a*), after corrosion tests in amyl (*b*) and its vapors (*c*)

of yield strength was 226–251 MPa (Figure 5, *c*), which was little different from the yield strength of the welded joints, produced along the rolled metal, but was lower than in the base metal. A similar pattern was observed for the tensile strength of these welded joints — 301–313 MPa (Figure 5, *d*).

The exposure of the specimens of joints welded in a transverse direction, in the amyl vapors contributed to a decrease in the yield strength to 254–261 MPa, and almost did not affect the value of the tensile strength, which was equal to 298–305 MPa.

The strength coefficient of the welded joints after the tests in amyl increased a bit as compared to the base metal and was 0.67 for the specimens welded along the rolled metal, and 0.66 for the transverse specimens.

For the specimens welded in the longitudinal direction, after the effect of amyl vapors, a decrease in relative elongation from 0.7 to 0.5 % was noted, for the transverse specimens, this indice did not changed and amounted to 0.8 %. The strength coefficient of the welded joints both for longitudinal specimens and transverse specimens after the action of amyl vapors was the same and amounted to 0.64.

The fracture of all the investigated specimens of welded joints of 2219 alloy occurred along the fusion line of the weld with the base metal (Figure 6), where during the thermal cycle of welding, grain boundaries are flashed and decomposition of an oversaturated solid solution of copper in aluminium occurs. Such structural changes are accompanied by precipitation and coagulation of strengthening phases, which causes thickening of grain boundaries.

As is evidenced by the analysis of the surface of fractures of the broken specimens of welded joints of the alloy, regardless of the direction of the rolled metal of semifinished products, their reliefs have a predominantly skewed character with a tough cell structure, the formation of which is accompanied by significant plastic deformations of the specimen material. The center of microcracking is the inclusions of intermetallic phases, which remain in the metal in the process of manufacturing semifinished products and do not dissolve in the conditions of arc welding.

CONCLUSIONS

1. Welded joints of aluminium 2219 alloy, made by single-pass nonconsumable electrode welding along (L) and across (T) the rolled metal, heat-treated to the T81 condition, are resistant to corrosion cracking and intergranular corrosion. The resistance to exfoliating corrosion in amyl and its vapors is evaluated by the point 2. According to a ten-point scale in accordance with GOST 9.502, the corrosion resistance of the base metal of the aluminium 2219 alloy in the T81 condition in amyl is evaluated by a point 2, which corresponds to the resistance group «highly resistant»; in amyl vapors — by a point 4, which corresponds to the resistance groups «resistant».

2. The resistance of welded joints of 2219 alloy to general and local corrosion in amyl and its vapors is not affected by the direction of welding process of semifinished products relative to the rolled metal and thermal welding conditions.

3. After soaking in amyl and amyl vapors, the ductility and strength indices of the welded joint specimens increase as compared to similar indices before the corrosion tests. The strength coefficient of the welded joints in the longitudinal direction after soaking in amyl is equal to 0.67, in the transverse direction it is 0.66, and after the action of amyl vapors for the joints welded in the longitudinal and transverse directions are the same and amount to 0.64. All the experimental specimens of welded joints of the alloy are fractured along the fusion line of the weld with the base metal, where during the thermal cycle of welding, a decomposition of an oversaturated solid solution of copper in aluminium and flashing of grain boundaries and coagulation of strengthening phases occur. This is accompanied by thickening of grain boundaries as a result of precipitation of phases during crystallization. Irrespective of the direction of welding relative to the rolled metal, its fractures of the experimental specimens during their breaking have a tough nature of the relief.

The work was performed with the support of SE «DB Pivdenne» (state registration number 011811006291s) in 2018.

REFERENCES

1. Rao, P.S., Sivadasan, K.G., Balasubramanian, P.K. (1996) Structure-property correlation on AA 2219 aluminium alloy workpieces. *Bulletin of Materials Sci.*, 19(**3**), 549–557.
2. Li, H., Zou, J., Yao, J., Peng, H. (2017) The effect of TIG welding techniques on microstructure, properties and porosity of the welded joint of 2219 aluminium alloy. *J. of Alloys and Compounds*, **727**, 531–539.
3. Zhang, D., Wang, G., Wu, A. et al. (2019) Study on the inconsistency in mechanical properties of 2219 aluminium alloy TIG-welded joints. *J. of Alloys and Compounds*, **777**, 1044–1053.
4. Grilli, R., Baker, M.A., Castle, J.E. et al. (2010) Localized corrosion of a 2219 aluminium alloy exposed to a 3.5 % NaCl solution. *Corrosion Sci.*, 52(**9**), 2855–2866.
5. Zhang, D., Wu, A., Zhao, Y. et al. (2021). Effects of the number of welding passes on microstructure and properties of 2219-C10S aluminium alloy TIG-welded joints. *J. of Mater. Eng. and Performance*, **5**, 3537–3546.
6. Wan, Z., Meng, D., Zhao, Y. et al. (2021) Improvement on the tensile properties of 2219-T8 aluminium alloy TIG welding joint with weld geometry optimization. *J. of Manufacturing Processes*, **67**, 275–285.

7. Niu, L.Q., Li, X.Y., Zhang, L. et al. (2017) Correlation between microstructure and mechanical properties of 2219-T8 aluminium alloy joints by VPTIG welding. *Acta Metallurgica Sinica*, 30(**5**) 438–446.
8. Zhang, D.K., Wang, G.Q., Wu, A.P. et al. (2019) Effects of post-weld heat treatment on microstructure, mechanical properties and the role of weld reinforcement in 2219 aluminium alloy TIG-welded joints. *Acta Metallurgica Sinica*, 32(**6**), 684–694.
9. Gupta, R.K., Panda, R., Mukhopadhyay, A.K. et al. (2015) Study of aluminium alloy AA2219 after heat treatment. *Metal Sci. and Heat Treatment*, 57(**5**), 350–353.
10. Lu, Y., Wang, J., Li, X. et al. (2018) Effects of pre-deformation on the microstructures and corrosion behavior of 2219 aluminium alloys. *Mater. Sci. and Engin.: A*, **723**, 204–211.
11. Chen, S., Li, F., Liu, Q. et al. (2020) Effect of post-aging heat treatment on strength and local corrosion behavior of ultrafine-grained 2219 Al alloy. *J. of Mater. Engin. and Performance*, 29(**5**), 3420–3431.
12. Zhang, D., Li, Q., Zhao, Y. et al. (2018) Microstructure and mechanical properties of three-layer TIG-welded 2219 aluminium alloys with dissimilar heat treatments. *Ibid.*, 27(**6**), 2938–2948.
13. Zhu, Z.Y., Deng, C.Y., Wang, Y. et al. (2015) Effect of post weld heat treatment on the microstructure and corrosion behavior of AA2219 aluminium alloy joints welded by variable polarity tungsten inert gas welding. *Materials & Design (1980–2015)*, **65**, 1075–1082.
14. Peng, X.N., Qu, W.Q., Zhang, G.H. (2009) Influence of welding processes on mechanical properties of aluminium alloy 2219. *J. of Aeronautical Materials*, **2**, 57–60.
15. Bai, J.Y., Yang, C.L., Lin, S.B. et al. (2016) Mechanical properties of 2219-Al components produced by additive manufacturing with TIG. *The Int. J. Adv. Manuf. Technol.*, 86(**1**), 479–485.
16. Rao, S.K., Reddy, G.M., Rao, K.S. et al. (2005) Reasons for superior mechanical and corrosion properties of 2219 aluminium alloy electron beam welds. *Materials characterization*, 55(**4–5**), 345–354.
17. AMS-QQ-A-250/30A. *Specifications. Aluminium alloy 2219. Sheet and plate* [in Ukrainian].
18. GOST 7512–82: *Nondestructive testing. Welded joints. Radiography method* [in Ukrainian].
19. GOST 9.908–85: *Unified system of corrosion and ageing protection. Metals and alloys. Methods for determination of corrosion and corrosion resistance indices* [in Russian].
20. GOST 9.904–82: *Unified system of corrosion and ageing protection. Aluminium alloys. Accelerated test method for exfoliating corrosion* [in Russian].
21. GOST 9.021–74: *Unified system of corrosion and ageing protection. Aluminium and aluminium alloys. Accelerated test method for intercrystalline corrosion* [in Russian].
22. GOST 1497–84 (ISO 6892-84, CT CMEA 471-88) *Metals. Methods of tension test* [in Russian].
23. GOST 9.502–82 (CT CMEA 6194–88): *Unified system of corrosion and ageing protection. Inhibitors of metals corrosion for aqueous systems. Methods of corrosion tests (with modifications Nos 1, 2)* [in Russian].

ORCID
L.I. Nyrkova: 0000-0003-3917-9063,
T.M. Labur:0000-0002-4064-2644

CONFLICT OF INTEREST
The Authors declare no conflict of interest

CORRESPONDING AUTHOR
L.I. Nyrkova
E.O. Paton Electric Welding Institute of the NASU
11 Kazymyr Malevych Str., 03150, Kyiv, Ukraine
E-mail: lnyrkova@gmail.com

SUGGESTED CITATION
L.I. Nyrkova, T.M. Labur, E.I. Shevtsov, O.P. Nazarenko and A.V. Dorofeev (2021) Corrosion-mechanical resistance of 2219 alloy welded joints, under simulated service conditions. *The Paton Welding J.*, **10**, 18–27.

JOURNAL HOME PAGE
https://pwj.com.ua/en

Received 27.08.2021
Accepted: 11.11.2021

https://doi.org/10.37434/tpwj2021.10.04

MATHEMATICAL MODELING OF MELTING TEMPERATURE RANGE AND PHASE COMPOSITION OF MULTICOMPONENT NICKEL ALLOYS

S.V. Maksymova, V.V. Voronov and **P.V. Kovalchuk**

E.O. Paton Electric Welding Institute of the NASU
11 Kazymyr Malevych Str., 03150, Kyiv, Ukraine

ABSTRACT

Modern brazing filler metals for brazing high-temperature nickel alloys are complex alloys, where the components should provide the required level of strength, high-temperature resistance, high-temperature corrosion resistance and other service properties of brazed joints. However, establishing the optimum composition to obtain the desired set of properties is a non-trivial task, requiring considerable investment of time and money. The work is a study of applicability of the method of mathematical modeling of thermodynamic processes (CALPHAD) during development of multicomponent filler metals for brazing high-temperature nickel alloys. During performance of investigations, using CALPHAD computational procedure, melting temperature ranges were determined for a number of alloys of Ni–Cr–Co–Al–(Me)–Ta system. Calculated data were obtained on the influence of adhesion-active elements of groups IV and V of the periodic table on liquidus temperature and phase composition of the base nickel alloy. In particular, their impact on the quantity and thermal stability of γ′-phase and σ-phase was determined. Thermodynamic calculated data, obtained with application of mathematical modeling method, were used during development and investigation of a number of promising filler metals for brazing high-temperature nickel alloys, including single-crystal high-temperature nickel alloy ZhS-32VI.

KEY WORDS: brazing filler metal, brazing, high-temperature nickel alloys, mathematical modeling (CALPHAD), adhesion-active components, titanium, niobium, tantalum, γ′-phase, σ-phase

Service properties of gas-turbine engines and stationary units are largely determined by the properties of high-temperature nickel alloys (HTNA), which are the main material for turbine blade manufacture [1].

For a long time the required level of characteristics of casting HTNA was reached due to alloying of the nickel base by an ever greater number of components, the summary action of which had a positive influence on long-term strength, ductility, fatigue, oxidation resistance, etc. [1, 2]. Here, the empirical «trial and error» method had been the main method for a long time at development of high-temperature nickel alloys [3]. It is quite obvious, however, that in such a case, if more than 10–15 elements are used for alloying the nickel high-temperature alloys, it is rather difficult to find an optimum composition to obtain the sought complex of properties, as it requires considerable time and cost. In this connection, the methods of mathematical calculation and engineering of modern high-temperature alloys become a necessary tool [2–7].

The above-said is also valid at development of filler metals for brazing the high-temperature nickel alloys. As the modern nickel alloys may contain more than ten alloying elements, then the filler metals for their brazing, as a rule, are also complex alloys, which contain depressants and elements, ensuring the required strength, heat resistance, high-temperature corrosion resistance and other service properties of brazed joints [4, 8].

In a number of studies [6–11] it is noted that the modern programs of mathematical modeling of the thermodynamic processes are based on physical theories of thermal, diffusion and thermodynamic phenomena, which can adequately reflect the pattern of physicochemical processes taking place in multicomponent nickel systems, both at solidification (cooling), and at heating. The authors show that application of the calculation methods for thermodynamic processes allows plotting the constitutional diagrams for multicomponent systems in broad ranges of temperatures and concentrations, as well as calculating the type, volume fraction and composition of phases for equilibrium and nonequilibirum conditions of phase transformations.

In particular, the concept of CALPHAD method (CALculation of PHAse Diagrams) by prediction of stable phases, their composition, as well as thermodynamic properties in those areas of the phase diagram, where experimental data are absent, enables plotting the phase diagrams [12–14].

So, for Ni-based multicomponent alloys typical is a microstructure, which usually consists of solid solution (γ-matrix), dispersed particles of γ′-phase, carbides and topological close-packed phases (TCP). To determine the volume fraction of each of these phases, it is necessary to have an estimate of the energy Gibbs functions [3]. Thus, CALPHAD method combines all the exper-

Copyright © The Author(s)

imental data on phase equilibria in the system and all the thermodynamic data, obtained during performance of thermochemical and thermophysical investigations.

This is the most completely realized in JMatPro software package (Java-based Materials Properties) of Sente Software Company [15–19].

This software package is designed for modeling a wide range of properties of multicomponent systems on different base (Fe, Al, Ti, Ni, Co, etc.), contains specialized thermodynamic bases for modeling the processes of cooling (solidification) or heating of materials.

The objective of this study is determination of the possibility of prediction of the melting temperature range and phase composition of multicomponent nickel alloys by application of the methods of computational alloys design, namely the methods of computer thermodynamics (CALPHAD) in combination with the methods of statistical processing of the obtained results.

Computational procedure. For thermodynamic calculations of the melting range of the studied brazing filler metals, a special JMatPro program was used for modeling the properties of multicomponent steels and alloys. This software package allows performance of thermodynamic calculations for multicomponent systems, also on nickel base, with determination of the type, and volume fraction of the precipitating phases (γ-, γ′-, MC, $M_{23}C_6$, M_6C, M_3B_2, etc.), chemical composition of the phases and the temperature field of their existence.

Thermodynamic calculations are based on evaluation of energy Gibb's functions for each phase for the specified temperature [13]:

$$\Delta G = \Delta G_0 + \Delta G_i^m + \Delta G_i^{xs},$$

where ΔG_0 is the phase free energy in its pure form; ΔG_i^m is the ideal energy from phase component mixing; ΔG_i^{xs} is the excess free energy from phase component mixing.

Free energy (ΔG_m) for a multicomponent system can be represented by the following equation:

$$\Delta G_m = \sum_i x_i \Delta G_0^i + RT \sum_i x_i ln(x_i) + \\ + \sum_i \sum_{j \rangle i} x_i x_j \sum_v \Omega_v (x_i - x_j)^v,$$

where x_i is the mole fraction of component i; ΔG_0^i is the free energy of the phase for pure component i; T is the temperature; R is the universal gas constant; Ω_v is the coefficient of interaction which depends on v value (in practice, v is usually not higher than 2) [13].

The base system for development of experimental filler metals for HTNA brazing was selected, allowing for the influence of each specific element on the properties of high-temperature nickel alloys. Ni–Cr–Co–Al– (Me) system is promising as a base. In view of the need to ensure the heat resistance, and high-temperature strength and to make the brazing filler metal composition close to that of the base metal, the base system alloys were additionally doped by tantalum, tungsten and molybdenum. Here, the limits of aluminium and tantalum content in experimental brazing filler metals were selected, proceeding from the considerations of ensuring the high-temperature strength of the alloy due to formation of the required volume fraction of the strengthening γ′-phase Ni_3 (Al, Ta, Ti). The content of niobium and titanium in the alloy was limited due to liquation susceptibility of these elements and local melting of interdendritic areas of the base material during brazing [2, 20].

Discussion of the results. During investigations a range of the values of liquidus and solidus temperatures was obtained, as well as the calculated phase composition of the experimental alloys. The calculated data were furtheron subjected to processing by statistical analysis methods, in order to plot the liquidus surfaces, which would allow assessment of the influence of the alloying elements on the melting temperature of the alloys of this system (Figure 1.)

So, for instance, it was determined that an increase of the quantity of tantalum from 2.5 to 10 wt.% in the base alloy allows lowering its liquidus temperature from 1371 to 1322 °C (Figure 2). The solidus temperature of the alloy here decreases from 1340 to 1261 °C. It is quite understandable that such a liquidus temperature is too high for the filler metal, which is designed for brazing the high-temperature nickel alloys.

Base metal alloying by zirconium almost does not change the liquidus temperature, but leads to a significant lowering of the solidus temperature — to 1060 °C (for an alloy with 2.5 wt.% Ta) and up to 991 °C (for an alloy with 10 wt.% Ta). Temperature lowering is related to formation of a low-temperature eutectic that contains zirconium and tantalum in its composition (Figure 3).

Doping of the base alloy by titanium and niobium leads to a significant lowering of melting temperature of the alloy. In this case titanium (Figure 4, curve *3*) has a stronger influence on lowering of the melting temperature than niobium does (Figure 4, curve *2*). However, temperature lowering to the required level can be achieved only at simultaneous addition of these elements and an increased tantalum content (Figure 4, curve *4*).

It is known that strengthening of γ-solid solution matrix by fine particles of γ′-phase ensures the required level of performance of the high-temperature nickel alloys at increased temperatures, due to slowing down of the dislocation movement. Therefore, during investigation of the microstructural components, special attention was given to studying the influence of alloying by the

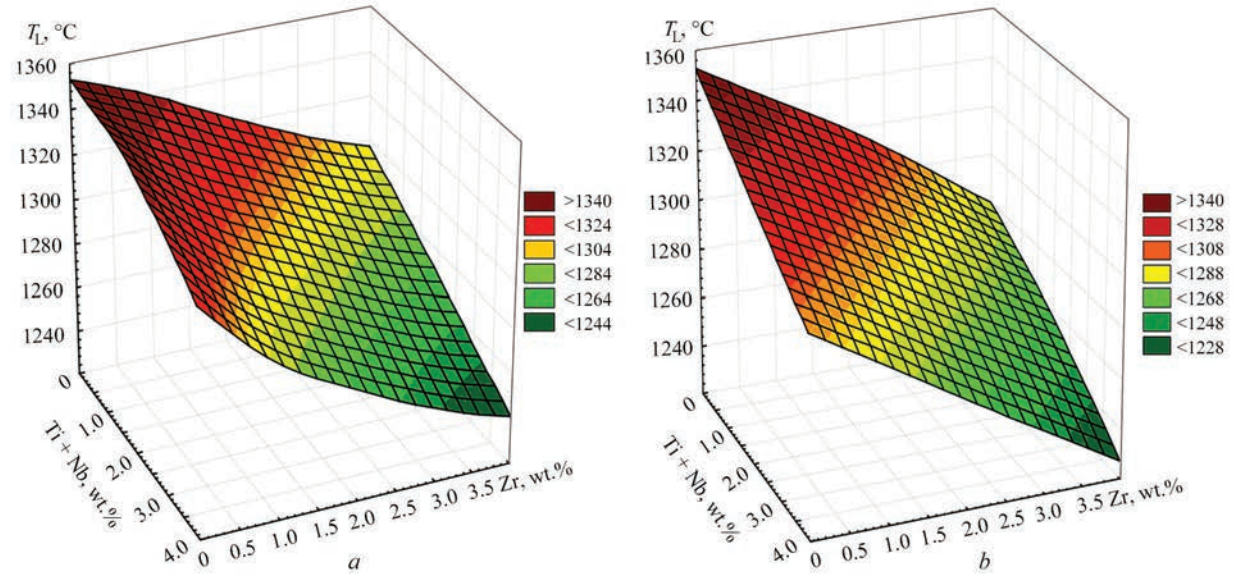

Figure 1. Liquidus surfaces of experimental brazing filler metals of Ni–Cr–Co–Al(Me:Ti, Nb, Zr) system with 5 (*a*) and 7.5 wt.% (*b*) tantalum

adhesion-active elements on formation of strengthening γ′-phase. This phase consists of Ni_3Al intermetallics, and in addition to aluminium it may have titanium, niobium and tantalum in its composition [21].

In particular, when studying the influence of tantalum on the calculated quantity of γ′-phase, it was found that increase of the amount of tantalum (up to 10 wt.%) leads to an increase of the temperature range of γ′-phase existence (Figure 5), although this range still is somewhat smaller than in the commercial single-crystal alloy ZhS-32VI (Figure 5, curve *5*).

Additional alloying by titanium and niobium significantly increases (up 1100 °C) the temperature of the start of γ′-phase dissolution (Figure 6), even though it slightly decreases the range of its existence (to 1210–1225 °C) (Figure 6, curves *3* and *4*).

It should be also noted that additional alloying by γ′-forming elements promotes a slight lowering of the quantity of one of TCP phase varieties (σ-phase), and at simultaneous alloying by titanium and niobium the appearance of this phase is recorded only at temperatures above 600 °C. On the other hand, however, the maximum temperature of existence of this phase in the alloy also rises significantly to 1100 °C (Figure 7, curve *4*).

The attempts to additionally lower the quantity of σ-phase by addition of rhenium to the alloy, which is known to be a good σ-stabilizer [6], lead to shifting of the range of σ-phase existence from the temperatures of 600–1110 to 685–1180 °C (Figure 8).

Calculated data obtained using computer thermodynamics method were applied during development and investigation of a number of promising filler metals for brazing single-crystal high-temperature nickel alloy ZhS-32V1.

Thus, during investigations it was found that the method of mathematical modeling of thermodynamic process (CALPHAD) using JMatPro software package can be successfully applied during development of multicomponent filler metals for brazing high-temperature nickel alloys, in particular, for prediction of liquidus temperature and tentative phase composition that will allow considerable reduction of the cost of time and material resources.

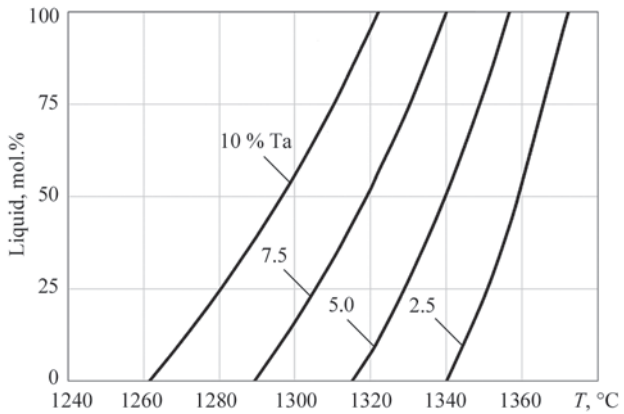

Figure 2. Dependence of melting range on the quantity of tantalum in the base alloy of Ni–Cr–Co–Al–(Me)–Ta system

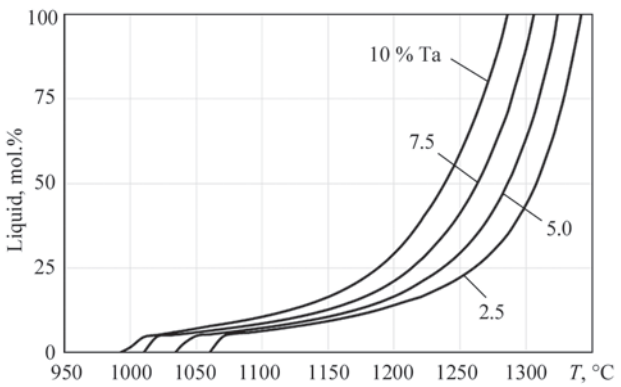

Figure 3. Dependence of melting range on alloying by tantalum and zirconium of the base alloy of Ni–Cr–Co–Al–Ta–2Zr system

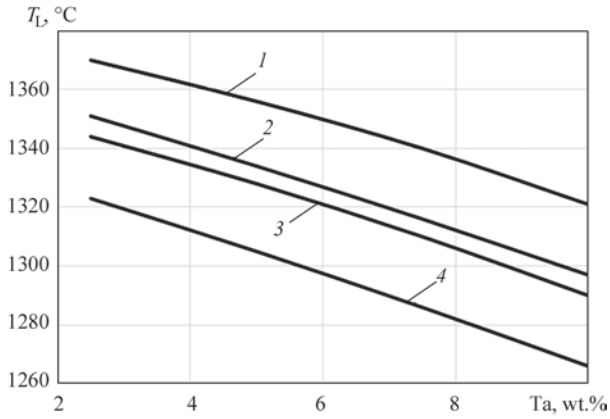

Figure 4. Dependence of liquidus temperature of the alloy of Ni–Cr–Co–Al–Me–(Nb, Ti) system on the content of adhesion-active components: *1* — Ta; *2* — Ta + 2 Nb; *3* — Ta + 2 % Ti; *4* — Ta + + 2 % Ti + 2 % Nb

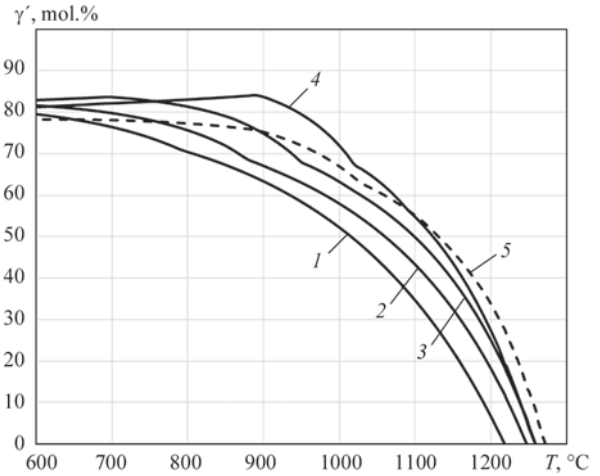

Figure 5. Dependence of volume percent of γ′-phase on Ta quantity in the base alloy of Ni–Cr–Co–Al– (Me) system: *1* — 2.5 % Ta; *2* — 5 % Ta; *3* — 7.5 % Ta; *4* — 10 % Ta; *5* — nickel alloy ZhS-32VI

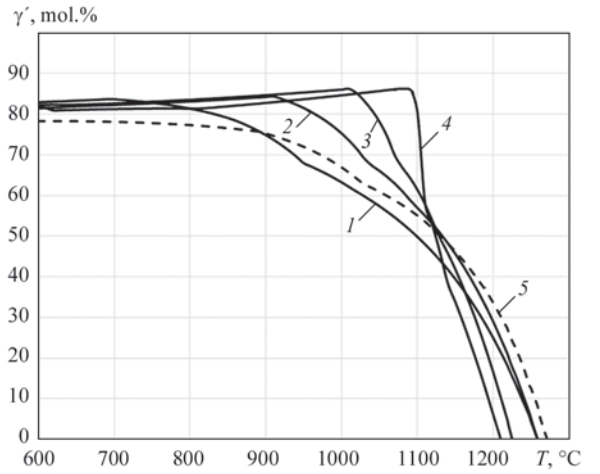

Figure 6. Dependence of volume percent of γ′-phase in the alloy of Ni–Cr–Co–Al–Ta–(Nb, Ti) system on the content of adhesion-active components: *1* — 7.5 % Ta; *2* — 7.5 % Ta + 2 % Nb; *3* — 7.5 % Ta + 2 % Ti; *4* — 7.5 % Ta + 2 %Ti + 2 % Nb; *5* — high-temperature nickel-alloy ZhS-32VI

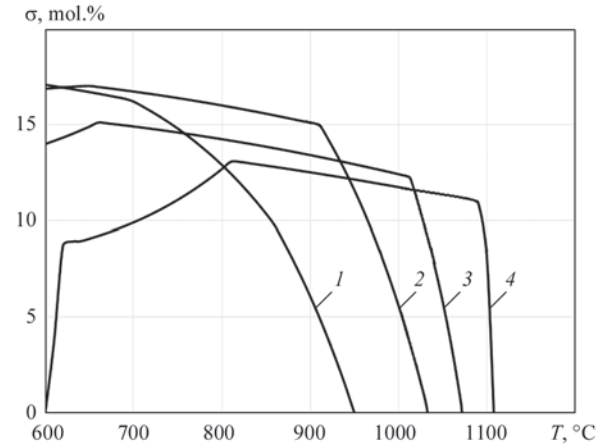

Figure 7. Dependence of volume percent of σ-phase in the alloy of Ni–Cr–Co–Al–Ta– (Nb, Ti) system on the content of adhesion-active components: *1* — 7.5 % Ta; *2* — 7.5 % Ta + 2 % Nb; *3* — 7.5 % Ta + 2 % Ti; *4* — 7.5 % Ta + 2 % Ti + 2 % Nb

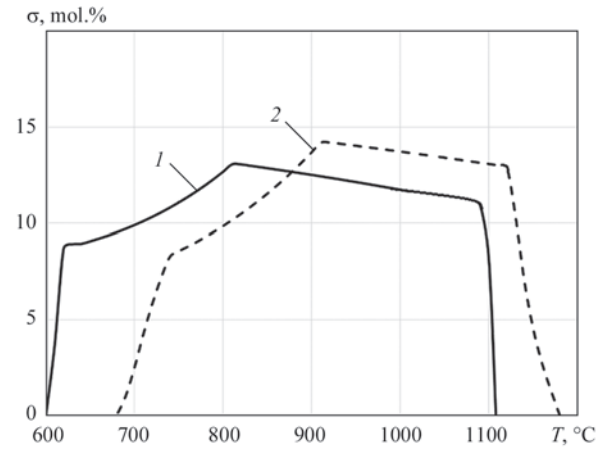

Figure 8. Dependence of volume percent of σ-phase in the alloy of Ni–Cr–Co–Al–Ta–(Nb, Ti) system on rhenium content: *1* — without rhenium; *2* — 2 % Re

CONCLUSIONS

During performance of the investigations it was found that the method of computer modeling of the thermodynamic processes (CALPHAD) with application of JMatPro software package can be effectively used during development of multicomponent filler metals for brazing high-temperature nickel alloys, in particular, for prediction of the liquidus temperature and phase composition of the filler metal.

Proceeding from the conducted computational studies, it was established that:

- increase of the amount of tantalum from 2.5 to 10 wt.% in the base alloy of Ni–Cr–Co–Al–Ta system does not allow considerably lowering its liquidus and solidus temperatures;
- zirconium addition to the base alloy composition almost does not change the liquidus temperature of the base alloy, but it leads to an essential lowering of solidus temperature (991 °C). This is related to appearance of

a low-temperature eutectic in the alloy, which contains zirconium and tantalum in its composition;

● base alloy doping by titanium and niobium leads to a significant lowering of the alloy melting temperature. Here, the influence of titanium is stronger than that of niobium;

● additional alloying by titanium and niobium significantly increases (up to 1100 °C) the calculated temperature of the start of γ′-phase dissolution (Figure 6), although it somewhat decreases the range of its existence (to 1210–1225 °C);

● when studying the curves of the alloy microstructure, it was found that additional alloying by γ′-forming elements promotes a slight lowering of the quantity of σ-phase, and at simultaneous alloying by a certain quantity of titanium and niobium, the appearance of this phase is recorded only at temperatures above 600 °C;

● attempts to further lower the quantity of σ-phase, by adding rhenium to the alloy lead to shifting of the interval of σ-phase existence from 600–1110 to 685–1180 °C.

REFERENCES

1. Kuznetsov, V.P., Lesnikov, V.P., Popov, N.A. (2016) *Structure and properties of monocrystalline high-temperature nickel alloys*. Ekaterinburg, Izd-vo Ural. Un-ta [in Russian].
2. Kablov, E.N., Petrushin, N.V., Svetlov, I.L., Demonis, I.V. (2007) Casting heat-resistant nickel alloys for perspective aircraft GTE. *Tekhnologiya Lyogkikh Splavov*, **2**, 6–16 [in Russian].
3. Zhou, Shihuai, Wang, Yougan, Zhu, J. et al. (2004) Computational tools for designing Ni-base superalloys. In: *Proc. of the Int. Symp. on Superalloys*. DOI: 10.7449/2004/Superalloys_2004_969_975
4. Kablov, E.N. (2005) Heat-resistant structural materials. *Litejnoe Proizvodstvo*, **7**. URL: https://viam.ru/sites/default/files/scipub/2005/2005-204274.pdf
5. Gaiduk, S.V., Kononov, V.V., Kurenkova, V.V. (2017) Application of integrated calculation-analytic method for multi-criterion optimizing of compositions of casting heat-resistant nickel alloys. *Suchasna Elektrometal*., 126(**1**), 44–51. DOI: doi.org/10.15407/sem2017.01.08 [in Ukrainian].
6. Saunders, N., Fahrmann, M., Small, C.J. (2000) The application of CALPHAD calculations to Ni-based superalloys. *Superalloys*, 803–811. DOI: 10.7449/2000/Superalloys_2000_803_811.
7. Markl, M., Müller, A., Ritter, N. et al. (2018) Development of single-crystal Ni–base superalloys based on multi-criteria numerical optimization and efficient use of refractory elements. *Metall. Mater. Transact. A*, **49**, 4134–4145. DOI: 10.1007/s11661-018-4759-0
8. Kablov, E.N. (2001) *Cast blades of gas turbine engines (alloys, technology, coatings)*. Moscow, MISiS [in Russian].
9. Petrushin, N.V., Chabina, E.B., Nazarkin, R.M. (2012) Development of heat-resistant intermetallic alloys based on γ′-phase with high melting temperature. Pt 1. *Metallovedenie i Termicheskaya Obrabotka Metallov*, **2**, 32–38 [in Russian].
10. Petrushin, N.V., Chabina, E.B., Nazarkin, R.M. (2012) Development of heat-resistant intermetallic alloys based on γ′-phase with high melting temperature. Pt 2. *Ibid*., **3**, 20–23 [in Russian].
11. Huang, W., Chang, Y.A. (1999) A thermodynamic description of the Cr–Ni–Re–Al system. *Mater. Sci. and Eng. A*, **259**, 110–119.
12. Perrut, M. (2015) Thermodynamic modeling by the CALPHAD method and its applications to innovative materials. *Aerospace Lab.*, **9**, 1–11. DOI : 10.1276212015.AL09.10
13. Saunders, N. (1996) Phase diagram calculations for Ni-based superalloys. *Superalloys*, 101–110.
14. Lukas, H.L., Fries, S.G., Sundman, B. (2007) *Computational thermodynamics: The Calphad method.* Cambridge University Press. 15. https://www.sentesoftware.co.uk/jmatpro
15. Saunders, N., Guo, Z., Li, X. et al. (2003) Using JMatPro to model materials properties and behavior. *JOM*, 55(**12**), 60–65. DOI:10.1007/s11837-003-0013-2
16. Sidorov, A. (2015) JMatPro – program package for modeling of properties of steels and alloys. CAD and graphics. *Sovremennye Tekhnologii — v Promyshlennost*, **3**, 2–4 [inRussian].
17. Tapia, A.S. (2006) *Computational design of nickel based superalloys for industrial gas turbine components*. University of Florida.
18. Schillé, J.-P., Guo, Z., Saunders, N., Miodownik, A.P. (2011) Modeling phase transformations and material properties critical to processing simulation of steels. *Materials and Manufacturing Processes*, 26(**1**), 137–143. DOI: 10.1080/10426910903153059
19. Petrushin, N.V., Ospennikova, O.G., Visik, E.M. et al. (2012) Heat-resistant alloys of low density. *Litejnoe Proizvodstvo*, **6** [in Russian]. URL: https://viam.ru/sites/default/fi les/scipub/2011/2011-205933.pdf
20. Morozova, G.I. (1992) *Phenomenon of γ′-phase in heat-resistant nickel alloys* [in Russian]. URL: https://viam.ru/ sites/files/scipub/ 1992-201097.pdf

ORCID

S.V. Maksymova: 0000-0003-0158-5760,
V.V. Voronov: 0000-0002-0410-1154,
P.V. Kovalchuk: 0000-0002-2313-5982

CONFLICT OF INTEREST

The Authors declare no conflict of interest

CORRESPONDING AUTHOR

S.V. Maksymova
E.O. Paton Electric Welding Institute of the NASU
11 Kazymyr Malevych Str., 03150, Kyiv, Ukraine
E-mail: maksymova.svitlana15@ukr.net

SUGGESTED CITATION

S.V. Maksymova, V.V. Voronov and P.V. Kovalchuk (2021) Mathematical modeling of melting temperature range and phase composition of multicomponent nickel alloys. *The Paton Welding J*., **10**, 28–32.

JOURNAL HOME PAGE

https://pwj.com.ua/en

Received 07.07.2021
Accepted: 11.11.2021

https://doi.org/10.37434/tpwj2021.10.05

ELECTROSLAG TECHNOLOGIES FOR REPAIR OF THROUGH-THICKNESS CRACKS IN THICK PARTS

S.M. Kozulin[1], **I.I. Lychko**[1] and **H.S. Podyma**[2]

[1]E.O. Paton Electric Welding Institute of the NASU
11 Kazymyr Malevych Str., 03150, Kyiv, Ukraine
[2]National Technical University of Ukraine «Igor Sikorsky Kyiv Polytechnic Institute»
6/2 Dashavska Str., 03056, Kyiv, Ukraine

ABSTRACT

Results of investigations are presented, which were performed in order to develop a highly-productive technology for repair of through-thickness cracks in thick parts in their operation site. The aim of the work is to study and establish the main principles of a high-efficient technology of repairing defects of the type of through-thickness cracks in thick parts in their operation site by the method of consumable nozzle multipass electroslag welding. The main tasks of the study were selection of principal diagram of electroslag welding, development of a procedure for calculation of geometrical parameters of edge preparation, that the most fully meet the conditions for formation of sound metal of the welded joint in a wide gap, development of basic principles of the technique of making welds and creation of routing technology of repair. Performed studies were the base for development of decision taking algorithms and general principles of the technology for repair of large-sized parts of unique equipment in its operation site, using the proposed method. Technological recommendations for repair of through-thickness cracks in such parts are based on the following postulates, elaborated proceeding from the features of the proposed method: domain of rational values of welding specific energy, providing sound weld formation, techniques allowing hot crack prevention in the weld central parts, conditions of minimizing the welding stresses when welding rigid joints, conditions of controlling the weld chemical composition that provide reduction of the fraction of base metal participation in weld formation, and lowering of harmful impurities level in it, and recommendations on selection of electrode and auxiliary materials, etc. Technological recommendations were successfully tried out in six cement works at repair of through-thickness cracks in rotary kiln tires.

KEY WORDS: multipass electroslag welding, consumable nozzle, through-thickness cracks, repair, specific heat input, hot cracks, welding voltages, decision taking algorithm, technology recommendations

Restoration of worn-out or fractured parts of machines is an environmentally friendly and resource-saving production [1]. The main task of repair production is the effective restoration of reliability of machines as a result of the most optimum use of residual life of their parts.

In the cost of repaired machines, the share of spare parts amounts to about 70 % [2]. Since the cost of parts restoration amounts to 50–60 % of the cost of their manufacture, an increase in the volumes of parts restoration is a real way to reduce the cost of repairing machines and units. 5–6 times reduction in the number of operations during restoration as compared to manufacturing and 20–30 times shortening in the cost of materials provides the prime cost of parts restoration, making 40–80 % of the cost of new ones. The production practice shows that scientifically substantiated technology and organization of defective parts restoration allow providing the service life of restored parts, which is close to the service life of new ones, equal to it, and in some cases even exceeds it [1–3].

Repair technologies with the use of welding processes are fundamentally different from those used in serial production of welded structures, mainly in the difficulty of creating universal technological recommendations. This is caused by the fact that defects to be eliminated, as a rule, differ significantly in nature, shape and sizes and it leads to the formation of non-standard large welding gaps, as well as atypical shape of edges preparation as a result of removal of defective metal. Therefore, each case of repair requires the development or specification of certain modes of welding, especially the technique of its realization. Before offering the technology of repair, it is necessary to carefully analyze the causes of failure of a part, evaluate technological characteristics of the whole part and especially the fatigue strength [1–3].

When correcting most unique parts, the specific conditions for repair works include: large cross-sections of parts, wide gaps, high rigidity of assembly, impossibility of dismantling of a repaired part as well as mechanical and high-temperature treatment, high carbon content and harmful impurities in cast steels of type 35L, etc. In addition, the repair of fractured parts of the equipment that is included into the production line with a continuous mode of operation should be carried out promptly to minimize losses of an enterprise from underproduction, which is also an urgent task. This requires the maximum possible structurization of tasks and creation of an algorithm for taking grounded technological decisions [4].

Copyright © The Author(s)

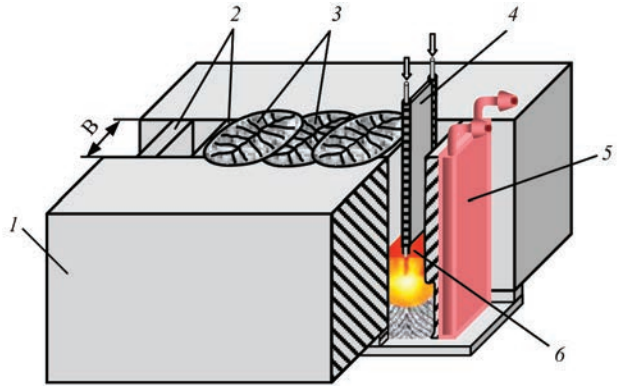

Figure 1. Scheme of the method of CNMEW of massive products with a large intersection of joining elements: *1* — welded part; *2* — forming partitions; *3* — welds; *4* — consumable nozzle; *5* — forming device cooled with water; *6* — slag pool; *B* — welding gap

The aim of the work is the research and development of basic principles of highly-efficient technological process of restoration of defects of the type of through-thickness cracks in parts of large thickness at the site of their operation applying the method of consumable nozzle multipass electroslag welding (CNMEW).

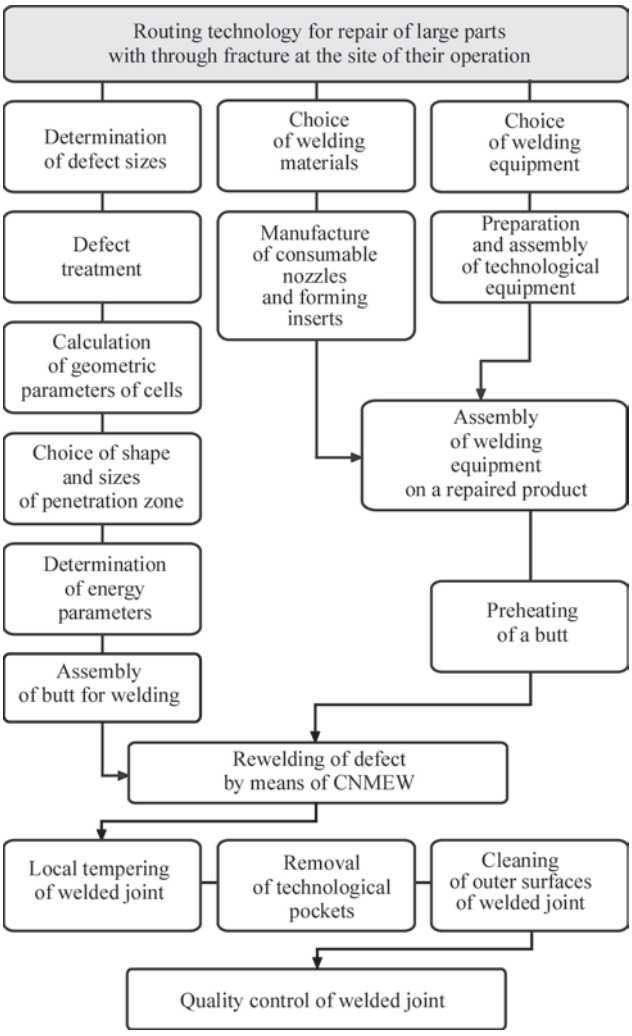

Figure 2. Algorithm for taking decisions during repair of through-thickness cracks in large steel parts of units at the site of their operation

The main tasks of the work are the choice of principal diagram of ESW, development of procedure for calculation of geometric parameters of edges preparation that most completely corresponds to the conditions for the formation of a sound welded joint metal in a wide gap, development of basic postulates of the technique of welds producing, as well as creation of routing repair technologies.

The known methods of repair of through-thickness cracks in parts of large thickness at the site of their operation using methods of welding differ in a low efficiency, hard working conditions of performers and do not always guarantee the satisfactory quality of welded joints [5, 6].

Analysis of the technical level of existing repair methods [6, 7] showed that restoration of large parts with defects of the type of through-thickness cracks is reasonable from technical and economical point of view, applying CNMEW method for joining the metal of large thickness (Figure 1) [8].

Based on the results of the carried out investigations, the algorithm for taking decisions (Figure 2) and general principles of the technology for repair of large parts of the unique equipment at the site of its operation using the proposed CNMEW method were elaborated.

Technological recommendations for repair of through-thickness cracks in such parts at the site of their operation are based on the following postulates elaborated in relation to the features of the proposed method. The main of them are:

- procedure of calculation of geometric parameters of cells and forming inserts depending on the width of a gap (60–120 mm), formed after removal of metal in the area of a crack and over the thickness of a part being repaired [9];
- domain of rational values of specific welding energy, providing a sound weld formation [10];
- technological techniques that provide prevention of hot cracks in the central parts of the welds [11];
- conditions for minimizing welding stresses during welding of rigid joints [12];
- conditions for regulating chemical composition of the weld, providing a decrease in the share of the base metal participation in the formation of a weld and a decrease in the level of harmful impurities in it [10];
- recommendations for choosing electrode and auxiliary materials, etc.

For successful realization of the technology of repairing through-thickness cracks on the site of defective

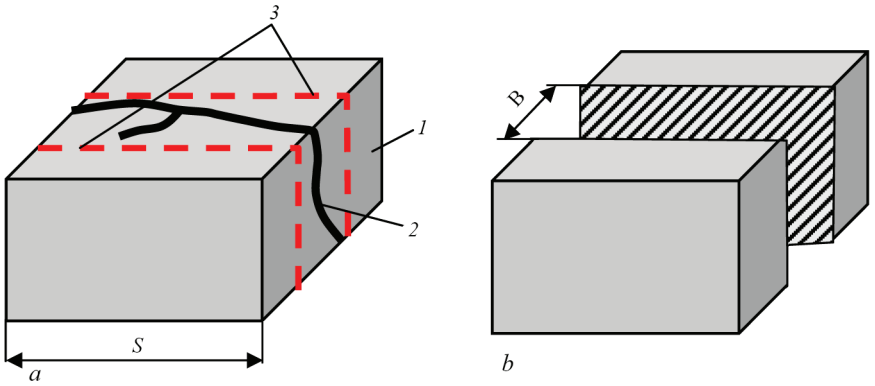

Figure 3. Scheme of layout (*a*) and removal of defective metal in the area of a through-thickness crack (*b*): *1* — part subjected to repair; *2* — through-thickness crack; *3* — plane of a cut; *B* — welding gap

parts operation using the proposed CNMEW method, it is necessary to carry out the following operations:

- determine sizes of the area of laying a through-thickness crack using visual inspection and with the help of a portable device for ultrasonic flaw detection, for example, UD2-12;
- remove a defective area with a crack by making two through parallel cuts of a product using oxyfuel cutting or by an oxygen lance (Figure 3, *a*). The distance between the planes of a cut is chosen in such a way as to cover the entire area of laying and branching of a crack;
- having measured the value of the formed gap *B* (Figure 3, *b*), choose the desired width of welded cells S_c from the domain of their technological ratios [9]. Determine the thickness of the forming inserts S_n from the expression $S_p = 0.04B + 34$, where *B* is the welding gap, mm;
- determine the required number of cells for rewelding of the formed opening from the expression

$$n = \frac{S - S_c}{S_c + S_p} + 1, \qquad (1)$$

where *S* is the thickness of a welded butt (fractured part), mm; S_c is the width of the cell, mm; S_p is the thickness of the insert, mm;

- determine the distance between the axes of rewelded cells (step) *t* (Figure 4, *a*) from the expression [9]:

$$t = 2k\sqrt{\left[1 - \frac{B^2}{B^2 + 4h(B+h)}\right]\left(\frac{S_c}{2} + 0.577h + 13\right)^2}, \qquad (2)$$

where $k = 0.85–0.95$; *B* is the gap; *h* is the depth of the base metal penetration.

- set the input and output technological pockets;
- make the layout of the butt in the places of mounting inserts *4* (Figure 4, *a*), which form an assembly to perform the first (central) pass. Install the water-cooled devices *3* to the outer surfaces of the inserts;
- choose the required penetration depth of the base metal and in accordance with the proposed procedure [10] determine the value of the specific heat energy of the process and expected sizes of welds in the cross-section;
- produce consumable nozzles *5* (Figure 4, *a*) and assemble the welding apparatuses of type AShP113M over the butt [13];
- calculate the time of rewelding a crack at a successive fulfilment of passes by a one welding apparatus from the expression:

$$t_w = \frac{H}{V_w} n + (n-1) t_p, \qquad (3)$$

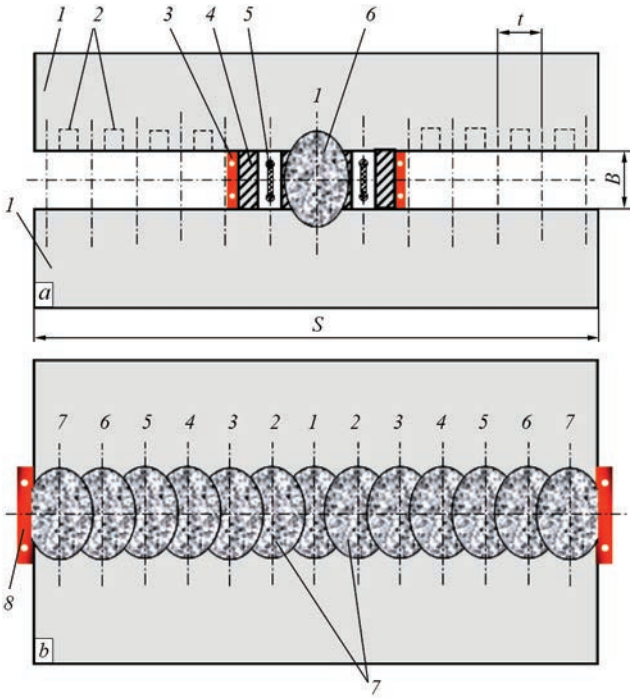

Figure 4. Scheme of butt layout, rewelding of central cell (*a*) and performance of adjacent passes by CNMEW (*b*): *1* — welded regions of defective part; *2* — places for mounting of forming inserts; *3*, *8* — water cooling device; *4* — insert; *5* — consumable nozzle; *6* — central weld; *7* — adjacent welds; *S* — thickness of part (length of through-thickness crack); *B* — gap; *t* — step of cells

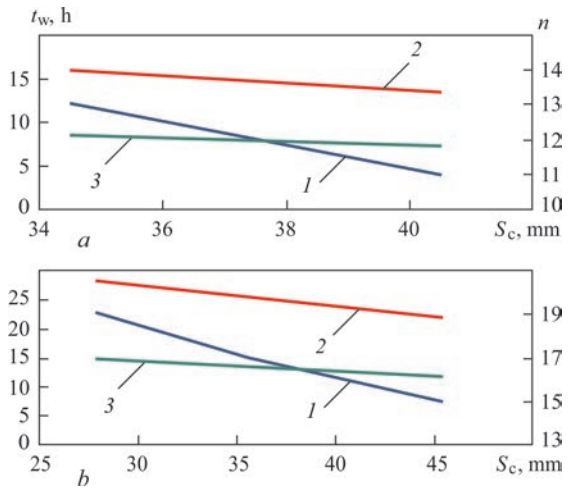

Figure 5. Change in the number of rewelded cells in the opening n and time of opening rewelding t_w, depending on the width of cells S_c: *a* — weldable intersection — 900×355 mm; *b* — 1200×475 mm; *1* — number of cells; *2* — rewelding of a cell successively one-by-one; *3* — welding simultaneously of two cells at a time

where H is the butt height (weld length), mm; v_w is the welding speed, m/h; n is the number of cells for opening rewelding; t_p is the pause time between the end of the preliminary rewelding and the start of the rewelding of the subsequent cell; h (depending on the level of mechanization of assembly and adjusting works this time is t_p = 0.25–0.4 h).

● determine the machine time of welding the butt by CNMEW using simultaneously two welding apparatuses by the formula

$$t_{w2} = \frac{H}{V_w}\left(\frac{n-1}{2}+1\right)+\left(\frac{n-1}{2}\right)t_p, \qquad (4)$$

● carry out a preheating of the assembly metal of the first pass to a temperature of 150–200 °C and perform rewelding of the central cell 6 (Figure 4, *a*);

● after rewelding of the central cell, perform other passes in pairs in the direction from the middle of the butt (central weld) to its edges (Figure 4, *b*);

● after welding of the entire butt is completed, remove the technological pockets, disassemble the welding equipment, mount a portable electric kiln on the welded joint and perform a local high tempering (for steel 35L) in the conditions: temperature of 620–650 °C with an exposure of 6–8 h and cooling together with the kiln to a temperature of 30–80 °C;

● carry out cleaning of outer surfaces of the welded joint with the help of a manual grinding tool;

● perform testing of the quality of the welded joint with the help of a portable device for ultrasonic flaw detection.

In each particular case of repair fulfilment, the necessary number of passes, sizes of welds and time of butt rewedling will be determined depending on the sizes of the cross-section of a repaired part and a degree of branching of a through-thickness crack [14]. The time spent on rewelding of a crack depends on its extension, value of branching, welding gap, number of passes to fill the edges opening, as well as a step between the centers of the holes, formed by the forming inserts.

A number of holes in the opening grows with a decrease in the set hole width and forming inserts. Figure 5 shows a change in the required number of forming holes depending on their width, designed for rewelding cracks in parts with the thickness of 900 and 1200 mm. It also shows diagrams of changing time of rewelding the butt in CNMEW successively of one hole at a time, as well as respectively in rewelding of the opening of two holes simultaneously.

From Figure 5 it follows that in terms of preserving the optimal efficiency of repair works:

a) width of the cells of edge opening should be 40–45 mm;

b) during rewelding of the opening of two cells simultaneously, the total time for welding a butt is almost twice reduced.

For example, for CNMEW of the butt with the cross-section 1000 (thickness) ×420 (length) mm with a gap of 70 mm, the width of the rewelded opening cells will be 43 mm, and for the forming inserts it will be 37 mm. To reweld such opening, it will be necessary to perform 13 passes, producing welds of an elliptical shape with the size of 105×130 mm (thickness and width of the weld, respectively). The machine time of one butt welding by means of a one apparatus will amount to 22–23 h, and simultaneously by two apparatuses it will be 12–13 h.

Technological recommendations were successfully tested on six cement works during repair of through-thickness cracks in the tires of rotating kilns [10, 14, 15]. Cross-sections of the restored (repaired) tires are: 900×355; 900×420; 900×475 and 1200×475 mm.

CONCLUSIONS

1. Based on the performed investigations, the principles of technology and technique of repairing through-thickness cracks in parts of a large thickness at the operation site of large-sized equipment applying the method of CNMEW, algorithm of taking decisions, special technological equipment and adaptation were developed.

2. The application of the developed technology allowed 1.5–3.0 times reducing the total time of restoration works as compared to two-arc automatic submerged welding. As compared to electric arc methods of welding, the use of CNMEW for repairing

through-thickness cracks excludes the formation of defects in the form of lacks of penetration, hot cracks, pores, slag inclusions, etc., which is confirmed by high service properties of restored parts.

REFERENCES

1. Panteleenko, F.I., Lyalyakin, V.P., Ivanov, V.P., Konstantinov, V.M. (2003) *Restoration of machine parts:* Refer. Book. Ed. by V.P. Ivanov. Moscow, Mashinostroenie [in Russian].
2. Shcherbakov, Yu.V., Kashfullin, A.M. (2018) *Current methods of restoration and strengthening of parts:* Tutorial. Perm, Prokrost [in Russian].
3. Eltsov, V.V. (2012) *Repair welding and surfacing of machine parts and mechanisms:* Tutorial. Tolyatti, Izd-vo TGU [in Russian].
4. Garf, M.G. (1979) *Taking decisions at multiple criteria.* Moscow, Znanie [in Russian].
5. Dennis, D., Harwig, P., Fallara, V. et al. (1999) A Narrow-groove process proves robust in a massive repair. The narrow — groove submerged arc welding process is used to repair a kiln tire. *Welding J.*, **1**, 45–48.
6. Kozulin, S.M., Lychko, I.I., Kozulin, M.G. (2007) Methods of reconditioning rotary kilns (Review) *The Paton Welding J.*, **10**, 33–39.
7. Sushchuk-Slyusarenko, I.I., Lychko, I.I., Kozulin, M.G., Semenov, V.M. (1989) *Electroslag welding and surfacing in repair works*. Kiev: Naukova Dumka [in Russian].
8. Yushchenko, K.A., Kozulin, S.M., Lychko, I.I., Kozulin, M.G. (2014) Joining of thick metal by multipass electroslag welding. *The Paton Welding J.*, **9**, 30–33.
9. Kozulin, S.M. (2011) Selection of the groove shape for repair of through cracks by multilayer electroslag welding. *Ibid.*, **3**, 32–35.
10. Kozulin, S.M. (2011) *Multipass electroslag welding with consumable nozzle at repair of unique equipment.* In: Syn. of Thesis for Cand. of Tech. Sci. Degree. Kyiv [in Ukrainian].
11. Kozulin, S.M., Lychko, I.I., Kozulin, M.G. (2010) Increase of resistance of welds to formation of crystalline cracks in repair of bands of kiln furnaces using electroslag welding. *The Paton Welding J.*, **1**, 32–34.
12. Kozulin, S.M., Lychko, I.I. (2011) Deformations of welded joints in multilayer electroslag welding. *Ibid.*, **1**, 22–27.
13. Paton, B.E., Yushchenko, K.A., Kozulin, S.M., Lychko, I.I. (2019) Electroslag welding process. Analysis of the state and tendencies of development (Review). *Ibid.*, **10**, 33–40.
14. (2006) Welding technology of repair of large-sized thickwall structures. In: *Proc. of Sci.-Tech. Int. Conf. on Modern Problems of Improvement of Welding Production Effectiveness (15–17 November 2006, Tolyatti)*. TGU, Vol. 1, 119–124.

ORCID

S.M. Kozulin: 0000-0002-8368-4545,
I.I. Lychko: 0000-0002-4977-7473,
H.S. Podyma: 0000-0002-0825-3235

CONFLICT OF INTEREST

The Authors declare no conflict of interest

CORRESPONDING AUTHOR

S.M. Kozulin
E.O. Paton Electric Welding Institute of the NASU
11 Kazymyr Malevych Str., 03150, Kyiv, Ukraine
E-mail: kozulin@paton.kiev.ua

SUGGESTED CITATION

S.M. Kozulin, I.I. Lychko and H.S. Podyma (2021) Electroslag technologies for repair of through-thickness cracks in thick parts. *The Paton Welding J.*, **10**, 33–37.

JOURNAL HOME PAGE

https://pwj.com.ua/en

Received 28.07.2021
Accepted: 11.11.2021

https://doi.org/10.37434/tpwj2021.10.06

IMPROVING THE RELIABILITY OF POWER COMPLEX EQUIPMENT BY ELECTRIC ARC SPRAYING

A.V. Hruzevych[1] and **V.V. Shvets**[2]

[1]Trypillia TPP PJSC «Centrenergo»
1 Promyslova Str., 08720, Ukrainka, Ukraine
Institute of Magnetism of the NASU and Ministry of Education and Science of Ukraine
36-b Akademik Vernadsky Blvd, 03142, Kyiv, Ukraine
[2]Chief Technologist Department «REZON», LLC
1 Geofizychna Str., 49057, Dnipro, Ukraine

ABSTRACT

The aim of the work is studying the efficiency of spraying application to improve the reliability of TPPs power equipment. A feasibility study indicated that the introduction of spraying technology can reduce losses in case of TPPs emergency shutdowns by 1.5–3.0 times a year, and the estimated extension of the service life of surfaces increases by 1.7–2.5 times. Since the main type of wear in the feed-water economizer (FWE) of TPP boilers is ash wear, and corrosion between the spacing bars, a comprehensive solution was proposed for the problem of extending the service life of boiler waterwall tubes and economiser tubes through development of new heat-resistant and wear-resistant thermal coatings.

KEY WORDS: spraying, welding, thermal power plant, ash wear, corrosion, electric arc coating

A significant number of failures in the operation of thermal power plant (TPP) equipment is predetermined by damages in boiler equipment, especially heating surfaces. Factors that lead to their malfunction can be divided into operational and nonoperational damages. The first group includes ash wear (typical for feed-water economizer (FWE) tubes), electrochemical and high-temperature corrosion (tubes of radiation and convective part of the boiler), metal overheating, etc. Nonoperational damages to TPP heating surfaces are most often caused by metallurgical and technological defects in the metal of tubes, low-quality manufacture, etc. [1]. Experience shows, that damages not in all heating surfaces of the boiler lead to a sudden shutdown of the power unit. In this regard, damages to FWE tubes in all cases cause failure of equipment. The main cause for such failures is ash wear. According to [2, 3], at individual power units, a number of failures caused by ash wear of boiler tubes, reaches 60 %. The mechanism of erosion wear of FWE tubes, which, according to the generally accepted theory, is caused by the effect of volatile ash particles, having high hardness and abrasiveness, is well studied [4, 5]. However, choosing an effective method of protection against wear is still a difficult task. Since the main type of wear of tube elements of TPP power equipment is ash wear and corrosion, in order to improve their reliability, service life and effi-

Figure 1. Electric arc spraying

Copyright © The Author(s)

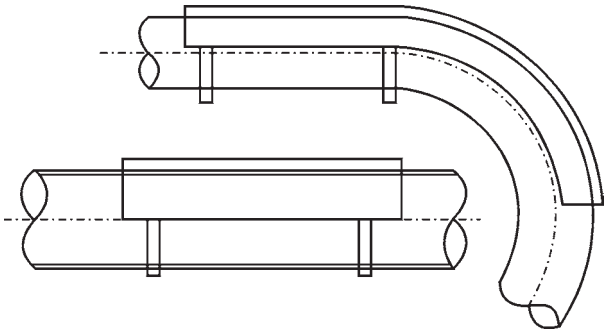

Figure 2. Individual sealing rings for protection of bends and straight sections of tubes

ciency, it was proposed to use electric arc spraying as a method of thermal modification of heating surfaces (Figure 1).

The most vulnerable areas of FWE are the first and second return bends downstream with the gas flow in opening to the section until the first spacing bars, inner and outer return bends, extreme coils from the back side of the convection shaft over the whole width. Traditionally, for individual protection of coils, sealing rings of a segment shape are used (Figure 2) [6], which are mounted on the front part of tubes downstream with the gas flow. Butt plates (Figure 3) are mounted also in other areas prone to intense ash wear.

In connection with a significant wear of technological equipment, the issue of its effective repair is now very acute, which provides the restoration of serviceability, increase in reliability, extension in the service life while reducing the costs on repair and restoration works [7]. One of the ways to improve the reliability of power plant equipment [8, 9] is its protection against ash and corrosion wear by spraying. An intensive wear of heat exchange surfaces of TPP boilers, in particular, waterwall tubes and economizer tubes, is predetermined by the use of coal dust with most of the solid noncombustible impurities as a fuel [10–12]. According to classification criteria, analysis of damages [13] shows that the main cause of damage to boiler tubes is corrosion and erosion wear. According to [14], in some units its share reached 60 %. Especially often erosion affects FWE coils. Abrasive ash particles, which are captured by flue gases at a high speed, hit the surface of the tubes and cause ash wear (Figure 4).

On the surface of waterwall tubes of 12Kh1MF steel, at temperatures elevated to 585 °C, films of iron oxides are formed, which have a weak adhesion to the steel surface and are easily worn by abrasive particles. Wear of the outer surface of tubes occurs uniformly over a large area and is localized in certain places. When the critical thickness of the tube wall is reached, it bursts, which leads to the shutdown of the power unit. The heat load on the outer wall

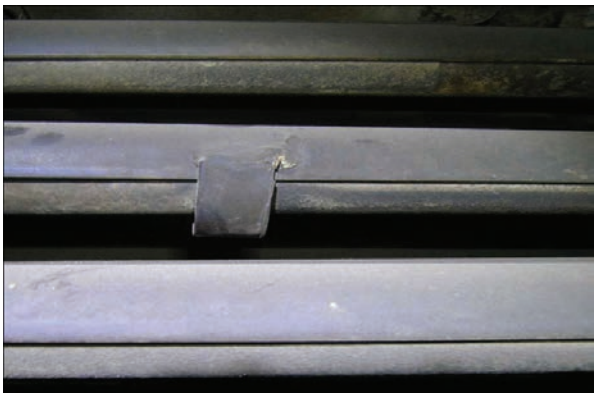

Figure 3. FWE tubes with butt plates of ash wear protection

of the tube is also increased because of the deposition of salts on the inner surfaces of waterwall tubes, which, in addition, experience corrosion and erosion damages. Therefore, the development of new effective methods to improve the reliability of TPP power equipment is an urgent direction. Damages of tube elements of heating surfaces of TPP power equipment have a nature of creep mechanisms with manifestation of fatigue, erosion and gas corrosion (oxidation) because of extremely high operating conditions, associated with high temperatures, cyclic loads and aggressive working environment, as well as because of abrasive action of coal fuel combustion products [11, 12]. Since the main type of wear on the water economizer of TPP boilers is ash wear and between the spacing bars corrosion exists, the works [12, 15] proposed a comprehensive solution to the problem of extending the service life of waterwall tubes of boilers and economizer tubes by developing new heat-resistant and wear-resistant thermal coatings [16, 17]. As a result, in the structure of such coatings, during the operation of boiler tubes and economizer tubes, dispersion hardening processes will take place as a result of precipitation of fine phases of carbides, nitrides and intermetallics, which will significantly increase their service properties during operation [18]. The aim of the article is to study the use of electric arc spraying, performed by LLC «REZON» (metallization) to improve the reliability of power equipment of TPP.

Figure 4. Nature of damage to the FWE tube with a diameter of 32×6 mm as a result of action of ash wear

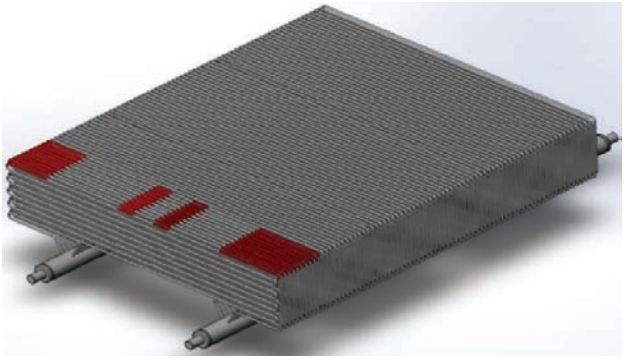

Figure 5. Areas of intensive ash wear of FWE tubes: straight sections and bends

Materials and methods. One of the challenging methods to improve the reliability of power equipment is electric arc spraying. The V.Karpenko Physico-Mechanical Institute of the NAS of Ukraine together with LLC «REZON» developed a technology for protection of heating elements of thermal power plants from ash wear and gas corrosion [19, 20], which involves the deposition of scarcely-alloyed electric arc coatings of the flux-cored wire on the surface of waterwall tubes and tubes of feed-water economizers in order to effectively protect them from ash wear and gas corrosion at operating temperatures of up to 600 °C. This technology allows increasing life of the protected tubes. The use of metallization will allow:

- providing corrosion and erosion resistance to tube sections at elevated temperatures;
- not increasing the total weight of heating surfaces;
- not complicating the access to separate packages of coils;
- not complicating visual observation of the outer surface of tubes also in the locations of spacing bars;
- reducing the labour consumption of the proposed measures by eliminating operations for the manufacture of shells, assembly of welded joints for sealing rings.

Table 1. Mechanical characteristics of tubes before metallization

σ_t, MPa	δ, %	ψ, %
50.3	28.8	60
According to the requirements of TU 14-3-460:2009/TU U 27.2-05757883-207:2009 «Seamless steel tubes for steam boilers and pipelines»		
420–560	24	45

Table 2. Structural characteristics of tubes before metallization

Specimen	Score of the Widmanstaetten structure according to the scale of TU 14-3-460	Score of banding orientiaion according to the scale of TU 14-3-460	Graffitization score in accordance with 3 SOU-N EE 20.321:2009
Cut from FWE	0	0	1 (graphitization was not detected)

Therefore, the use of metallization is the most advantageous method of protecting tubes of heating surfaces. The heat resistance of the metal of the Fe–Cr–B–Al alloying system is provided by the formation of Al_2O_3 oxide film on its surface, which is characterized by high chemical and thermal stability. At elevated temperatures, the diffusion of oxygen and nitrogen into the transition layers leads to the formation of iron Fe_2O_3 oxides and aluminium AlN nitrides, which reduces the heat resistance of coating. In order to mitigate the negative effect of these oxides, silicon is introduced into the coating system, which promotes the formation of a diffusion layer of SiO_2, preventing the oxidation of the subscale layer. The wear resistance of coating is provided by the content of fine iron-chromium carbides $(Fe, Cr)_7O_3$ and spinels $(Fe, Cr)_2O_3$ in the coating. To restore worn-out and protect the new most vulnerable sections of FWE tubes (Figure 5) of the boiler TPP-210A in the conditions of power engineering production of Ukraine, the technology of electric arc metallization was tested.

The technological stages of thermal spraying included the following operations:

- preliminary preparation of the base metal surface;
- spraying;
- external inspection and quality testing of the geothermal heat pump.

To provide a high-quality sprayed layer in accordance with the recommendations [10], the following parameters were tested:

- condition of the tube surface;
- distance of material deposition;
- inclination angle of the torch tip to the sprayed surface of the tube element;
- surface temperature of the base metal in the process of spraying;
- uniformity of coating thickness;
- feed rate of the sprayed material.

Electric arc compressed air jet spraying of heating surfaces was carried out at two thermal power plants in 2013. FWE Coils, which were once in operation at the unit No.2 of the Trypillia TPP (TpTPP) after two years of operation were disassembled and subjected to spraying by metallization. Before spraying, reference specimens were cut out from the tubes to determine mechanical and metallographic properties of the metal of the coils that were in operation. The results of mechanical tests to determine the tensile strength were shown in Table 1.

While carrying out metallographic analysis, the examinations were carried out around the whole perimeter of the tube at a magnification of ×100 and ×500. The ferritic-pearlitic structure of the metal over

Table 3. Composition of sprayed layer

Number of specimen	Content of alloying elements,%								
	Fe	Cr	Al	Si	Ni	Cu	Ti	Zn	Mo
1	76.04	11.76	5.41	5.36	0.17	0.08	0.14	0.13	0.05
2	77.39	11.27	5.58	4.66	0.15	0.09	0.11	0.1	0.09
3	75.13	11.33	5.52	5.67	0.19	0.09	-	0.04	-
4	76.95	12.37	6.04	3.5	0.18	0.11	0.11	0.06	0.04

the whole cross-section of the examined specimen was the same. The results are given in Table 2.

During the mechanical and metallographic tests of tube specimens, no deviations from the standard requirements [21] were found, after which it was decided to apply a protective coating by metallization. The works on coating were carried out on the repair site of the TpTPP and Zmiivska TPP according to the developed procedure [22]. To perform works on applying a protective coating on the tubes of heating surfaces, a set of equipment was used, which included: apparatus for sandblast treatment, electric arc metallizer, filter drier, cassettes with flux-cored wire, electrical cabinet, power source. In the process of spraying, an in-process control was performed, in which the quality of preparation of heating surfaces for spraying was subjected to testing, mode of spraying, order of applying layers of sprayed metal, granularity and color of the coating were subjected to testing. Spraying was performed without the use of a substrate. The tubes after metallization were not subjected to heat treatment.

After spraying of the protective layer, the coils were mounted on the steam boiler of supercritical pressure TPP-210 A, station unit No. 1, block A. According to the project for the boiler TPP-210 A, as a fuel, the coal of grade ASh was used. During operation of the boiler on the coal of grade ASh, the temperature of gases in the zone of the coils location was within 700–900 °C, and the composition of the furnace gases was approximately the following: CO – 50–70 mg/m^3; O_2 – 5 %; SO_2 – 2863 mg/m^3; NO_x – 1187 mg/m^3. Chemical composition of coal ASh ash from cyclone ash collectors (%): SiO_2 = 51.4, CaO = 3.8, MgO = 1.6, Fe_2O_3 = 15.3, Al_2O_3 = 22.4, K_2O = 3.3, Na_2O = 1.5. At the Uglegorsk TPP (Ugl.TPP), two heating surfaces were subjected to spraying: steamer (St. 12Kh1MF) between the spacing bars and bends near the walls of the steam boiler of supercritical pressure TPP-312 A, station unit No.4. Similarly, FWE (steel 20 (st.)) of the steam boiler of supercritical pressure TPP-312 A, station unit No.2 was subjected to spraying. According to the project for the boiler TPP-312 A, as a fuel, the coal of grade G was used. It was found that at the Tp.TPP and Ugl.TPP, the main type of wear on FWE was ash wear, and between the spacing bars — corrosion wear. Therefore, spraying on the heating surfaces was performed by one and the same material. The composition of the spray layer is given in Table 3. At the Trypillian TPP, the composition was tested by the X-ray fluorescent spectrometer NITON XL2.

Electric arc spraying was carried out in 2013 on the most abrasive-worn sections of coils of FWE boilers TPP-210 A and TPP-312 A, corrosion-damaged sections of coil of steamer tubes in the spacing bars of the boiler TPP-312 A (low pressure). Photos of sprayed coils are shown in Figure 6.

After spraying and during operation, the cuts from the heating surfaces of tubes were performed, whose microstructure should meet the requirements [21] for reliable operation. At the Uglegorsk TPP after metallization, for metallographic examination from the sprayed steamer (low pressure) tube 2 reference specimens were cut out: one — directly from the bend (with spraying on the surface), and the second one (reference) — at a distance of 150 mm from the

Figure 6. Appearance of sprayed coils

Figure 7. Appearance of tube bend and its surface after spraying

sprayed zone. The sections were made by successive grinding and polishing. The etching of sections was performed in a 4 % solution of nitric acid in ethyl alcohol. For metallographic analysis, the microscope MIM-8M was used at a magnification of ×100 and ×500 times. The structure of the reference specimen is a ferrite-pearlite. Styloscopy was performed in a stationary styloscope SL-13. To external inspection, sprayed tubes and bends were subjected. Mechanical tests were carried out on flattening and determination of mechanical properties. At the Trypillia TPP after carrying out metallization of FWE coils with a diameter of 32×6 mm St.20, coils (production specimens) were cut out. Then, specimens were cut out of them, which were tested on flattening. Delamination of the coating layer occurs after bringing together the inner sides to H_{in} = 15 mm. Bringing of the sides together was performed up to H_{in} = 10 mm. The sprayed layer was subjected to measuring hardness in the ultrasonic hardness meter TKM-459.

At the Trypillia TPP, two variants of welding steel tubes after metallization were investigated. The first is an electric arc welding of tubes after metallization by 2.5 mm TsU-5 electrodes with the tubes that did not pass metallization. The second is welding by TsU-5 electrodes during alignment of tubes between each other that passed metallization. Welding was performed in accordance with [23]. Before welding the edges of tubes were treated at an angle of 40–45° with cleaning in the region of ends. Diameter of the rod of TsU-5 electrodes is 2.5 mm. According to the appearance, the welds are in a satisfactory condition. Cracking, pores, cavities, undercuts and other outer defects were not observed. The surface layer of tubes with metallization in the area of welded joint are cleaned for testing using non-destructive methods. Ultrasonic testing did not detect inner defects in the butt welds. Microstructure of metal in the near-weld zone and in the welds area in both cases is satisfactory. When conducting X-ray fluorescent analysis of welded joints, a slight increase in chromium content was revealed. An increased silicon content in welded joints is obviously associated with insufficient quality preparation. During mechanical tests of the weld, the fracture of the specimen occurs mainly over the base metal, indicating satisfactory mechanical properties of the weld. Microstructure of metal in the near-weld and weld zone in both cases is within the normal limits.

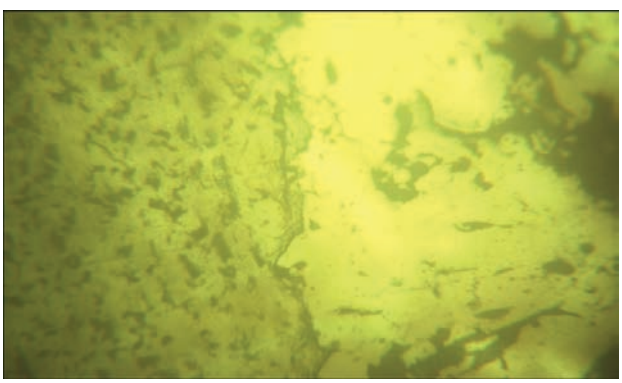

Figure 8. Microstructure (×500) of metal specimen with a sprayed layer

Results and discussion. The inspection of tubes and bends showed that the sprayed layer has a rough surface with a metallic luster. At a detailed consideration of surface sprayings, separated large crystals are distinguished on it, which give it a significant roughness. Spraying has a uniform and solid distribution over the outer surface of the bends. As a result of performed spraying of tubes and bends at the Trypillia TPP, the photos of their macrostructure (Figure 7), as well as microstructure of the tube after spraying were made (Figure 8). The structure after metallization did not undergo changes and complied with the standard requirements.

With the help of high-quality spectral analysis, it was found that a sprayed protective layer of FWE tube, produced by the method of electric arc metallization, represents a composite with a strengthening carbide phase in a metal matrix and contains such alloying elements as chromium and aluminium. The composition of the carbide phase is about 40 %. The base metal is carbon steel (alloying elements were not detected). In the microstructure of sprayed tubes from steel of grade 20 (Figure 9), the orientation on

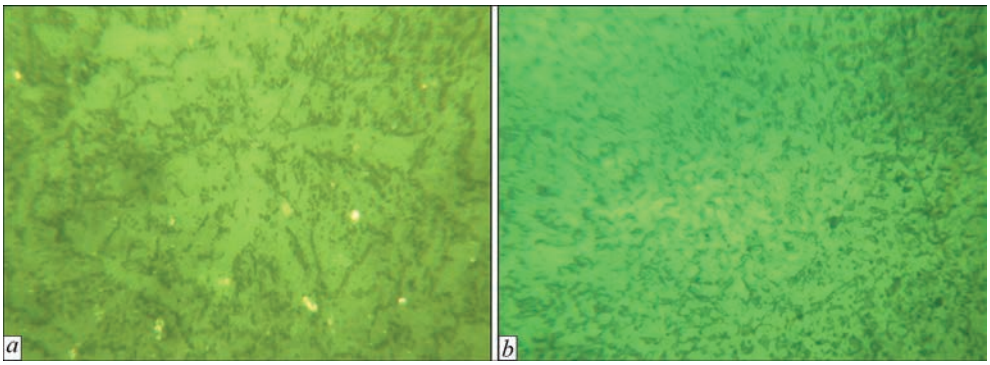

Figure 9. Microstructure of sprayed tubes from steel of grade 20: *a* — ×500; *b* — ×100

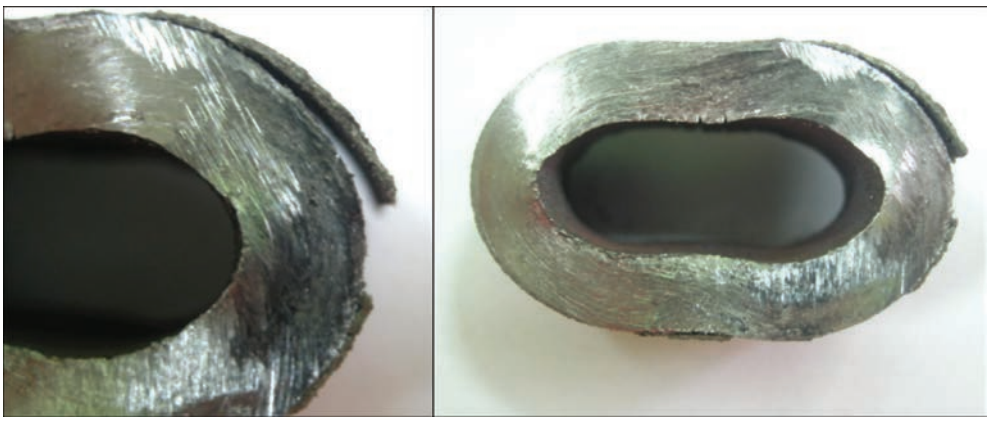

Figure 10. Specimens after tests on flattening

the Widmanstatten structure should not exceed the 3rd point of the scale of the 2nd Appendix B «Scales of banding orientation and Widmanstatten structure of boiler tube metal» [21].

When conducting metallographic examination of steamer tubes of the Uglegorsk TPP it was found that the initial structure of the tube metal is characterized by a significant banded orientation, which is a deviation from the standards and indicates a poor thermal treatment of tubes after rolling in the process of their manufacture. The structure of the sprayed specimen is ferrite-pearlite as in the reference one; visible structural changes were not found. Under the sprayed layer, a narrow borderline band of the base metal with a thickness from 0.07 to 0.15 mm is seen, which was subjected to interaction with a sprayed layer. The structure of the matrix of this band is the same as in the base metal — ferrite-pearlite. Within this band, the used etcher did not provide the inclusions of the sprayed material. However, it can be assumed that diffusion inclusions should be present in it.

The used etcher was not able to reveal any structural components in the structure of spraying (special chemical reagents were not used). However, it allowed establishing a loose-layer and porous (not monolithic) structure of spraying, caused by the technological

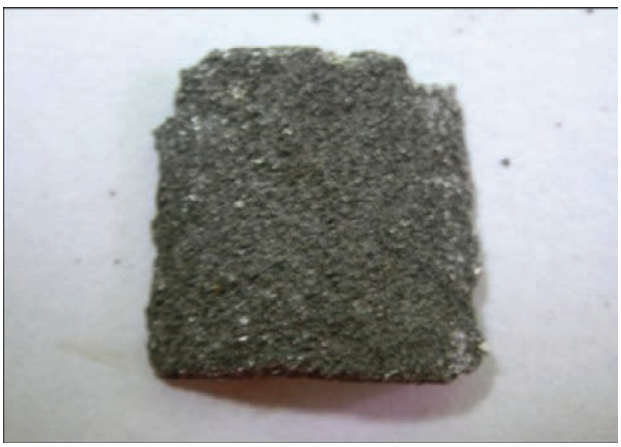

Figure 11. Delaminated layer after test on flattening

Figure 12. Macrostructure of sprayed tubes after six years of operation

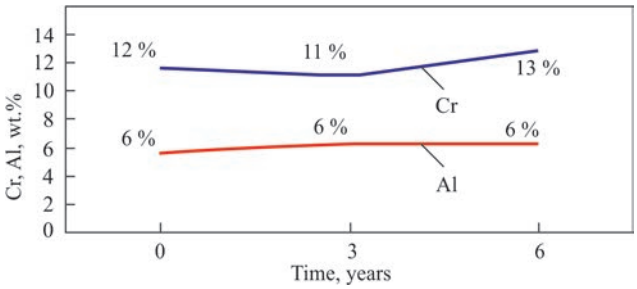

Figure 14. Change in the concentration of chromium and aluminium in the surface coating layer depending on service life

features of electric arc metallization. In both cases, the thickness of the sprayed layer varies in different sections of the tube. Thus, in the frontal point of the tube, the thickness of spraying reaches 0.42 mm, and on the side points it amounts to 0.2 mm. Taking into account the boundary layer of the base metal, which was subjected to diffusion of the sprayed material in it, it can be stated that the largest spraying thickness is 0.57 mm (on the frontal part of the bend). When carrying out technological tests on flattening cracks, tears over the base metal of the tube were not detected. After tests on flattening (Figure 10) for a delaminated layer (0.55 mm) (Figure 11), the X-ray fluorescence analysis was conducted, which showed the following chemical composition, wt.%: 11.7–12.21 Cr; 0.12 Ni; 4.0–5.65 Si; 4.37–5.87 Al; 0.37–0.44 S. Photo of the macrostructure of sprayed tubes after six years of operation is shown in Figure 11.

Destruction of the surface layer occurs by a delamination of large fragments of the sprayed layer. During mechanical tests for determining the tensile strength of the tube after spraying, the results were obtained given in Table 4.

The obtained results of mechanical tests meet the requirements of TU 14-3-460: 2009/TU U 27.2-05757883-207:2009 [21]. The areas of the sprayed layer has the hardness *HRC* 54–58. The surface layer under the delaminated coating has the following chemical composition, wt.%: 91.47 Fe; 2.78 Cr; 3.9 Si; 1.1 Al; 0.26 S. Hardness of the surface under the spraying layer is *HB* 200–217. Thus, the obtained

Table 4. Results of mechanical tests

σ_t, MPa	δ, %	ψ, %
51.1	28.2	58
TS 14-3-460:2009/TS 27.2-05757883-207:2009		
420–560	24	45

Table 5. Composition of sprayed layer after three-year operation at TPP

Number of specimen	Content of alloying elements, %				
	Fe	Cr	Al	Si	Ni
1	Base	11.41	5.67	5.67	0.15
2	Same	10.89	5.87	5.5	0.17

Table 6. Composition of sprayed layer after six-year operation at TPP

Number of specimen	Content of alloying elements, %				
	Fe	Cr	Al	Si	Ni
1	Base	12.9	6.67	7.9	0.1
2	Same	12.7	5.79	7.1	0.1

results may indicate that the base metal after spraying did not undergo significant changes in microstructure and mechanical properties and corresponded to the requirements of technical conditions. After a three-year operation of tubes and bends at the Trypillia TPP, a spectral analysis of the coating surface layer. Layer composition was changed insignificantly (Table 5).

When carrying out cuts after six years of operation, macro- and microstructure of sprayed tubes (Figures 12, 13), the composition of the surface layer were also recorded (Table 6). Technological tests on flattening, the measurement of hardness was not carried out. During operation, the surface becomes more rough, on the surface protruding carbides of different size are visible.

Examination of microstructure before and after the wear in the flow of a coal dust at the operating parameters of FWE show reorientation of the carbide frame in the matrix.

The surface diffusive layer has the following chemical composition, wt.%: 3.27 Cr; 1.87 Si; 0.9 Al; 0.3 S.

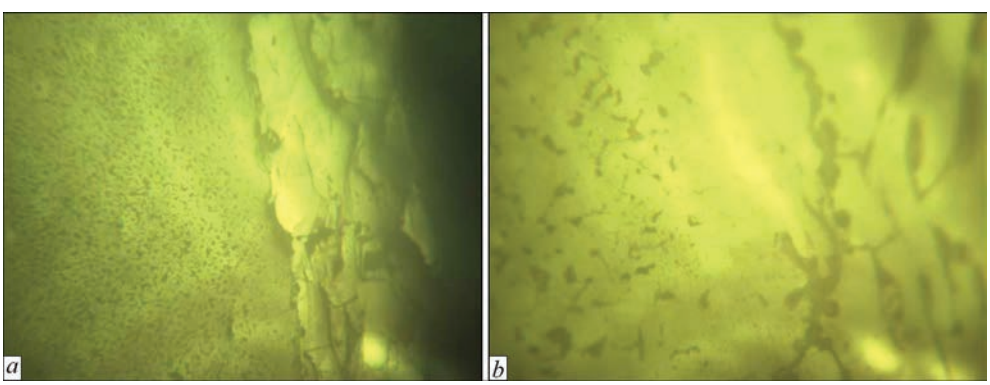

Figure 13. Microstructure of sprayed tubes after six years of operation: *a* — ×100; *b* — ×500

Table 7. Data from thinning of tube walls

Number of unit	Heating surface	Surface, working environment	Grade of material	Number of coil	Number of tube	Thinning, mm				Service life, h
						Left side	Right side	Outer	Inner	
1	FWE	ASh	St.20	152	1	–0.4	–0.4	–0.5	+0.2	11296
1	FWE	Same	Same	150	Same	–0.5	–0.5	–0.8	+0.1	12138
1	FWE (after spraying)			151		+0.4	+0.5	+0.7	+0.2	9084

Horizontal lines in Figure 14 show that during six years, the concentration of chromium in the surface layer almost did not change and even slightly increased, its accumulation in the surface layer occurs. An increase in the concentration of aluminium in the surface layer is most likely associated with precipitation of aluminium-containing elements, formed in the process of combustion of organic fuel on the tubes of coils.

Destruction of the surface layer during testing of specimens occurs by cracking of the coating into tiny fragments and its spalling. As is seen, the exposure of coatings at operating parameters leads to a change in the mechanics of their fractures, which is possibly caused by the change in the structure of the disperse phases. It was impossible to measure the hardness of the sprayed layer. The hardness of the surface under the spraying layer is *HB* 180. At each power plant, data from the actual thickness of the walls of the tubes of heating surfaces are collected, applying destructive and nondestructive methods. When carrying out cuts from tubes, data from tube thickness, microstructure and mechanical properties are fixed. To measure thinning of tubes, the procedure of direct measurement of the thickness of the wall is used. The summary data from thinning of the walls of tubes before spraying, as well as the time of each cut specimen are summarized in Table 7.

Analyzing data from thinning, it can be concluded that in all cases, with an increase in the operation time, the value of thinning the wall from the ash wear grows as well. The greatest intensity of the ash wear is observed on the first two tubes of steel 20 of extreme FWE coils. This phenomenon is most likely associated with a designing feature of the gas tract of a coal-dust П-shaped boiler. At the outlet from the upper radiation part, in a rotary chamber, the gases change their direction and the largest particles of fuel combustion products are thrown into the periphery of the general flow. An increase in their density in the flow contributes to the intensification of the ash wear of 20 extreme FWE coils [24]. After metallization of the surface of tubes of FWE coils, a decrease in the intensity of the ash wear of the coils was revealed. While measuring the thickness of the wall on the reference cuts, thinning was not recorded. Thus, in this case, it is possible to allow the presence of the influence of hardness on the rate of ash wear and conclude that with an increase in hardness wear resistance grows. This observation is agreed with a model of erosion wear [23].

CONCLUSIONS

In the work, the use of the method of electric arc spraying (metallization), performed by LLC «Rezon» to improve the reliability of the power equipment of TPP, was studied. According to the obtained data on mechanical, chemical and structural state of the tube metal and the coating layer, it can be concluded about the positive experience of introducing a method of electric arc spraying as a promising and highly effective method for increasing the reliability of power equipment. At the Trypillia TPP, two variants of welding tubes of steel 20 after metallization were investigated. The first is an electric arc welding of tubes after metallization by TsU-5 electrodes of 2.5 mm with the tubes that did not pass metallization. The second is welding by TsU-5 electrodes during alignment of tubes that passed metallization, with each other. When carrying out X-ray fluorescence analysis of welded joints, a slight increase in chromium content was revealed. An increased content of chromium in the welded joint is obviously associated with insufficient quality of surface preparation. During mechanical tests of the weld, fracture of the specimen occurs mainly over the base metal, indicating satisfactory mechanical properties of the weld. Microstructure of metal in the near-weld and weld zone in both cases is within the norm [21]. A lack of corrosion damages in the places of mounting the studied coils and a significant erosion wear of the FWE tube walls, as compared to untreated spraying, with conventional methods of individual protection of coils, indicates a successful realization of the technology, as is evidenced by an increase in the life of the boiler tube.

REFERENCES

1. Shrajber, A.A., Yatsenko, V.P. (2008) Modeling of abrasive wear of convective heat exchange surfaces of boiler. *Problemy Zagalnoi Energetyky*, **17**, 37–40 [in Russian].
2. *Accident rate in the facilities of electrical power engineering of Ukraine in 2004.* http://mpe.kmu.gov.ua/minugol/control/uk/doccatalog/list.

3. *Inspection of technology violoation in electrical power engineering of Ukraine in fourth quarter of 2005*. http://mpe.kmu.gov.ua/minugol/control/uk/doccatalog/list
4. Soltani, M., Chahartaghi, M., Majid Hashemian, S., Faghih Shojaei, A. (2020) Technical and economic evaluations of combined cooling, heating and power (CCHP) system with gas engine in commercial cold storages. *Energy Conversion and Management*, **214**. Article number: 112877.
5. Yang, S., Zhang, L., Fan, J., Sun, B. (2021) Experimental study on erosion behavior of fracturing pipeline involving tensile stress and erosion prediction using random forest regression. *J. of Natural Gas Sci. and Engin*., **87**. Article number: 103760.
6. Maidanik, M.N., Tugov, A.N., Vereshchetin, V.A. (2020) Assessment of Boiler Units' Technical State Based on Quality Indicators. *Thermal Engineering*, 67**(4)**, 216–222.
7. Kiselev, S.P., Kiselev, V.P., Maximovsky, E.A. et al. (2019) Mechanism of formation of intermetallic coatings by the cold spray technology. *J. of Physics*, Conf. Series, **1677**, 1. Article number: 012136.
8. Sethi, A.K. (2020) Studies on hard surfacing of structural steel by gas thermal spraying process. In: *Proc. of Int. Conf. on Mechanical and Energy Technologies*, **21**, 1436–1440.
9. Shatov, A.P. (2009) *Welding and repair of metal structures of anticorrosion coatings*. Moscow, MGTU [in Russian].
10. Panteleenko, F.I., Snarsky, A.S., Krylenko, A.V. (2012) Peculiarities of structure degradation and mechanical properties of components of furnace and heat-and-power engineering equipment after long term service. *Nauka i Tekhnika*, **1**, 16–20 [in Russian].
11. Som Dutt Sharma, S.D., Saluja, R., Moeed, K.M. (2013) A review on the effect of preheating and/or post weld heat treatment (PWHT) on hardened steel. *Int. J. of Technical Research and Applications*, **1**, 5–7.
12. Feng, L., Yang, N. (2019) Stainless steel welding and development trend of welding technology. In: *IOP Conf. Series: Earth and Environmental Sci.*, **252**, 2, Article number: 022117.
13. Yatsenko, V.P. (2006) Prediction of erosion wear of heat exchange surfaces ob boiler equipment. *Problemy Zagalnoi Energetyky*, **13**, 81–85 [in Russian].
14. Birkin, P.R., Lear, R., Webster, L. et al. (2020) In-situ detection of single particle impact, erosion/corrosion and surface roughening. *Wear*, **464–465**. Article number: 203527.
15. Korzh, V.M. (2005) *Thermal treatment of materials*. Kyiv, Ekotekhnologiya [in Ukrainian].
16. Lashchenko, G.I. (2012) *Modern technologies of welding production*. Kiev, Ekotekhnologiya [in Russian].
17. Hirohata, M., Takeda, F., Konishi, H., Itoh, Y. (2018) Effect of weld line direction and paint orientation on corrosion and paint deterioration characteristics of welded part of steel. *Corrosion Engin. Sci. and Technology*, 53**(8)**, 591–600.
18. *Instruction on restoration of worn-out and new bends and straight pipe areas of heating surfaces of high-pressure boilers by gas powder surfacing*. I 34-70-027-87 [in Russian]. http://online.budstandart.com/ru/catalog/doc-page?id_
19. doc=68749.
20. Grechneva, M.V., Goppe, G.G. (2015) Gas powder spraying of heating surface pipes of boiler units of thermal power stations. *Vestnik IrGTU*, **11**, 106, 23–27 [in Russian].
21. Malchevsky, I.A., Bespalov, S.A. (2017) *Prospective scientific and technical developments. Energetyka ta Energoefektyvnist*. Kyiv, Akademperiodyka [in Ukrainian].
22. TU U 14-3-460:2009/TU U 27.2-05757883-207:2009*: Seamless steel pipes for steam boilers and pipelines* [in Russian]. https://files.stroyinf.ru/Index2/1/4293733/4293733499.htm
23. *TI* 00130044.25101.00549: *Deposition of protective coating on coils of feed-water economizer and water wall tubes of boiler TP-100. Lviv, SE Lviv Design Bureau.* https://patonpublishinghouse.com/eng/journals/as/2019/05/04/
24. RD.15.027–89: *Welding, heat treatment and inspection of pipe systems of boilers and pipelines in mounting and repair of power plant equipment.* http://docs.cntd.ru/document/1200026674
25. Ruff, A.W., Wiederhorn, S.M. (1979) Erosion by solid particle impact. *Treatise on Mater. Sci. and Technol.*, **16**, 69–126.

CONFLICT OF INTEREST

The Authors declare no conflict of interest

CORRESPONDING AUTHOR

A.V. Hruzevych
Trypillia TPP PJSC «Centrenergo»
1 Promyslova Str., 08720, Ukrainka, Ukraine
E-mail: hruzevych6635@kpi.com.de

SUGGESTED CITATION

A.V. Hruzevych and V.V. Shvets (2021) Improving the reliability of power complex equipment by electric arc spraying. *The Paton Welding J*., **10**, 38–46.

JOURNAL HOME PAGE

https://pwj.com.ua/en

Received 20.08.2021
Accepted: 11.11.2021

https://doi.org/10.37434/tpwj2021.10.07

EFFECT OF THE ANGLE OF INCIDENCE OF ABRASIVE PARTICLES ON THE EROSIVE WEAR RESISTANCE OF HVOF-SPRAYED COMPOSITE COATINGS

M. Szymura

Silesian University of Technology Department of Welding
18A Konarskiego Str., 44-100, Gliwice, Poland

ABSTRACT

The study presents test results concerning resistance to impingement erosion caused by solid particles transported in the gas stream. The angle at which the erosive jet affected the HVOF-sprayed coatings made using the Ni–WC flux-cored wire amounted to 30° and 90°. The study included microhardness measurements and the microscopic metallographic specimens of the deposited (sprayed) coatings.

KEY WORDS: thermal spray, wire-high-velocity oxy-fuel (W-HVOF), erosion, flux cored wire

High-quality erosive wear resistant coatings can be obtained using processes where particles of deposited materials are accelerated to supersonic velocity (e.g. the high velocity oxy fuel process (HVOF)). Presently, HVOF process-related tests are primarily concerned with coating formed through the melting of the coating material in the form of powder. In comparison with the powder, the coating material in the form of a wire is cheaper to manufacture and can be sprayed at higher deposition rates [1, 3, 8, 10].

Erosive wear processes reduce the service life of various machinery parts. In industry, erosion is estimated to be responsible for the wear of approximately 8 % of machine elements. Welding technologies enable the deposition of erosion-resistant coatings and layers [4, 9, 10].

The intensity of the erosive wear of sprayed coatings depends, among other things, on the angle of incidence of abrasive particles. In erosion resistance tests, composite Ni–WC coatings may demonstrate the unequal loss of volume in relation to the extreme angles of incidence of the erosive jet. Available reference publications present test results concerning the erosive wear resistance of HVOF powder sprayed coatings. However, related publications do not contain quantitative data making it possible to compare the intensity of the erosive wear of HVOF-sprayed coatings (deposited using the composite wire) in relation to various impact angles of abrasive particles. The above-named lack of information inspired an attempt to identify the effect of the angle of incidence of the erosive jet on the erosive wear resistance of HVOF-sprayed coatings deposited using the wire [1, 2, 6, 7, 10].

Copyright © The Author(s)

The study presents test results concerning resistance to impingement erosion triggered by solid particles contained in the gas jet striking the surface at an angle of 30° and 90°. The HVOF-sprayed coatings (made using an Ni–WC flux-cored wire) used in the tests had various thicknesses. The scope of the tests also included microhardness measurements and microscopic metallographic tests of deposited coatings.

Test materials. The HVOF spraying process involved the use of a HARDFACE NICARBW flux-cored wire (manufactured by Welding Alloys company) having a diameter of 2.4 mm, providing the obtainment of composite weld deposit containing particles of tungsten carbide in the nickel alloy matrix (group Ni20 in accordance with PN-EN 14700:2014-06). The core of the wire contained cast and crushed irregularly-shaped particles of tungsten carbide sized restricted within the range of 150 to 350 μm. The mass content of tungsten carbide particles in the wire amounted to 50 %. Recommendations concerning the use of the HARDFACE NICARBW wire include the cladding of surfaces exposed to intense erosive wear. According to the manufacturer, the wire can also be used in arc spraying [11]. The base material used in the tests had the form of specimens (75×25×15 mm) cut out of a plate made of unalloyed steel S355JR (according to PN-EN 10025-2:2019-11).

Tests. *Erosive wear resistance tests.* The tests, aimed to identify the significance of differences in the erosive wear resistance of coatings in relation to various angles of incidence (of abrasive particles), were performed using the Student's *t*-test, adopting significance level $\alpha = 0.05$. The thicknesses of the coatings amounted to approximately 100, 200 and 300 μm.

Table 1. Parameters used in the spraying of coatings

Oxygen flow rate, l/min	Propane flow rate, l/min	Air flow rate, l/min	Wire feed rate, cm/min	Spraying distance, mm
180	40	500	46,0	150

The tests of erosive wear resistance were performed in relation to two impact angles 30° and 90° respectively. The study involved the performance of 6 erosive wear resistance tests in relation to each coating thickness and each angle of incidence. Before spraying, the specimens were subjected to dry abrasive grit blasting. The HVOF spraying process was carried out using the Metatherm HVOF-W1000 system manufactured by Metatherm Verschleißschutz GmbH company. In this system, the wire is continuously feeding into the propane/oxygen flame. The droplets created from wire, are deposited to the prepared substrate with compressed air [12]. The technological parameters used when making the coatings are presented in Table 1.

The tests concerning resistance to erosion resulting from the impingement of solid particles in the gas jet were performed in accordance with the ASTM G76-18 standard using abrasive particles (Al_2O_3) having a nominal size of 50 μm. During the tests, the feed rate of the abrasive particles amounted to 2.2 g/min, whereas their velocity in the compressed air jet amounted to approximately 70 m/s. The nozzle tube was located 10 mm away from the specimen surface. The time of each test amounted to 10 minutes. The identification of the erosive wear resistance of the coatings involved measurements concerning the loss of mass and density. Before and after each test, specimens were weighed using a laboratory balance with an accuracy of up to 0.0001 g. Measurements of coating density involved one specimen representing a given coating thickness. The average coating density was determined using the laboratory balance on the basis of three measurements of the density of a given coating, weighed in air and in liquid. The loss of volume was determined (using formula (1)) on the basis of the loss of mass and the average density of a given coating. Related results are presented in Table 2.

$$V_1 = \frac{M_1}{\rho} \cdot 10^3, \tag{1}$$

where V_1 — loss of coating volume, mm^3; M_1 — loss of specimen mass, g; ρ — coating density, g/cm^3.

In accordance with the concept of the Student's *t*-test, first it was necessary to verify if erosion resistance-related test results were characterised by normal distribution and whether their variances were the same. The hypothesis of the normal distribution of the test results was verified using the Shapiro–Wilk test, adopting significance level $\alpha = 0.05$. In addition to the volume losses of in relation to the coating having a thickness of approximately 200 μm and an incidence angle of 90°, calculated values of W_d were restricted within the range, the ends of which were quantiles of distribution. In relation to the above-presented test results there was no basis for rejecting the hypothesis of the normal distribution in relation to a significance level of 0.05. Because of the assumptions of the Student's *t*-test, further analysis only involved groups of erosion test results characterised by normal distribution. The hypothesis of the equality of the variances

Table 2. Test results concerning the erosive wear resistance of the HVOF-sprayed coatings made using the Ni–WC flux-cored wire

Coating thickness, μm	Loss of coating volume, mm^3						
	1	2	3	4	5	6	Average value for individual levels
Approx. 100	0.2935*; 0.2348**	0.2054*; 0.3131**	0.2837*; 0.3620**	0.3815*; 0.3033**	0.3522*; 0.2837**	0.3033*; 0.2739**	0.3033*; 0.2951**
Approx. 200	0.3252*; 0.3153**	0.3449*; 0.3350**	0.2365*; 0.3547**	0.3941*; 0.2168**	0.3350*; 0.3843**	0.3449*; 0.3646**	0.3301*; 0.3285**
Approx. 300	0.3467*; 0.2674**	0.3764*; 0.3764**	0.2972*; 0.3665**	0.3071*; 0.2476**	0.2774*; 0.4061**	0.3665*; 0.2278**	0.3286*; 0.3153**
In relation to all results							0.3206*; 0.3130**

*In relation to an incidence angle of 30°.
**In relation to an incidence angle of 90°.
The loss of the volume of sprayed coatings was identified using formula (1). The density of the coating having a thickness of approximately 100 μm amounted to 10.2219 g/cm^3; that having a thickness of 200 μm amounted to 10.1487 g/cm^3 and that having a thickness of 300 μm amounted to 10.0954 g/cm^3.

Table 3. Microhardness results (*HV*0.1) related to the cross-section of the HVOF-sprayed coatings made using the Ni–WC flux-cored wire

Coating thickness, μm	Point of measurement of coating matrix microhardness			Average microhardness of coating matrix, *HV*0.1	Point of measurement of tungsten carbide microhardness in the coating			Average microhardness of tungsten carbides in the coating, *HV*0.1
	1	2	3		4	5	6	
Approx. 100	398	299	375	357	2107	1834	1660	1867
Approx. 200	443	386	324	384	1842	1917	1685	1815
Approx. 300	361	458	346	388	1707	1774	2116	1866

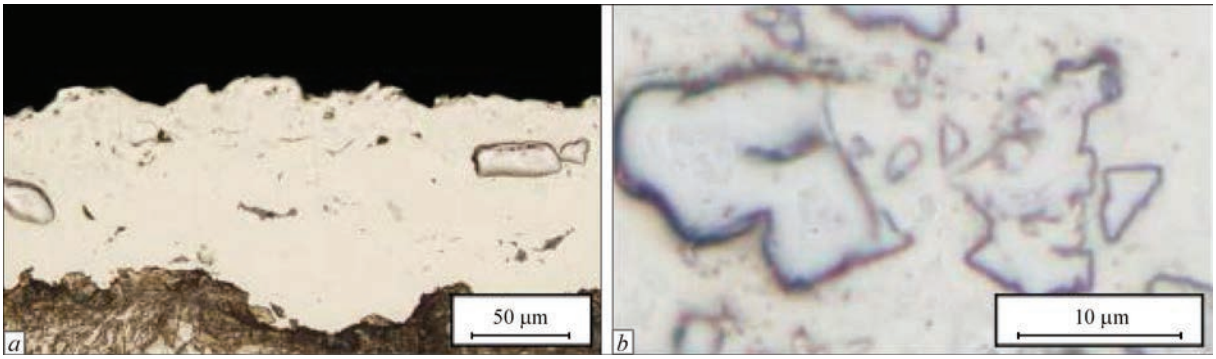

Microstructure of deposited coatings having a thickness of approximately: *a* — 100 μm, mag. ×400; *b* — 200 μm, mag. ×1000

of groups of erosive wear resistance test results was verified using the Hartley test. As the calculated values of H_{calc} were not restricted within the critical set in relation to a significance level of 0.05, there was no basis to reject the hypothesis subjected to verification. The calculated value of the Student's *t*-test was lower than the critical value $t_{0.05;\,10}$ of the aforesaid test. Because of the foregoing, it can be stated that the volume loss values obtained in the tests concerning the erosive wear resistance of coatings of given thicknesses did not differ significantly in terms of the angle of incidence (30° and 90°) of the erosive jet.

Microhardness measurements. The microhardness of the coatings sprayed using the Ni–WC wire was measured using the Vickers hardness test performed in accordance with the PN-EN ISO 6507-1:2018-05 standard. The cross-section of one specimen representing a given thickness of the coating was subjected to 3 measurements concerning the microhardness of the matrix and the microhardness of tungsten carbides. The obtained microhardness test results are presented in Table 3.

Metallographic tests. The identification of the quality and the porosity of the coatings as well as the content of the reinforcing phase and the size of its particles required the performance of microscopic metallographic tests. The metallographic tests of selected coatings involved the use of a light microscope and cross-sectional metallographic specimens. The results of the metallographic test results are presented in Figure *a* and *b*. The computer-aided analysis of the images of the specimen microstructure enabled the determination of coating porosity (Table 4) as well as the volume fraction and the geometrical dimensions of tungsten carbide particles.

The distribution of tungsten carbides in the coatings was not uniform. The measured content of tungsten carbides in the coatings did not exceed 33.3 % by volume, whereas their size was restricted within the range of approximately 1 to 62 μm.

Analysis of test results. The test results concerning the erosive wear resistance of the coatings deposited using the Ni–WC flux-cored wire revealed that, regardless of the coating thickness and the angle of erosive jet incidence, the coatings were characterised by high erosion resistance. The average loss of coat-

Table 4. Test results related to the porosity of the HVOF-sprayed coatings made using the Ni–WC flux-cored wire

Coating thickness, μm	Coating porosity, %
Approximately 100	2.0
Approximately 200	2.6
Approximately 300	2.9

ing density as regards individual coating thicknesses (determined in the test based on the ASTM G76-18 standard) was restricted within the range of 0.3033 to 0.3301 mm^3 in relation to an incidence angle of 30° and within the range of 0.2951 to 0.3285 mm^3 in relation to an incidence angle of 90°.

The tests aimed to determine the significance of differences in erosive wear resistance in relation to various angles of incidence (of abrasive particles) involved the use of the Student's *t*-test statistics. In relation to adopted level of significance $\alpha = 0.05$, in terms of the coatings having a thickness of approximately 100 and that of 300 μm, the calculated values of the Student's *t*-test were lower than critical value $t_{0,05;\,10}$ of the aforesaid test. Therefore, it can be stated that volume loss values obtained in the erosive wear resistance tests of coating thicknesses in relation to related angles of erosive jet incidence (30° and 90°) did not differ significantly. The foregoing could probably be ascribed to the composite structure of the coating (hard particles of tungsten carbide in the relatively soft nickel alloy matrix) affected by two models of wear, i.e. brittle cracking (reinforcing elements) and plastic deformation (matrix) [6]. It should be emphasized that the volume losses identified in the erosive wear resistance tests are not a permanent material feature as they may change along with changes of related parameters [5, 10]. The low porosity of the sprayed coatings, restricted within the range of 2.0 to 2.9 %, favours the lower intensity of erosive wear [10].

The average values of the microhardness of the matrix in individual coatings were restricted within the range of 357 *HV*0.1 to 388 *HV*0.1, whereas the microhardness range in relation to a given coating thickness was between 99 *HV*0.1 and 119 *HV*0.1. The cross-sectional microhardness of tungsten carbide particles was restricted within the range of 1660 *HV*0.1 to 2116 *HV*0.1.

The microscopic metallographic tests did not reveal the separation of the coating from the substrate or the presence of cracks in the coating in any of the analysed variants of coating thickness. The arrangement of tungsten carbides in the coating was not uniform. The size of tungsten carbide particles in the coating was restricted within the range of approximately 1 to 62 μm. The highest identified content of tungsten carbide particles amounted to 33.3 % by volume. The above-named value was lower than the volume fraction of tungsten carbide grains contained in the core of the flux-cored wire used in the spraying process. The most probable reasons for the decrease in the content of tungsten carbide particles in the coating include their dissolution during the spraying process, directing the particles outside the surface being coated as well as the reflection of the particles against the substrate or their improper deposition in the coating.

CONCLUSIONS

The tests concerning the properties of HVOF-sprayed composite coatings made using the Ni20 flux-cored wire justified the formulation of the following conclusions:

1. The values of volume losses identified in the erosive wear resistance tests of the coatings in relation to an erosive jet angle of 30° and that of 90° did not differ significantly.

2. The average microhardness of the coating matrix was restricted within the range of 357 *HV*0.1 to 388 HV0,1, whereas the average microhardness of the tungsten carbide particles was restricted within the range of 1815 *HV*0.1 to1867 *HV*0.1.

3. The arrangement of tungsten carbides in the deposited coatings was not uniform. The measured content of tungsten carbide particles in the coatings did not exceed 33.3 % by volume, which indicated the lower amount of tungsten carbides in the coating than that in the composite material which was used to make the coatings. The size of tungsten carbide particles in the coatings was restricted within the range of approximately 1 to 62 μm. Regardless of the thickness of the coatings, their porosity did not exceed 2.9 %.

Publication was supported by Own Scholarship Fund of the Silesian University of Technology in the year 2019/2020; grant number: 31/FSW18/0003-03/2019.

REFERENCES

1. Berger, L. M., Saaro, S., Naumann, T. et al. (2008) Microstructure and properties of HVOF-sprayed chromium alloyed WC–Co and WC–Ni coatings. *Surface and Coatings Technology*, 202(**18**), 4417–4421.
2. Chen, Y., Wu, Y., Hong, S. et al. (2020) The effect of impingement angle on erosion wear characteristics of HVOF sprayed WC–Ni and WC–Cr_3C_2–Ni cermet composite coatings. *Materials Research Express*, 7(**2**), 026503.
3. Cheng, D., Xu, Q., Trapaga, G., Lavernia, E.J. (2001) The effect of particle size and morphology on the in-flight behavior of particles during high-velocity oxyfuel thermal spraying. *Metallurg. and Mater. Transact. B*, **32B**, 525–535.
4. Eyre, T.S. (1976) Wear characteristics of metals. *Tribology Int.*, 9(**5**), 03-212.
5. Hussainova, I., Kubarsepp, J., Pirso, J. (2001) Mechanical properties and features of erosion of cermets. *Wear*, 50(**1–12**), 818–825.

6. Kleis, I., Kulu, P. (2008) *Solid particle erosion: Occurrence, prediction and control*. Springer-Verlag London Limited, 19–21, 107–108.
7. Oka, Y.I., Ohnogi, H., Hosokawa, T., Matsumura M. (1997) The impact angle dependence of erosion damage caused by solid particle impact. *Wear*, **203**, 573–579.
8. Qiao, L., Wu, Y., Hong, S. et al. (2021) Wet abrasive wear behavior of WC-based cermet coatings prepared by HVOF spraying. *Ceramics Int.*, 47(**2**), 1829–1836.
9. Staniša, B., Ivušić, V. (1995) Erosion behaviour and mechanisms for steam turbine rotor blades. *Wear*, **186**, 95–400.
10. Tu, J.P., Liu, M.S., Mao, Z.Y. (1997) Erosion resistance of Ni–WC self-fluxing alloy coating at high temperature. *Wear*, 209(**1–2**), 43–48.
11. *Welding Alloys Group' catalogue* (2018) Cored Wires. Hardfacing. Cladding – Weld overlay – Surfacing.
12. *User manual HVOF-W1000* (2013) HVOF-W1000 Hochgeschwindigkeitsflammspritzanlage für Draht.

CORRESPONDING AUTHOR
M. Szymura
Silesian University of Technology Department of Welding
18A Konarskiego Str., 44-100, Gliwice, Poland
E-mail: m.szymura.jr@gmail.com

SUGGESTED CITATION
M. Szymura (2021) Effect of the Angle of incidence of abrasive particles on the erosive wear resistance of HVOF-sprayed composite coatings. *The Paton Welding J.*, **10**, 47–51.

JOURNAL HOME PAGE
https://pwj.com.ua/en

Received 22.09.2021
Accepted: 11.11.2021

https://doi.org/10.37434/tpwj2021.10.08

PRODUCTION OF TITANIUM INGOTS WITH REGULATED OXYGEN CONTENT BY ELECTRON BEAM MELTING

S.V. Akhonin[1], **O.M. Pikulin**[1], **V.O. Berezos**[1], **A.Yu. Severin**[1] and **O.G. Erokhin**[2]

[1]E.O. Paton Electric Welding Institute of the NASU
11 Kazymyr Malevych Str., 03150, Kyiv, Ukraine
[2]SC «SPC «Titan» of the E.O. Paton Electric Welding Institute of the NASU»
26 Raketna Str., 03028, Kyiv, Ukraine

ABSTRACT

Comprehensive research work was performed to produce ingots of Grade 2 titanium alloy of 600 mm diameter with regulated oxygen content of 0.12–0.16 % and an ingot of Grade 3 titanium alloy of 1100 mm diameter and up to 3 m length by the method of electron beam cold-hearth melting in the production facilities of SC «SPC «Titan» of the E.O. Paton Electric Welding Institute of the NAS of Ukraine» in multifunctional electron beam unit UE5810. A method of forming the charge billet and a formula for calculation of the amount of TiO_2 powder for alloying are proposed. Defectfree ingots of titanium alloys of Grade 2 and Grade 3 with regulated oxygen content were produced and the range of deviation of its distribution in the ingot metal of ± 0.02 % was provided. It is shown that the proposed modes of electron beam heating of the consumable billet, metal melting in the cold hearth and in the mould, as well as the melting rate ensure complete dissolution of titanium dioxide particles in the cold hearth, and absence of defects in the produced ingots, enriched in oxygen.

KEY WORDS: electron beam cold hearth melting; electron beam unit; titanium ingot; oxygen; regulated oxygen content; titanium dioxide; melting rate; macrostructure

Titanium, as one of the most important modern structural materials, is becoming more and more often used in medicine, construction industry and production of consumer goods. However, just about 5 % of titanium raw materials that are mined in the world today are processed into metallic titanium and its alloys, which are of greatest importance for many sectors of industry. Here, it should be noted that titanium-based alloys, the strength of which is 4–5 times higher than that of pure titanium, are now becoming ever wider applied [1, 2].

At present, alongside a stable global tendency to increase the use of titanium alloys in different industries, the issue of the high cost of titanium and its alloys remains unsolved [3]. The cost of titanium alloys is inseparably connected with the technology of producing them and ensuring the required mechanical properties. In order to increase the level of mechanical properties, titanium alloys have expensive alloying elements (aluminium, vanadium, zirconium, silicon, molybdenum) in their base [3]. However, it should be noted that sparsely-alloyed titanium alloys have been more and more widely accepted in recent years, in which the expensive alloying elements are replaced by inexpensive and available elements, namely iron, carbon, oxygen and nitrogen [4, 5]. At alloying by such elements it is taken into account that α-stabilizers are nitrogen, oxygen and carbon, which ensure the greatest increase of strength in titanium alloys, and β-stabilizer is iron.

In the small concentration range (up to 0.02 wt.%) each one hundredth fraction of oxygen increases the ultimate strength and yield limit of titanium by approximately 1.0–1.25 kgf/mm^2. Oxygen has the most noticeable effect on the mechanical properties of titanium at its concentration of up to 0.6 wt.% in the metal [6]. In this case, a considerable increase of strength is observed at relatively small drop of the ductility properties. At the same time, at oxygen concentration of more than 0.7 wt.%, titanium completely looses its capacity for plastic deformation. Thus, controlling oxygen content in the metal to a certain extent allows reaching an optimum ratio of ductility and strength characteristics of the titanium alloy. Therefore, oxygen can be regarded as a promising alloying element to produce new titanium alloys. It is particularly important for medical products, for which corrosion resistance and biocompatibility come to the fore, alongside the mechanical properties. Unlike other alloying components (for instance, vanadium) oxygen is safer [6–8].

Over the last decades, local and foreign metallurgists performed a number of studies on producing titanium, alloyed by oxygen [6, 7, 9], both from the gas phase during chamber electroslag remelting [7, 9], and with application of titanium dioxide powder as an alloying element at its addition to the charge billet [10, 11].

Copyright © The Author(s)

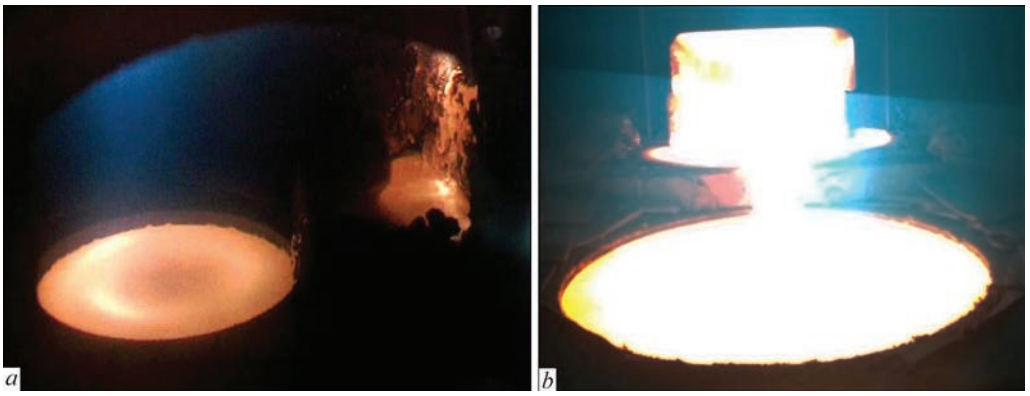

Figure 1. The process of producing titanium alloy ingots of Grade 2 (*a*) and Grade 3 (*b*)

It should be noted that today titanium and its alloys are produced by the following special electrometallurgy methods: vacuum-arc and plasma-arc remelting; vacuum-induction, electroslag and electron beam melting of titanium [12, 13]. The technology of vacuum-arc remelting of the consumable electrode became the most widely accepted. However, electron beam cold hearth melting (EBCHM) is the most promising from the viewpoint of metal refining, removal of nonmetallic inclusions of high and low density.

At titanium alloying by titanium dioxide powder it should be taken into account that its melting temperature is equal to 1870 °C that is higher than titanium melting temperature (1670 °C), so that titanium dioxide will not melt, but dissolve in the melt. In its turn, EBCHM is a technology, which, owing to an independent heat source, enables regulating the charge billet melting rate is a wide range, which allows regulation of the duration of the metal staying in the liquid overheated state. Thus, EBCHM technology can be regarded as the most efficient one for obtaining titanium ingots, alloyed by oxygen.

So, taking into account the experience of studies performed by the authors in work [11], it was proposed to conduct at PWI investigations on producing ingots of oxygen-doped titanium alloys. During investigations a batch of ingots of Grade 2 titanium alloy of 600 mm diameter with regulated oxygen content within 0.12–0.16 % an of and ingot of Grade 3 titanium alloy of 1100 mm diameter with regulated oxygen content within 0.28–0.32 % were melted in the production facilities of SC «SPC «Titan» of the E.O. Paton Electric Welding Institute of the NAS of Ukraine» in a multifunctional electron beam unit UE5810 (Figure 1).

Materials and investigation procedures. In order to obtain a uniform regulated oxygen content in ingots of titanium alloys of Grade 2 and Grade 3, a method to form the charge billet was proposed, which is based on that a water-dispersed emulsion of TiO_2 powder (Figure 2) is uniformly applied along its length as an alloying element, with further drying of the charge billet.

To obtain the specified level of oxygen in the metal, the required quantity of TiO_2 powder is calculated by the following formula:

$$M[TiO_2] = K(M_{in}[O]_{sp}\,\% - M_{bil}[O]_{bil}\,\%),$$

where $M[TiO_2]$ is the weight of TiO_2 powder for preparation of its water-dispersed emulsion; $K = 0.025$ is the coefficient of proportionality, which allows for oxygen percentage in TiO_2 powder; M_{in} is the ingot weight; $[O]_{sp}$ % is the specified oxygen percentage in the ingot; M_{bil} is the charge billet weight; $[O]_{bil}$ % is the oxygen percentage in the charge billet.

Considering that the melting temperature of TiO_2 powder is almost 200 °C higher than that of pure titanium, oxygen-enriched zones appear at its dissolution in the melt. In its turn, in keeping with titanium-oxygen constitutional diagram, titanium with a higher oxygen content has a higher melting temperature than that of pure titanium. The authors of work [14] established that at melt overheating above the titanium melting temperature by more than 150 °C, increase or decrease of the inclusion diameter two times, extends or shortens the dissolution time two times, accordingly, and at melt overheating by less than 150 °C increase or decrease of inclusion diameter two times extends or shortens the dissolution time three times, respectively. If the melt does not have enough time to

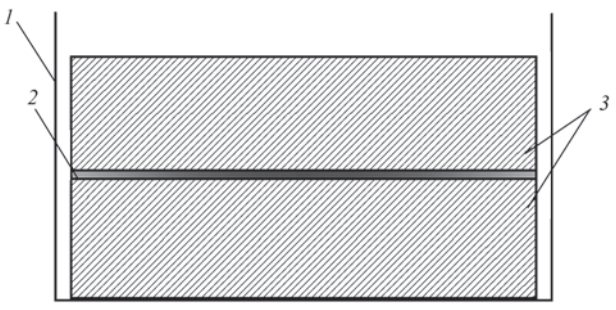

Figure 2. Scheme of the cross-section of the charge billet: *1* — nonconsumable box; *2* — layer of TiO_2 powder; *3* — charge billet

Figure 3. Ingot of Grade 3 titanium alloy of 600 mm diameter after EBCHM

homogenize before pouring into the mould, the oxygen-enriched metal can solidify ahead of the crystallization front, as its solidification temperature is higher, and it can form a zone of higher hardness in the ingot [14]. Here, micropores can form. Thus, it is necessary to reach a higher temperature of the melt, overheating the metal and soaking it in such a state the longer, the thicker is the TiO_2 layer in the charge billet.

Thus, only the homogenized melt, kept for the required time in the cold hearth, should be poured into the mould. Therefore, it is necessary to take into account the cold hearth geometry and the melting rate [14]. Based on the investigations performed by the authors in work [14], and taking into account the geometry of the cold hearth in electron beam unit UE5810, modes of electron beam heating of the consumable billet, metal melting in the cold hearth and in the mould, as well as the melting rates for ingots of 600 and 1100 mm diameter, were proposed. Thus, the total specific heating power was equal up to 0.14 kW/cm^2 for ingots of 600 mm diameter, and up to 0.11 kW/cm^2 for ingots of 1100 mm diameter. Here, the melting rate was 270 kg/h for 600 mm ingots, and 275 kg/h for 1100 mm ingots.

The process of producing the titanium ingots, alloyed by oxygen, was conducted as follows. Preparation of the initial charge billet was performed, along the length of which water-dispersed emulsion of TiO_2 powder was uniformly applied as an alloying element, with further drying of the charge billet. Then, electron beam cold hearth remelting of this initial charge billet was performed. The ingot was produced by periodically pouring the melt portions from the cold hearth into the mould, where its heating and periodical drawing were performed. The process was carried on up to deposition of the ingot of the required length. After that the ready ingot was cooled in a chamber to the required temperature under vacuum.

As a result of the conducted melting operations, titanium alloy ingots of Grade 2 of 600 mm diameter (Figure 3) and of Grade 3 of 1100 mm diameter and up to 3 m length were produced.

Examination of the quality of the produced ingots showed that their surface after cooling in vacuum is clean, oxidized or alpha layers are absent. The depth of surface defects in the form of corrugations which are characteristic for electron beam melting, is not more than 1–3 mm. Defects in the form of tears, cracks or lacks-of-fusion are absent.

Produced ingots of Grade 2 titanium alloy of 600 mm diameter were used to cut out transverse templates at 150 mm distance from the head and bottom part and from the ingot middle to study oxygen distribution along its length and cross-section. In Grade 3 titanium ingot of 1100 mm diameter the transverse templates were cut out from its head and bottom part.

Investigation results and their discussion. Investigations of the chemical composition of the ingots produced by the proposed method showed (see Table 1) that the impurity element content meets the requirements of the standards for titanium alloys of Grade 2 and Grade 3. Analysis of the results of studying the chemical composition of ingots with regulated oxygen content (see Table 1) showed that the proposed process of alloying by titanium dioxide powder and method to calculate its required quantity allows rather precisely reaching the required level of oxygen in the ingot metal under the condition of exact following of the melting modes.

Hydrogen concentration in the metal of the studied ingots did not exceed 0.002 %. No increased content of nitrogen was revealed, either in the bottom, or in the head part of the ingots, its maximum concentration being 0.02 %. Iron concentration in the studied ingot metal was in the range from 0.08 up to 0.13 %.

The quality of titanium ingot metal is due to absence of nonmetallic inclusions in it, particularly in the form of nitrogen-containing alpha particles or titanium nitrides, leading to formation of defects, which negatively affect the titanium alloy mechanical properties.

Therefore, after machining of the surface layer of the produced ingots (Figure 4), ultrasonic flaw detection method was used to detect inner defects in the form of nonmetallic inclusions, pores and discontinuities. Investigations of the ingot metal were conducted by sequential manual scanning of the side surface by the radius along the entire longitudinal axis of the ingot. To guarantee covering of the entire ingot volume, all of its side surface was scanned. Ultrasonic testing of the ingot metal was performed using ultrasonic

Table 1. Chemical composition of metal of titanium alloy ingots of Grade 3 of 1100 mm diameter and of Grade 2 of 600 mm diameter produced by EBCHM, wt.%

Alloy	Ingot part	Sampling location	C	Fe	O	N	H	Other elements (max), total
Grade 3	Top	Surface	0.01	0.08	0.29	0.01	0.002	0.13
		1/2 of radius	»	»	0.27	»	»	0.11
		Center	»	0.09	»	»	»	»
	Middle	Surface	»	0.10	0.29	»	»	0.12
	Bottom	Surface	0.02	»	0.30	0.02	»	»
		1/2 of radius	0.01	0.11	»	0.01	»	0.10
		Center	»	»	»	»	»	»
	ASTM B977-13		≤0.08	≤0.30	≤0.35	≤0.05	≤0.003	≤0.40
Grade 2	Top	Surface	0.02	0.11	0.13	0.01	0.002	0.13
		1/2 of radius	0.01	0.10	»	»	»	0.11
		Center	»	»	0.12	»	»	0.14
	Middle	Surface	»	»	0.15	0.02	»	0.11
		1/2 of radius	0.02	0.09	0.14	»	»	0.13
		Center	0.01	0.10	»	0.01	»	0.14
	Bottom	Surface	0.02	0.13	0.16	»	»	0.16
		1/2 of radius	0.01	0.11	»	»	»	0.14
		Center	»	»	0.15	»	»	»
	ASTM B977-13		≤0.08	≤0.30	≤0.25	≤0.03	≤0.003	≤0.40

converter P121-1.25-40-M-003 of 1.25 MHz frequency, which provides a smaller attenuation factor and better signal/noise ratio. During ingot examination, multiple small amplitude echoes typical for cast metal were observed which resulted from signal reflection from the grain boundaries. Performed testing did not reveal any pulses, which could be interpreted as non-metallic inclusions, pores or shrinkage cavities.

Macrostructural studies of the produced ingots were conducted on transverse templates, which were cut out to study the uniformity of oxygen distribution over the ingot cross-section. The structure was revealed by template etching in 15 % solution of fluoric acid with addition of 3 % nitric acid at room temperature. As a result, it was found that the ingot metal is dense, homogeneous, with absence of differently etched zones in the ingot cross-section. The studied metal is characterized by crystals close to the equiaxed ones of 25 to 50 mm size for ingots of 1100 mm

Figure 4. Appearance of an ingot of Grade 3 titanium alloy of 1100 mm diameter after machining

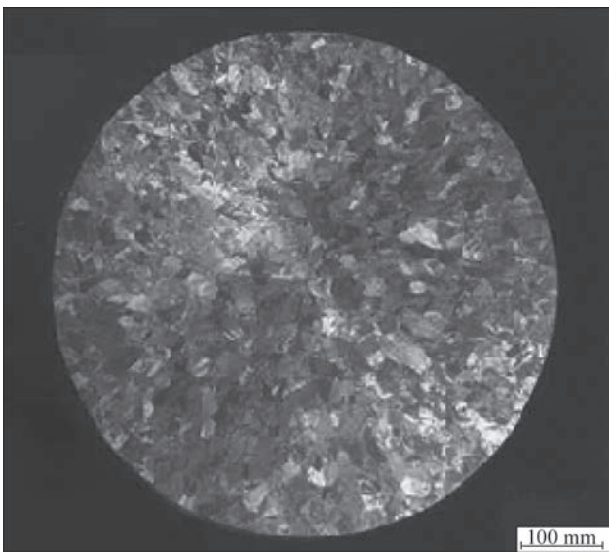

Figure 5. Macrostructure of an ingot of 600 mm diameter of Grade 2 alloy

diameter and of 10–30 mm size for ingots of 600 mm diameter. No difference is found in the structure of the ingot central and peripheral zones (Figure 5).

The microstructure of the grain, produced as a result of cast metal melting, is characterized by packets of α-phase plates oriented in one direction towards the grain boundary.

Thus, EBCHM technology allows producing defectfree titanium ingots with regulated oxygen content that meet the standard requirements, and the proposed formula for calculation of the quantity of TiO_2 powder for alloying allows achieving not more than ± 0.02 % range of oxygen distribution deviation in the ingot metal.

CONCLUSIONS

1. Proceeding from the research results, a method to form the charge billet and a formula for calculation of the quantity of TiO_2 powder for alloying were proposed that allowed producing defectfree titanium ingots with regulated oxygen content, while ensuring a not more than ± 0.02 range of its distribution deviation in the ingot metal.

2. It is shown that the proposed modes of electron beam heating of the consumable billet, metal melting in the cold hearth and the mould, as well as the melting rate ensure complete dissolution of titanium dioxide particles in the cold hearth and absence of oxygen-enriched defects in the produced ingot.

REFERENCES

1. Olejnik, T.A., Guryanova, T.P., Kolobov, G.A. et al. (2010) Development of technologies for the extraction, enrichment and processing of titanium raw materials in the world and in Ukraine. *Metalurgiya: Zb. Nauk. Prats of ZGIA*, **22**, 44–59 [in Russian].
2. Chervony, I.F., Telin, V.V., Pozhuev, V.I. et al. (2007) Titanium and fields of its application. In: *Proc. of Int. Sci.-Tech. Conf. on Ti-2007 in CIS (15–18 Apr. 2007, Yalta)*. Kiev, 2007, 314–325 [in Russian].
3. (2013) *Titanium Metal: Market Outlook to 2018*. Sixth Ed. Roskill Information Services Ltd, USA.
4. Osipenko, A.V. (2015) Development of technology of producing raw materials for titanium alloys from substandard titanium sponge. *Eastern-European J. of Enterprise Technologies*, 4(**5**), 28–32 [in Russian]. http://nbuv.gov.ua/UJRN/Vejpte_2015_4%285%29__7
5. Cheng-Lin, Li, Yang, Yu, Wen-Jun, Ye et al. (2015) Effect of boron addition on microstructure and property of low cost beta titanium alloy. In: *TMS 2015, 144th Annual Meeting & Exhibition*, 1167–1172. https://link.springer.com/chapter/10.1007/978-3-319-48127-2_141
6. Davydov, S.I., Shvartsman, L.Ya., Ovchinnikov, A.V., Teslevich, S.M. (2006) Some peculiarities of titanium alloying with oxygen. In: *Proc. of Int. Sci.-Tech. Conf. on Ti-2006 in CIS (21–24 May, 2006, Suzdal, Russia)*. Kiev, Naukova Dumka, 253–257 [in Russian].
7. Ryabtsev, A.D., Troyansky, A.A. (2011) Refining and alloying of titanium in the process of electroslag remelting in a chamber furnace. *Advances in Electrometallurgy*, 9(**1**), 56–57.
8. Kollerov, M.Yu., Spektor, V.S., Skvortsova, S.V. (2015) Problems and prospectives of application of titanium alloys in medicine. *Titan*, 48(**2**), 42–53 [in Russian].
9. Ratiev, S.N., Ryabtseva, O.A., Troyansky, A.A. et al. (2010) Alloying titanium with oxygen from the gas phase in chamber electroslag remelting of titanium sponge. *Advances in Electrometallurgy*, 8(**2**), 87–92.
10. Egorova, Yu.B., Davydenko, L.V., Mamonov, I.M. (2015) Influence of oxygen alloying on mechanical properties of rods from titanium and Ti–6Al–4V alloy. *Int. Research J*., 41(**10**), Pt 2, 49–51 [in Russian]. DOI: https://doi.org/10.18454/IRJ.2015.41.154
11. Kostenko, V.I., Kruglenko, M.P., Kalinyuk, A.N., Pap, P.A. (2012) Production by of defect-free titanium ingots with controlled oxygen content by electron beam remelting. *Advances in Electrometallurgy*, 10(**1**), 29–32.
12. Kablov, E.N. (2012) Strategic trends of development of materials and technologies of their processing for the period up to 2030. *Aviats. Materialy i Tekhnologii*, **S**, 7–17 [in Russian].
13. Iliin, A.A., Kolachev, B.A., Polkin, I.S. (2009) *Titanium alloys. Composition, structure, properties*. Moscow, VILS-MATI [in Russian].
14. Akhonin, S.V., Kruglenko, M.P., Kostenko, V.I. (2011) Mathematical modeling of the process of dissolution of oxygen-containing refractory inclusions in a titanium melt. *Advances in Electrometallurgy*, 9(**1**), 13–18.

ORCID

S.V. Akhonin: 0000-0002-7746-2946,
O.M. Pikulin: 0000-0001-6327-3448,
V.O. Berezos: 0000-0002-5026-7366,
A.Yu. Severin: 0000-0003-4768-2363,
O.G. Erokhin: 0000-0003-2105-5783

CONFLICT OF INTEREST

The Authors declare no conflict of interest

CORRESPONDING AUTHOR

S.V. Akhonin
E.O. Paton Electric Welding Institute of the NASU
11 Kazymyr Malevych Str., 03150, Kyiv, Ukraine
E-mail: titan.paton@gmail.com

SUGGESTED CITATION

S.V. Akhonin, O.M. Pikulin, V.O. Berezos, A.Yu. Severin and O.G. Erokhin (2021) Production of titanium ingots with regulated oxygen content by electron beam melting. *The Paton Welding J*., **10**, 52–56.

JOURNAL HOME PAGE

https://pwj.com.ua/en

Received 22.06.2021
Accepted: 11.11.2021